**Università degli Studi di Napoli Federico II**

Doctoral Thesis

# NONLOCAL CONTINUUM MECHANICS: THEORETICAL AND FINITE ELEMENT FORMULATIONS

**Marzia Sara Vaccaro**

Dottorato di Ricerca in Ingegneria Strutturale,
Geotecnica e Rischio Sismico XXXIV ciclo

Thesis Advisor:

**prof. Francesco Marotti de Sciarra**

March 2022

# NONLOCAL CONTINUUM MECHANICS: THEORETICAL AND FINITE ELEMENT FORMULATIONS

Thesis by

Marzia Sara Vaccaro

In Partial Fulfillment of the Requirements

for the Degree of

Doctor of Philosophy

Università degli Studi di Napoli Federico II

Italy

March 2022

# Contents

# List of Figures

# Preface

According to classical notions in Continuum Mechanics, constitutive equations are those intrinsic relations providing response variables at a material point of a continuum as functions of variables evaluated at the same material point. Classical constitutive laws obey thus to the axiom of local action according to which response variables at a material point are not significantly influenced by the state of the continuum at distant material points.

However, the domain of application of local Continuum Mechanics strictly depends on the concept of length-scale. If the external characteristic length of a continuum (let us say: structural dimension, wavelength, etc.) is much greater than an internal characteristic length (granular distance, interatomic length, heterogeneities size, etc.), then classical constitutive laws can predict accurate results. On the contrary, if the external and internal characteristic lengths are comparable, local theories fail at predicting the effective mechanical behavior and necessity of nonlocality arises to account for long range interatomic attractions.

In nonlocal continuum field theories, the constitutive response at a material point of a continuum depends on the state of all points and thus is described by response functionals. The above mentioned concept regarding space nonlocality can be also applied to memory-dependent mechanical behaviors where a nonlocality in time is involved.

The present thesis aims at providing an in-depth treatment on nonlocal continuum field theories of elasticity leading to the formulation of a nonlocal finite element method. The plan is the following.

In Chapter 1, micro and nanotechnological applications concerning small-scale electromechanical devices are discussed along with detailed descriptions of their working mechanism. In Chapter 2 fundamental concepts of nonlocal mechanics are elucidated with reference to the Eringen's strain-driven integral model of elasticity, representing a milestone in scientific literature in the framework of early nonlocal theories.

Comprehensive investigations about Helmholtz's kernel and its peculiar properties are provided as essential aspects to prove the differential elasticity model equivalent to the integral constitutive law. The equivalent differential formulation is thus derived and exploited to reverse the Eringen's model of integral elasticity. Then, a discussion is made about issues emerging from the application of Eringen's theory to bounded structural domains and inconsistencies of

relevant nonlocal structural responses are detected.

In Chapter 3, a variational formulation is proposed to derive the general constitutive law of nonlocal elasticity in an abstract form. Firstly, a recent nonlocal elastic theory based on a stress-driven formulation is illustrated. It is shown that the stress-driven nonlocal model is able to overcome ill-posedness of the strain-driven nonlocal theory applied to structural problems and thus it is exploited in the chapter to investigate size-dependent mechanical behaviors of nano-structures. Then, the strain-driven two-phase theory of elasticity is illustrated along with an in-depth analysis about inconsistencies of limiting solutions for a vanishing mixture parameter. The two-phase mixture elasticity is then formulated according to the stress-driven approach and adopted to analyse structural schemes of applicative interest.

Nonlocal theories of elasticity are exploited in Chapter 4 to model the mechanical behavior of a nanocomposite microbeam conceived as a basic structural component of advanced electromechanical systems undergoing large displacements. The two-phase theory of elasticity is first applied to assess elastic properties of nanofillers, according to a novel approach based on Homogenization Theory. Then, the stress-driven integral elasticity is exploited to capture size effects on the flexural behavior of the nanocomposite structure. Elastostatics of the nano-reinforced beam undergoing large displacements is investigated and the relevant nonlocal elastic equilibrium problem is solved by an iterative solution procedure to perform geometrically nonlinear parametric analyses.

In Chapter 5, the stress-driven nonlocal elasticity is developed for structural assemblages. Notably, a well-posed methodology is formulated to account for size effects in nonlocal elastic structures involving concentrated and non-smooth distributed loadings, internal kinematic constraints, piecewise regular elastic and geometric properties. A constitutive differential formulation is provided involving prescription of non-classical interface conditions. Then, asymptotic behaviors of nonlocal response fields for vanishing nonlocal parameter are investigated. Finally, the proposed approach is exploited to solve assembled structural systems.

In Chapter 6, a nonlocal finite element formulation based on the stress-driven model is conceived, starting from the constitutive differential formulation for articulated structural systems illustrated in Chapter 5. A two-noded nonlocal finite element is developed and nonlocal shape functions are derived. They account for long range effects that are not confined into a single finite element but involve the entire structural assemblage; indeed, the number of nonlocal shape functions is equal to four times the number of the mesh elements. Then, a direct procedure to get nonlocal stiffness matrix and nodal force vector is

provided and an assemblage procedure is performed.

The proposed nonlocal finite element methodology is exploited to solve exemplar case-studies and a validation is performed comparing the obtained results with the corresponding closed form solutions. Finally. the nonlocal finite element formulation is applied to nano-structural assemblages to provide benchmark numerical results.

# Chapter 1

# Small-scale structures

Nowadays, design and realization of smaller and smaller smart electromechanical devices are attracting a lot of attention in Engineering Science. Before going deeper into modeling and analysis of small-scale continua, this chapter aims at providing an overview on the main engineering applications involving micro- and nano-structures.

First of all, the term micro/nano-electromechanical system indicates a smart device combining mechanical and electrical components. This kind of systems, also referred as M/NEMS, can sense, actuate and control on nano- and micro-scales to produce effects on macro-scale [1–7]. Starting from 1950's, micro and nanotechnologies have been progressively introduced in several fields such as Automotive, Aerospace, Electronical and Biomedical Engineering where they are used as small-scale actuators, sensors, switches, resonators and probes. Most relevant and recent applications of M/NEMS will be discussed in this section with detailed descriptions.

The recent advancements in small-scale science and technology are due to the fact that micro- and nano-devices exhibit several great advantages such as reduced size, high sensitivity and selectivity, low power consumption, low analyte requirement and quick response. Other specific advantages and features depend on the particular application of micro/nano systems, as will be explained in the following.

It is worth mentioning that typically materials adopted in design of micro/nano-electromechanical devices are Single-crystal silicon (Si), Polycrystalline Si (polysilicon), Silicon dioxide ($SiO_2$), Silicon nitride ($Si_3N_4$, $Si_xN_y$), Polycrystalline germanium (polyGe), Polycrystalline silicon-germanium (poly-Si-Ge), Gold (Au),

Aluminum (Al), Nickel-iron (NiFe), Titanium-nickel (TiNi), Silicon carbide (SiC). In the following, the most relevant applications of small-scale structures in Micro and Nano-Engineering are illustrated and discussed.

## 1.1 Sensing applications

A wide range of applications concerns sensing. In particular, the most used types of sensors and their working mechanism are summarized and described below.

- *Chemical sensors.* A chemical sensor device (also known as bio-sensor) can measure the amount of a specific substance from a sample or from the external environment. One of the simplest schemes is the cantilever based bio-sensor. It can be designed with a single micro/nanobeam or by adopting an array of cantilevers. In a chemical sensor array (CSA), each cantilever has a different probe coating. The coating acts as a receptor surface with the aim to react to a specific analyte. When the chemical substance in the sample is absorbed from the coating surface, the cantilever bends and its deflection provides a measurement of the analyte concentration in the sample. Thus, chemical sensor arrays are designed to be chemically discriminating since each coating surface must bend only with a specific analyte. Therefore CSA can be useful to detect the amount of different substances within a given sample.

- *Humidity sensors.* Sensing of humidity is performed by specific devices based on micro/nanobeams covered with a surface made of hygroscopic material (e.g. phosphoric acid). Absorption of water vapors by the beam coating surface causes deflection of the micro/nanobeam. Moreover, this absorption leads to a change in mass of the beam which also causes a change in resonance frequency. Deflections and resonance frequencies are thus related to the environment humidity. This kind of sensor is also classified as resonator since it is actuated in order to detect changes in resonance frequency providing a measurement of humidity.

- *Viscosity sensors.* Changes in viscosity can be measured by dipping the sensor in a viscous fluid. Indeed, viscus medium surrounding the micro/nanobeams shifts the resonance frequency according to the damping effect.

- *Temperature/heat sensors.* Temperature and heat sensors are based on small-scale structures made of two material with different thermal expansion coefficients. Changes in temperature or in heat make the beams bent. This kind of temperature sensors are used for photo thermal measurement since they are able to detect changes in temperature of $10^{-5}\,K$. While heat sensors can be used to study heat evolution during catalytic chemical reactions.

## 1.2 Transport devices

Other possible applications based on small structures deal with transport devices, as described below.

- *Atomic Force Microscope.* Scanning Force Microscope, also called Atomic Force Microscope, is a kind of MEMS based on a curved micro-cantilever having a nano-tip. Specifically, the Atomic Force Microscope is a scanning probe microscope with a high resolution (fractions of Angstrom). Thus, it is able to investigate matter at nanoscopic level. AFM is based on a micro-cantilever made of silicon or silicon nitride with a nanoscopic tip. In proximity of the sample, microbeam deflects due to attractive forces between the tip and the sample surface. Deflection of microbeam is measured by means of a laser beam that is reflected from the beam end to a position-sensitive photo-detector. Another method to detect displacements of the cantilever is adopting piezoresistive sensors embedded in the cantilever. Carbon nanotube are potentially ideal tip probe for Atomic Force Microscope because of their high stiffness and nanoscopic diameter. Indeed, image resolution is mostly influenced by the properties of the scanning probe.

- *Read/write storage devices.* In storage systems, nano/micro-structures are used as transport devices. Each beam has a probe tip at the end with a diameter of about $10\,nm$. The storage support is a polymer film on which the cantilevers are suspended so that the tips can move or detect matter in the film. In the reading process, tips detect presence or absence of matter in the polymer medium, i.e. 0 or 1 data bit; tips can also move matter in the writing process, i.e. create or erase a bit. This kind of read/write storage device has a storage capacity of $1\,Tbit/in^2$ and thus can be used in mobile devices. Fig.1.1, made by IBM Zurich Research Laboratory, represents the IBM's experimental "millipede" memory chip.

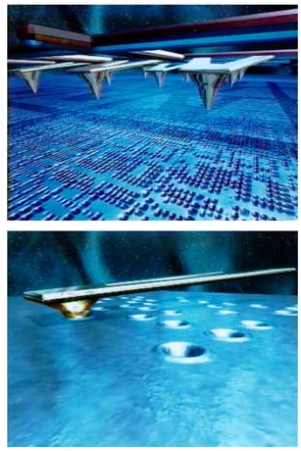

Figure 1.1: IBM experimental millipede nano-mechanical storage device (copyright of IBM Zurich Research Laboratory).

## 1.3 Small-scale accelerometers

Miniaturized accelerometers are characterized by reduced size, weight and cost, and can be effectively integrated with electronic circuits to obtain highly performance micro/nano-devices. Micromachined accelerometers have wide range of applications in Automotive for activity monitoring, stability control, navigation systems and high sensitivity sensoring. Applications of small-scale accelerometers deal not only with the automotive industry, but also with design of portable electronic devices like camcorders, smartphones, virtual reality systems and video games. Ultra-small accelerometers are also applied in biomedical Engineering for health care and activity monitoring. This kind of inertial sensors are typically silicon-based devices.

Specifically, a typical accelerometer is made of a fixed structure, a suspended element and a proof mass located at the end of the mechanical suspension. When an input acceleration is applied, the suspended beam undergoes relative displacements with respect to the fixed structure. In a piezoelectric accelerometer, a piezoelectric sensor detects strains in the suspension as a measure of the applied acceleration. In a capacitive accelerometer, the proof mass and the substrate electrode form a capacitor. Under the external acceleration, displacements of the suspended beam cause a variation of the gap between the fixed

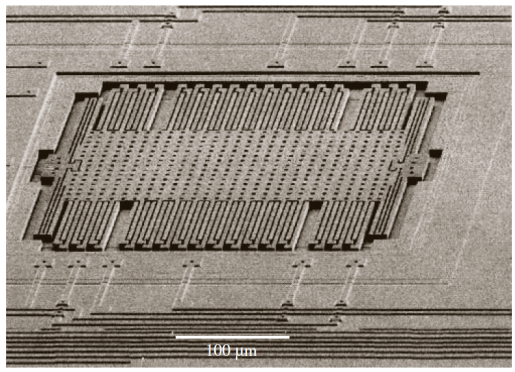


Figure 1.2: SEM micrograph of a polysilicon surface micromachined lateral accelerometer (Copyright Analog Devices Inc.) [8].

structure and the mass, so that the capacitance changes too. Capacitive accelerometers have a wide range of application since they are characterized by high sensitivity and low temperature-dependence. There are two basic types of capacitive accelerometers, i.e. vertical and lateral. In the first one the proof mass form a parallel-plate capacitor with the above substrate electrode. The mass moves in the direction perpendicular to the fixed substrate, thus changing the microscopic gap between suspensions and substrate.

A lateral accelerometer is made of arrays of suspended fingers attached to the proof mass and arrays of fixed fingers. The proof mass moves parallel to the substructure when a lateral acceleration is applied, thus changing the overall gap between the arrays of fingers. A SEM image of a later accelerometer is provided in Fig. 1.2 [8].

A specific type of accelerometer possessing efficient characteristics is the capacitive torsional accelerometer. The device consists of a glass substrate and a silicon structure. As shown in Fig.1.3 the silicon structure is made of a V-shape torsional beam and of four masses anchored at the ends of two beams [9]. The z-direction is the accelerometer sensing direction. Only two masses are curved and they are located at opposite sides with respect to the torsional beam. Thus, when an out of plane acceleration is applied, the two torsional structures anchored at the V-shape beam rotate reversely.

Under each silicon mass, an electrode is located on the glass substrate so that the silicon structure together with the electrodes make a capacitor. The

input acceleration changes the distance between the electrodes and thus the capacitance of the four capacitors, providing a measurement of the acceleration.

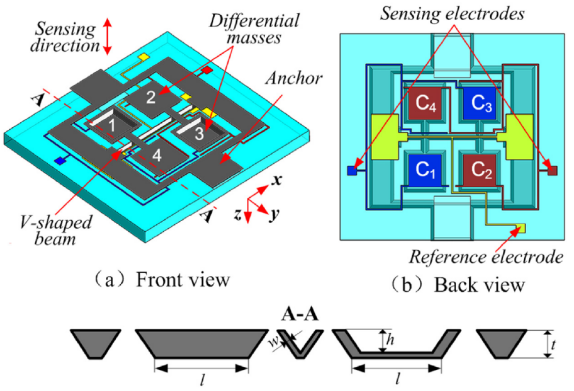


Figure 1.3: Front (a) and back (b) views of a double differential torsional micro-accelerometer based on V-shape beam [9].

## 1.4 M/NEMS resonators

Small-scale resonators are devices based on mechanically resonating structural elements that are electrically put in resonance. These electro-mechanical systems are used in sensing applications for mass detection or as bio-MEMS for chemical/biomedical purposes (such as virus or bacteria sensing). Other aims concern mass inertial sensing or timing applications where resonators are integrated into electronic circuits to provide a high quality clock signal. Indeed, miniaturized resonators exhibit high sensitivity, low power consumption, reduced size and integrability with circuits.

Resonators can be actuated in electrostatic or piezoelectric way [10, 11]. An exemplar scheme consists of a bridge actuated by electrostatic fields. In the simplest configuration, the resonator is composed of a doubly-clamped beam electrostatically actuated by DC (Direct Current) and AC (Alternating Current) voltages. First, the beam is pre-deflected by the DC voltage and then vibrated by the harmonic excitation with a frequency near to the first bending natural frequency of the resonator so that the beam is put in resonance condition.

Resonator-based devices can be successfully adopted for biological detection. For example, a simple scheme of a cantilever-based resonator can be adopted to detect virus particles. Detection is done comparing resonant frequencies of the unloaded cantilever and the virus-loaded cantilever. Thus, a single virus particle can be detected with mass even of the order of $fg$.

## 1.5 CNTs-based devices

Discovered simultaneously by Iijima and Ichihashi [12] and by Bethune [13], carbon nanotubes (CNTs) are an attractive subject of research thanks to their superior mechanical, electronic and optical properties. A single-walled carbon nanotube (SWCNT) is ideally obtained by rolling into a cylinder a perfect sheet of graphene, which is a monoatomic layer made of carbon atoms arranged in hexagonal rings. Of course, hexagons in contact must join coherently. Finally, two hemifullerene caps with appropriate diameter close the obtained cylinder. It is worth noting that each pair of carbon atoms is linked by a covalent bond, referred as C-C bond. As shown in Fig.1.4, different kinds of nanotubes can be obtained depending on how the graphene sheet is rolled. Thus some CNTs possess symmetry planes parallel and orthogonal to the nanotube axis while others are named "chiral" because it is impossible to superimpose them on their mirror image. However, the term "helical" can be also adopted instead of "chiral".

The way in which the nanotube is rolled is mathematically described by the vector of helicity $\mathbf{C}_h$ and by the angle of helicity $\theta_h$. Helical (or chiral) vector is expressed as

$$\mathbf{C}_h = n\mathbf{a}_1 + m\mathbf{a}_2\,, \tag{1.1}$$

where $n$ and $m$ are components of $\mathbf{C}_h$ in the coordinate system defined in the graphene sheet by vectors $\mathbf{a}_1$ and $\mathbf{a}_2$, that is

$$\begin{cases} \mathbf{a}_1 = a\mathbf{x} \\ \mathbf{a}_2 = \dfrac{a}{2}\mathbf{x} + \dfrac{a\sqrt{3}}{2}\mathbf{y} \end{cases} \tag{1.2}$$

where the parameter $a$ is defined as

$$a = |\mathbf{a}_1| = |\mathbf{a}_2| \simeq 2.49\text{Å}\,. \tag{1.3}$$

It can be easily shown that the modulus of the chiral vector is obtained as follows

$$|\mathbf{C}_h| = \sqrt{\mathbf{C}_h \cdot \mathbf{C}_h} = a\sqrt{n^2 + m^2 + nm}\,, \tag{1.4}$$

while the angle of helicity $\theta_h$ can be evaluated reversing the following function

$$cos\theta_h = \frac{\mathbf{C}_h \cdot \mathbf{a}_1}{|\mathbf{C}_h|\,|\mathbf{a}_1|} = \frac{2n+m}{2\sqrt{n^2+m^2+nm}}\,. \tag{1.5}$$

The vector of helicity (chirality) defines the direction orthogonal to the nanotube axis and its modulus is the length of the tube circumference. Hence, the corresponding nanotube diameter is related to $|\mathbf{C}_h|$ as follows

$$d = \frac{|\mathbf{C}_h|}{\pi}\,. \tag{1.6}$$

A carbon nanotube can be thus ideally constructed by rolling a graphene sheet in the direction defined by the chiral vector. Since chiral vector, chiral angle and diameter of CNTs can be got from the values of $n$ and $m$, thus the classification of single-walled nanotubes can be done in function of the pair $(n, m)$ which are always integer numbers. Indeed, the values of $n$ and $m$ express the number of hexagons separating the ends of the chiral vector, counted along the $\mathbf{a}_1$ and $\mathbf{a}_2$ directions, respectively.

An armchair CNT is characterized by the pair $(n, n)$ and by a 30° chiral angle. A zig-zag CNT is described by the pair $(n, 0)$ and by a 0° chiral angle. Armchair and zig-zag names refer to the positions of the carbon atoms at the end of nanotubes. Finally, a chiral CNT is given by $(n, m)$. Of course, the larger is $n$, or $m$, the larger is the diameter $d$ of the carbon nanotube. It is

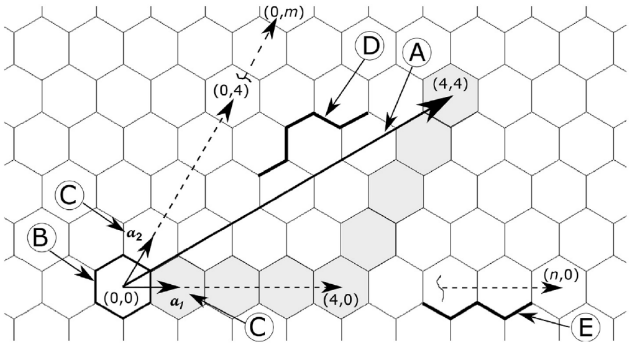


Figure 1.4: Graphene sheet with: A - chiral vector, B - hexagonal elementary cell, C - base vectors, D - armchair pattern, E - zig-zag pattern [14].

worth noting that single-walled carbon nanotubes typically have diameters in the range of $0.7 - 10\,nm$.

Multi-walled carbon nanotubes (MWCNTs) are made of sheets of graphene mutually arranged with a certain filamentary morphology. The easiest MWCNT to imagine is made of concentric and co-axial SWNTs with increasing diameter and it is referred as c-MWCNT.

Carbon nanotubes show different electronic properties depending on their geometry. Thus, they can behave like insulating, semiconductor or metallic materials depending on the values $(n, m)$. CNTs also exhibit great mechanical properties; indeed, they can be even one hundred times stronger than steel but six times lighter and they show an exceptional flexibility. These superior mechanical properties of carbon nanotubes are related to the strong bonds between the carbon atoms (with a $sp2$ hybridization). Indeed, bonds in the curved graphene sheet are stronger than in diamonds. The tensile strength can reach the value of $45\,GPa$ for single-walled CNT while ideal (defect-free) c-MWNTs can reach values of tensile strength even three times higher since they are made by perfect tubes concentrically combined. Euler-Young modulus is also the highest value known. It can be of the order of $1\,TPa$ for ideal carbon nanotubes without defects.

One of the most attractive applications of CNTs-based devices concerns sensing [15]. In particular, among chemical NEMS based on carbon nanotubes, gas sensors are one of the most promising devices. Indeed, CNTs gas sensors can be applied in biomedical fields, environmental monitoring, pharmaceutic industry and even in food and agriculture applications. This kind of sensors is characterized by an ultra-sensitivity so that they can be able to detect in real-time leakages of explosive gases (such as hydrogen) or toxic gases produced by industrial activities.

They can also be used in the field of environmental monitoring. Indeed, flue gases from power plants like nitrogen oxides or sulfur oxides, produce acid rain and photochemical smog and increase the ozone layer depletion and globe warming. Thus, real-time environmental monitoring and control are important to reduce these emissions and clean combustion systems. In the field of space exploration, ultra-sensitive NEMS are required as gas sensors to detect atmospheric components of other planets. Moreover, homeland security is another possible field of application for CNTs sensors.

Chemical nano-sensors are characterized by ultra-sensitivity, low cost, fast response time and low operating temperature. High-sensitivity is achieved increasing the contact surface between gas particles and sensing element, since sensing is mostly based on adsorption of gas molecules. Thus, carbon nanotubes

have gained much attention because they are ideal sensing elements due to their high surface-to-volume ratio and due to the presence of hollows. The working mechanism of CNT-based gas sensors is generally based on chemisorption. That is, adsorption and desorption of gas molecules change the conductance or resistance of nano-sensors.

Fig.1.5 shows a SWCNTs-based gas sensor on a flexible substrate [16]. Flexibility is required to adapt sensors to body skin in order to produce portable and wearable smart devices. The SWCNTs have a length of $30\,\mu m$ and diameter of 1–2 $nm$ and they are decorated with Cu particles to increase their sensitivity. When the sensor is exposed to hydrogen sulfide gas ( $H_2S$ ), molecules are absorbed by the surfaces of CNTs and this causes changes in the conductivity. Variation of electrical resistance is a measure of the sensor response, that is $\Delta R = (R_g - R_0)/R_0$ where $R_g$ and $R_0$ are the resistances before and after the exposure to the gas. These high-performance sensors can detect even small amount of $H_2S$, such as $5\,ppm$.

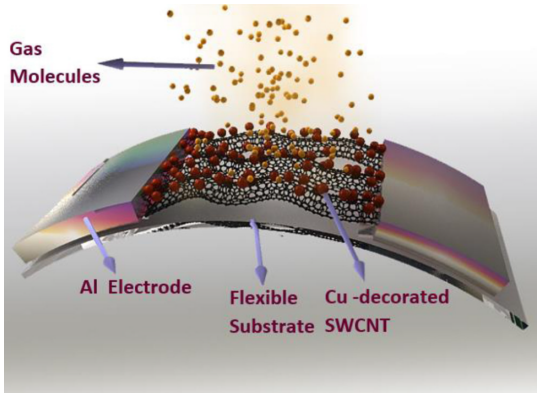


Figure 1.5: SWCNT-based hydrogen sulfide sensor on a flexible substrate [16].

CNT-based sensors are design to detect also ammonia, methane, carbon monoxide, benzene, nitrogen dioxide and other gases that can be dangerous for human and environmental health (see e.g. [17]). NEMS gas sensors can be also applied in monitoring of food quality and safety to avoid losses and spoilages and to detect pathogens and pesticides. Thanks to reduced sizes, CNT based sensors can be incorporated into smartphones or other portable devices, to control in real-time the state of food.

In health monitoring, breath analyses based on CNT sensors, can provide

a non-invasive and fast way to monitor physical conditions and detect diseases like Alzheimer's and Parkinson's pathologies, cancers, diabetes and sclerosis.

CNTs-based storing is another attractive field. Storage systems based on single-walled or multi-walled carbon nanotubes use simple electromechanical switching rules. An example of a memory cell based on a carbon nanotube is represented by a three-terminal cell made of a cantilever CNT and source, drain and gate electrodes. The cantilever nanotube acts as a bending conducting element connected to the source electrode and suspended on a silicon substrate. Drain and gate electrodes are located in the substrate. A "0-state" corresponds to the non-conducting state in which the CNT and the drain are not in contact. If a voltage is applied between the source and the gate electrodes then the nanotube is electrostatically actuated and bent. When the so-called pull-in voltage is applied, then the electrostatic force pulls the cantilever CNT in contact to the drain electrode. Now, the current is allowed to flow between the source and the drain electrodes and this represents the "1-state" or conducting state. Usually, gate voltages range between $5 - 20\,V$. A non-volatile memory cell can be got if the system remains stable in the conducting state. In this case, a pull-out voltage is applied to make the system returning into the non-conducting state.

Other types of devices are the so-called nano-mechanical resonators that are CNTs-based resonators [18, 19]. Low density along with high stiffness make CNTs-based devices attractive for many applications. Indeed, nano-resonators are applied for molecular scale investigations or as highly sensitive mass detection devices where particles absorption shifts the resonance frequency of the nano-resonators [20, 21]. Simple structural schemes for nano-mechanical resonators are cantilever or doubly-clamped (bridge) resonators, generally based on single-walled nanotubes. Other possible configurations are based on double-walled CNT. In this type of resonator, the inner nanotube is doubly-fixed while the second CNT (shorter than the first one) is free to vibrate around the inner one.

Thanks to their high-sensitivity, CNTs-based resonators are used to detect specifically DNA sequences related to some diseases. Indeed, nano-mechanical resonators have high resonance frequencies (of order of $MHz$ and $GHz$). Absorption of DNA causes shifts in resonant frequency that can be measured by means of optical methods. Thus molecular weight can be measured by comparing resonant frequencies of the unloaded and the DNA-loaded nanobeam. Nano-resonators can be also used to measure molecular weight of proteins at single-molecule resolution. In particular, interactions between proteins, or between proteins and DNA, can be investigated by NEMS resonators to detect

cancer and other specific diseases.

Interestingly, carbon nanotubes-based nano-structures are gaining a considerable attention by virtue of their remarkable features such as electrical conductivity, mechanical strength, high sensitivity and large surface area. Small-scale structures like carbon nanotube-based nano-trusses can be successfully adopted for design of ultra-sensitive devices, electronic nano-systems or energy storage devices [22–24].

# Chapter 2

# Eringen's nonlocal theory of elasticity

## 2.1 Nonlocal mechanics: early concepts

The increasing number of miniaturized structural devices and their importance in several technological fields have pushed the research towards the formulation of mathematical models able to capture mechanical small-scale effects. Indeed, analysis and modeling of size-dependent behaviors of micro- and nano-structures is a subject of current interest in Engineering Science with several potential applications as discussed in Chapter 1.

Development of simple and computationally convenient methodologies for model, design and optimization of modern devices and nanocomposites is the main motivation of many recent scientific investigations. In this context, a crucial point is to properly account for small-scale effects which are technically significant and cannot be overlooked. Indeed, size effects result in long range interactions due to intermolecular and interatomic forces that are predominant at the scale under consideration and must be properly addressed.

In its first formulation, continuum mechanics was based on the idea that the matter mechanically interacts through local forces [25–27]. However, local continuum mechanics is not able to model small-scale structures where size effects and long range interactions appear in the mechanical behavior. Moreover, some mechanical effects caused by micro- and nano-scale phenomena also appear at macro-scale such as stress-tip concentrations, dispersion of elastic waves, edge

effects, shear bands, dislocations and heterogeneities. In this context, classical local continuum theories are not able to capture the above mentioned scale phenomena and thus new methodologies must be explored to take into account complex mechanical effects.

Since classical local continuum theories fail in reproducing small-scale mechanical behaviors, assessment of size effects can be advantageously performed by making recourse to tools and techniques of nonlocal continuum mechanics rather than time consuming atomistic approaches [28–30]. Since first formulations and pioneering works [31, 32], nonlocal theories are based on the idea that stress at a given point of a continuum depends on local strain field on the whole domain. Thus, nonlocal theories of elasticity provide enriched continuum models with respect to classical theories and are able to capture small-scale phenomena avoiding computational expensive procedures [33, 34].

Notably, nonlocal approaches introduce a constitutive relation where long distance interactions exchanged within the body are described by internal parameters. One of the earliest theories of nonlocal integral elasticity was conceived by Eringen in [35, 36]. According to Eringen's model, nonlocal stress is the output of a convolution integral between the elastic strain field and a suitable attenuation function depending on an internal length-scale parameter. Since the elastic strain field is input of the integral constitutive relation, Eringen's model is also referred to as strain-driven nonlocal theory. Substantially, this nonlocal formulation provides a constitutive law which is not pointwise but it is based on an integral average. Eringen's approach provides an accurate tool to deal with screw dislocation and surface waves problems in unbounded domain, but when applied to structural problems some issues emerge due to incompatibility between constitutive and equilibrium requirements. Indeed, Eringen's model has been shown to provide failing results known as mechanical paradoxes in the scientific community [37–39], definitely clarified by [40] and acknowledged by the scientific community (see e.g. [41–45]).

The plan of the chapter is the following. Eringen's integral model of elasticity is first illustrated and an in-depth treatment on Helmholtz's averaging kernel and its peculiar properties is provided. Then, it is proven that the integral strain-driven formulation is equivalent to a differential constitutive formulation made of a differential equation equipped with constitutive boundary conditions. The equivalent differential formulation is then usefully exploited to discuss and clarify alleged paradoxical results in scientific literature. Finally, application limits of the strain-driven nonlocal model are illustrated and commented upon.

## 2.2 Strain-driven formulation

Eringen's nonlocal integral formulation has been conceived to solve Rayleigh waves dispersion and screw dislocation problems in unbounded domains [35,36]. It is based on the idea that the stress $\boldsymbol{\sigma}$ at a point $\boldsymbol{x}$ of a nonlocal body $\mathcal{B}$ is the output of a convolution between the local response to the elastic strain field $\boldsymbol{\varepsilon}^{el}$ and a scalar kernel $\phi_\lambda$ depending on a positive nonlocal parameter $\lambda$. That is,

$$\boldsymbol{\sigma}(\boldsymbol{x}) = \int_\Omega \phi_\lambda(\boldsymbol{x}-\bar{\boldsymbol{x}})\boldsymbol{E}(\bar{\boldsymbol{x}})\boldsymbol{\varepsilon}^{el}(\bar{\boldsymbol{x}})\, d\Omega_{\bar{\boldsymbol{x}}}\,, \tag{2.1}$$

where $\boldsymbol{E}$ is the local elastic stiffness tensor field and $\boldsymbol{x}$, $\bar{\boldsymbol{x}}$ are position vectors. Eq.(2.1) expresses the purely nonlocal Eringen's law of elasticity for a three-dimensional continuum that is a Fredholm integral equation of the first kind in the unknown elastic strain field. Eringen's model is also referred to as the strain-driven nonlocal theory since the elastic strain $\boldsymbol{\varepsilon}^{el}$ is source field of the integral convolution.

It is worth nothing that $\Omega$ represents the actual placement of the body and the symbol $d\Omega_{\bar{\boldsymbol{x}}}$ indicates that integration over $\Omega$ is performed with respect to the $\bar{\boldsymbol{x}}$ variable. The stress field $\boldsymbol{\sigma}$ must fulfil equilibrium conditions while the total strain field $\boldsymbol{\varepsilon}$, sum of non-elastic $\boldsymbol{\varepsilon}^{nel}$ and elastic $\boldsymbol{\varepsilon}^{el}$ strain fields, must fulfil kinematic compatibility. The relevant nonlocal elastic equilibrium problem based on Eq.(2.1) is thus represented by a set of integro-differential equations. That is,

$$\begin{cases} div\,\boldsymbol{\sigma}(\boldsymbol{x}) = -\mathbf{b}(\boldsymbol{x})\,, \\ \\ \boldsymbol{\sigma}(\boldsymbol{x}) = \displaystyle\int_\Omega \phi_\lambda(\boldsymbol{x}-\bar{\boldsymbol{x}})\boldsymbol{E}(\bar{\boldsymbol{x}})\boldsymbol{\varepsilon}^{el}(\bar{\boldsymbol{x}})\, d\Omega_{\bar{\boldsymbol{x}}}\,, \\ \\ \boldsymbol{\varepsilon}(\boldsymbol{x}) = sym\,\nabla\mathbf{u}(\boldsymbol{x})\,, \end{cases} \tag{2.2}$$

where $\boldsymbol{x} \in \Omega$. In Eq.(2.2), $\mathbf{u}$ is the displacement field and $\mathbf{b}$ represents the body forces.

Thus, it is worth nothing that when dealing with nonlocal continua, equilibrium and kinematics do not depend on the scale under consideration. Indeed, it only affects the constitutive law that must properly account for size effects.

The scalar averaging kernel $\phi_\lambda$ in Eq.(2.1) is an attenuation function with physical dimension $[\,L^{-3}\,]$ and it is described by a nonlocal parameter $\lambda > 0$ defined as the ratio between internal and external characteristic lengths. As will

be explained in the following, for $\lambda \to 0^+$ the classical elasticity law at internal points of the domain can be recovered from Eq.(2.1) if the attenuation kernel satisfies particular properties described in the sequel [46].

Now, let us apply the integral law in Eq. (2.1) to a one-dimensional domain. Specifically, we deal with the plane and linearised Bernoulli-Euler beam theory. Hereinafter, $x$ will denote the axial abscissa and $L$ the length of the beam, coinciding with the external characteristic length.

Let us indicate with $M$ the bending interaction and with $\chi^{el}$ the elastic flexural curvature field. Then, the strain-driven model applied to a Bernoulli-Euler beam leads to the following nonlocal constitutive relation between bending interaction $M$ and elastic curvature $\chi^{el}$, that is

$$M(x) = \int_0^L \phi_\lambda(x - \bar{x})\,(k_f\,\chi^{el})(\bar{x})d\bar{x}\,, \tag{2.3}$$

where $k_f := I_E$ is the local elastic bending stiffness given by the second moment of Euler–Young modulus E on beam cross-section.

The unknown elastic curvature is implicitly defined by Eq.(2.3) since it is input of the Eringen's convolution integral. The crucial point is that solution of this Fredholm equation in terms of elastic curvature may not exist for an assigned output bending moment fulfilling differential and boundary equilibrium conditions. In the following, this issue will be discussed in detail.

### 2.2.1 Averaging kernel and Green's function

The attenuation kernel $\phi_\lambda$ can be selected among exponential, Gaussian or power-law type functions. Averaging kernels usually adopted in one-dimensional formulations are

$$\begin{aligned} \phi_\lambda(x) &= \frac{1}{2c}\exp\left(-\frac{|x|}{c}\right), \\ \psi_\lambda(x) &= \frac{1}{c\sqrt{2\pi}}\exp\left(-\frac{x^2}{2c^2}\right), \end{aligned} \tag{2.4}$$

where $\lambda$ is the ratio between the internal $c$ and the external $L$ characteristic lengths. Kernel in Eq.$(2.4)_1$ is the bi-exponential function while Eq.$(2.4)_2$ is the normal distribution with zero mean and standard deviation equal to $\lambda$. Attenuation function in Eq.$(2.4)_1$ is also called special kernel due to the fulfillment of some particular properties discussed in the following [40].

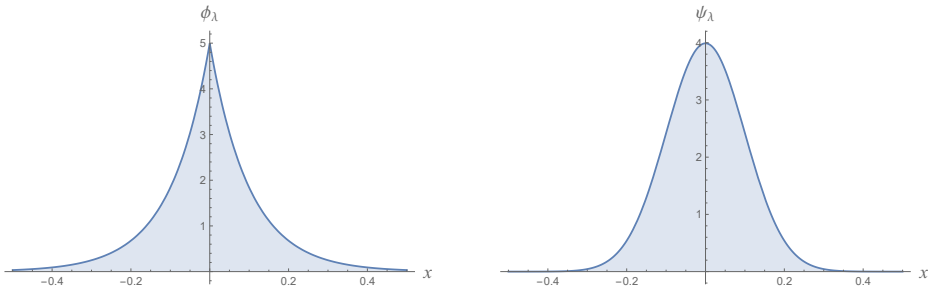


Figure 2.1: Averaging kernels: bi-exponential function (left) and normal distribution (right) for $\lambda = 0.1$.

First of all, the integral kernel $\phi_\lambda : \Re \to [0, +\infty[$ satisfies the properties of symmetry, positivity and limit impulsivity on the real axis as expressed below.

1. Symmetry and positivity
$$\phi_\lambda(x - \bar{x}) = \phi_\lambda(\bar{x} - x) \geq 0 \tag{2.5}$$
2. Normalisation
$$\int_{-\infty}^{+\infty} \phi_\lambda(x)\, dx = 1 \tag{2.6}$$
3. Limit impulsivity
$$\lim_{\lambda \to 0^+} \phi_\lambda(x) = \delta(x) \tag{2.7}$$
being $\delta$ the Dirac impulse.

An explicit expression of the previous formal definition for the impulsivity property is provided below in terms of distribution, that is
$$\lim_{\lambda \to 0^+} \int_{-\infty}^{+\infty} \phi_\lambda(x - \bar{x}) f(\bar{x}) d\bar{x} = f(x) \tag{2.8}$$
for any continuous function $f : \Re \to \Re$.

It is worth noting that for decreasing $\lambda$, the kernel's support reduces and the peak value reached by the function increases. On the contrary, for increasing

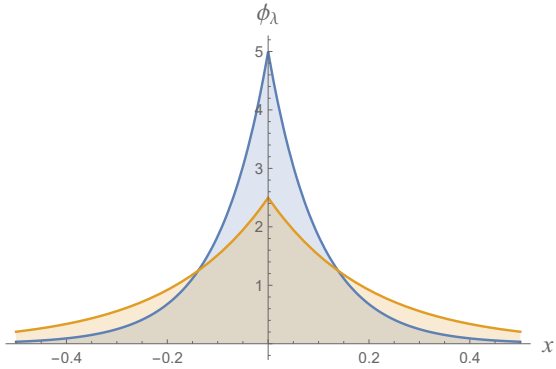


Figure 2.2: Special kernel in Eq.(2.4)$_1$ for $\lambda \in \{0.1, 0.2\}$.

$\lambda$ more and more abscissae of the domain are involved in the convolution law, increasing thus nonlocal effects.

As shown above, the limit impulsivity property is defined on the real axis. If a bounded domain is considered the property changes according to the following explanation.

First, let us consider a bounded one-dimensional domain e.g. the interval $[a, b]$ with $a, b \in \Re$. Then, we define the following function

$$g(x) = \begin{cases} 1, & x \in ]a, b[\,, \\ 1/2, & x = \{a, b\}\,. \end{cases} \tag{2.9}$$

Hence, the impulsivity properties in a bounded domain can be rewritten as follows

$$\lim_{\lambda \to 0^+} \int_a^b \phi_\lambda(x - \bar{x}) f(\bar{x}) d\bar{x} = g(x)\, f(x) \tag{2.10}$$

for any continuous real scalar function $f$.

That is, in the limit for $\lambda \to 0^+$, the special kernel tends to the Dirac impulse or to the halved Dirac impulse, depending on whether the abscissa of evaluation is an interior or exterior point of the domain. So if $x \in ]a, b[$, then for $\lambda \to 0^+$, the output of the convolution evaluated at $x$ is the source field $f(x)$. While if $x = \{a, b\}$, then for a vanishing nonlocal parameter only the halved local source field $f(x)/2$ is recovered.

Thus, by virtue of the impulsivity property, the local elastic law can be recovered from the nonlocal integral one when $\lambda \to 0^+$ and so goes for the solution of the relevant elastostatic problem except for boundary effects due to the fact the the kernel's support exceeds the structural domain at boundary abscissae. A simple explanation of this result is that for $\lambda \to 0^+$, at a regular boundary point, only one-half of the kernel's support will be included in the integration domain.

A proof of the impulsivity property can be found below.

**Proof 2.2.1** *Let us consider the convolution integral on the real axis between the special kernel $\phi_\lambda$ and any continuous function $f : \Re \to \Re$, that is*

$$\big(\phi_\lambda * f\big)(x) := \int_{-\infty}^{+\infty} \phi_\lambda(x - \bar{x}) f(\bar{x}) d\bar{x}\,, \tag{2.11}$$

*with the nonlocal length ratio parameter defined as $\lambda := c/L$. Right-hand side of Eq.(2.11) can be explicitly rewritten as follows*

$$\frac{1}{2c}\int_{-\infty}^{x} \exp\left(\frac{\bar{x} - x}{c}\right) f(\bar{x})\, d\bar{x} \;+\; \frac{1}{2c}\int_{x}^{+\infty} \exp\left(\frac{x - \bar{x}}{c}\right) f(\bar{x})\, d\bar{x}\,. \tag{2.12}$$

*Now, let us fix any $x^* \in \Re$ and make the following change of variables*

$$\begin{cases} z = \dfrac{\bar{x} - x^*}{c}\,, \\[2ex] dz = \dfrac{d\bar{x}}{c}\,. \end{cases} \tag{2.13}$$

*Then, the extremes of integration change as follows*

$$\begin{cases} \bar{x} \in ]-\infty, x^*] \Rightarrow z \in ]-\infty, 0]\,, \\[2ex] \bar{x} \in [x^*, +\infty[ \Rightarrow z \in [0, +\infty[\,. \end{cases} \tag{2.14}$$

*Thus, integral convolution (2.12) becomes*

$$\big(\phi_\lambda * f\big)(x^*) := \frac{1}{2}\left( \int_{-\infty}^{0} \exp(z)\, f(z\,c + x^*)\, dz \;+\; \int_{0}^{+\infty} \exp(-z)\, f(z\,c + x^*)\, dz \right). \tag{2.15}$$

*Taking the limit for* $\lambda \to 0^+$ *of Eq.*(2.15) *yields*

$$\lim_{\lambda\to 0^+} \big(\phi_\lambda * f\big)(x^*) := f(x^*) \tag{2.16}$$

*thus proving Eq.*(2.8).

*Let us consider the case in which the convolution integral is defined on a bounded domain* $[a,b]$ *with* $a,b \in \Re$, *that is*

$$\big(\phi_\lambda * f\big)(x) := \frac{1}{2c}\int_a^x \exp\left(\frac{\bar{x}-x}{c}\right) f(\bar{x})d\bar{x} \,+\, \frac{1}{2c}\int_x^b \exp\left(\frac{x-\bar{x}}{c}\right) f(\bar{x})d\bar{x}\,. \tag{2.17}$$

*Then, fixing any* $x^* \in ]a,b[$ *and considering the change of variables in* (2.13) *lead to the following change in the extremes of integration*

$$\begin{cases} \bar{x} \in [a,x^*] \Rightarrow z \in \left[\dfrac{a-x^*}{c}, 0\right], \\[2ex] \bar{x} \in [x^*,b] \Rightarrow z \in \left[0, \dfrac{b-x^*}{c}\right]. \end{cases} \tag{2.18}$$

*Then, being* $a < x^* < b$, *taking the limit for* $\lambda \to 0^+$ *yields the following result*

$$\begin{aligned} \lim_{\lambda\to 0^+} \frac{a-x^*}{c} &= -\infty\,, \\[2ex] \lim_{\lambda\to 0^+} \frac{b-x^*}{c} &= +\infty\,. \end{aligned} \tag{2.19}$$

*Taking into account result in* (2.19) *we get*

$$\lim_{\lambda\to 0^+} \left(\frac{1}{2}\int_{\frac{a-x^*}{c}}^{0} \exp(z)\, f(z\,c{+}x^*)dzx + \frac{1}{2}\int_0^{\frac{b-x^*}{c}} \exp(-z)\, f(z\,c{+}x^*)dz\right) = f(x^*)\,. \tag{2.20}$$

*If* $x^* = \{a,b\}$, *from* (2.20) *we get* $f(x^*)/2$ *as limiting result.*

Now, let us prove that the kernel in Eq.$(2.4)_1$ is a Green's function. This peculiar property will be adopted in the following. First, the bi-exponential kernel $\phi_\lambda$ can be described by the position

$$\phi_\lambda(x) = \begin{cases} \omega(x), & x < 0 \\ \\ \omega(-x), & x > 0 \end{cases} \tag{2.21}$$

where the function $\omega$ is defined as follows

$$\omega(x) := \frac{1}{2c} \exp\left(\frac{x}{c}\right). \tag{2.22}$$

Thus, first and second derivatives of the special kernel (2.22) are expressed as

$$\partial_x \phi_\lambda(x) = \begin{cases} \dfrac{1}{c}\omega(x), & x < 0 \\ \\ -\dfrac{1}{c}\omega(-x), & x > 0 \end{cases} \tag{2.23}$$

and

$$\partial_x^2 \phi_\lambda(x) = \begin{cases} \dfrac{1}{c^2}\omega'(x), & x < 0 \\ \\ \dfrac{1}{c^2}\omega'(-x), & x > 0\,. \end{cases} \tag{2.24}$$

As shown in Fig.2.3, the function $\partial_x \phi_\lambda$ has a jump discontinuity at x = 0, equal to $\dfrac{1}{c^2}$.

Taking into account Eqs.(2.21)-(2.24) we get the following second order differential equation

$$\phi_\lambda(x) - c^2\, \partial_x^2 \phi_\lambda(x) = \delta(x) \tag{2.25}$$

being $\delta$ the Dirac impulse and $x \in [a, b]$ with $a < 0 < b$. Thus, we can state the following proposition.

**Proposition 2.2.1** *The special kernel $\phi_\lambda$ is the Green's function solution of the differential equation (2.25) equipped with boundary conditions*

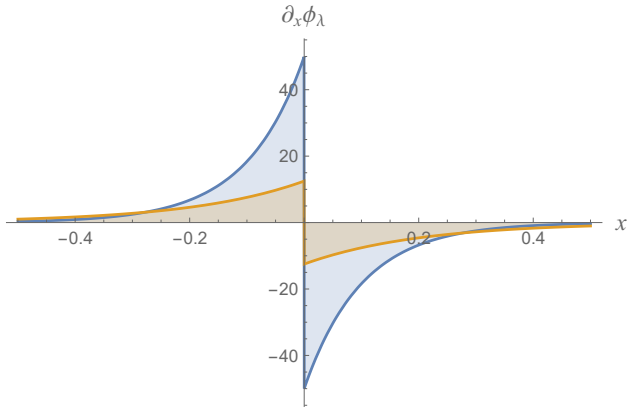


Figure 2.3: First derivative of special kernel in Eq.(2.4)$_1$ for $\lambda \in \{0.1,\, 0.2\}$.

$$\begin{cases} \partial_x \phi_\lambda(a) = \dfrac{1}{c}\phi_\lambda(a)\,, \\ \partial_x \phi_\lambda(b) = -\dfrac{1}{c}\phi_\lambda(b)\,. \end{cases} \tag{2.26}$$

*The differential problem Eqs.*(2.25)-(2.26) *admits a unique solution since the corresponding homogeneous problem admits only the trivial solution.*

By virtue of the peculiar properties of the Helmholtz bi-exponential kernel, a fundamental result of equivalence can be proven for the strain-driven integral model in Eq.(2.3). Indeed, the choice of the special kernel $\phi_\lambda$ as averaging function in the integral convolution law allows us to provide an equivalent differential formulation.

However, it is worth noting that the integral equation (2.3) in the unknown elastic curvature field $\chi^{el}$ and with the interaction bending field $M$ as prescribed by equilibrium requirements, is known as a Fredholm equation of the first kind. In general, solution to this kind of integral equation does not exist or, when it does, is not unique.

In order to prove the constitutive differential formulation equivalent to the strain-driven nonlocal model let us consider a beam of length $L := b - a$ with $a, b \in \Re$. Thus, bending interaction $M$ and flexural elastic curvature $\chi^{el}$ are real scalar functions defined as $\{M,\, \chi^{el}\} : [a, b] \to \Re$. The attenuation function

$\phi_\lambda : \Re \to [0, +\infty[$ is the special bi-exponential kernel described by the nonlocal parameter $\lambda := c/L$. The following proposition can be stated.

**Proposition 2.2.2** *For any $\lambda > 0$, the integral constitutive convolution*

$$M(x) = \int_a^b \phi_\lambda(x - \bar{x})\,(k_f\,\chi^{el})(\bar{x})d\bar{x} \tag{2.27}$$

*with the special kernel $(2.4)_1$, admits either a unique solution or no solution at all, depending on whether or not the bending interaction field fulfils the constitutive boundary conditions*

$$\begin{cases} \partial_x M(a) = \dfrac{1}{c} M(a)\,, \\ \partial_x M(b) = -\dfrac{1}{c} M(b)\,. \end{cases} \tag{2.28}$$

*If Eqs.(2.28) are fulfilled then the unique solution $\chi^{el}$ is obtained from the second order equation*

$$M(x) - c^2\,\partial_x^2 M(x) = k_f(x)\,\chi^{el}(x)\,. \tag{2.29}$$

Proposition 2.2.2 provides an equivalent differential formulation to the integral convolution. This equivalent constitutive law is made of a second order differential equation equipped with two constitutive boundary conditions.

The bending interaction field $M$ is assigned from equilibrium requirement. Thus, the unique solution in terms of elastic curvature $\chi^{el}$ is got from the differential equation (2.29) if and only if the boundary conditions (2.28) are satisfied by the equilibrated bending interaction. In case that the BCs are not satisfied, then no solution does exist.

Proof of Proposition 2.2.2 can be got as follows.

**Proof 2.2.2** *First, let us define the differential operator $\mathcal{L}_x$, that is*

$$\mathcal{L}_x := 1 - c^2\,\partial_x^2\,. \tag{2.30}$$

*Then, we apply $\mathcal{L}_x$ to the integral convolution (2.27) to get*

$$\mathcal{L}_x M(x) = \int_a^b \mathcal{L}_x \phi_\lambda(x - \bar{x})\,k_f(\bar{x})\chi^{el}(\bar{x})\,d\bar{x}\,. \tag{2.31}$$

*Remembering that the special kernel is the Green's function associated with the differential operator* $\mathcal{L}_x$ *, Eq.*(2.31) *can be rewritten as follows*

$$\mathcal{L}_x M(x) = \int_a^b \delta(x-\bar{x})\, k_f(\bar{x})\chi^{el}(\bar{x})\, d\bar{x} = k_f(x)\chi^{el}(x)\,, \tag{2.32}$$

*thus proving the differential equation* (2.29) *and, since the constitutive boundary conditions (CB) in Eqs.*(2.24) *are homogeneous, by linearity they are preserved by the convolution.*

Constitutive equation (2.29) has been widely adopted in scientific literature in recent treatments regarding nonlocal elastic beams, disregarding the constitutive boundary conditions (2.28). In [47], necessity of Eq.(2.28) has been deeply discussed and definitely clarified in [40] where the ill-posedness of the elastic equilibrium problem based on the strain-driven model has been finally proven.

Indeed, Proposition 2.2.2 puts into evidence that the nonlocal elastic convolution in Eq.(2.27) imposes stringent requirements to bending interaction fields since constitutively admissible bending fields must belong to the linear subspace of fields fulfilling the constitutive boundary conditions Eqs.(2.28). Compatibility between equilibrium requirements and constitutive boundary conditions is necessary to ensure the existence of solution for the relevant elastostatic problem of a nonlocal elastic beam.

Indeed, constitutive boundary conditions (2.28) relate the boundary values of bending and shearing fields for any value of $\lambda > 0$ and this is likely to be in contrast with the natural boundary conditions in all nonlocal elastic problems of applicative interest. As a consequence, no solution exists in general. This lack of existence was considered to be a paradox in the scientific literature, because existence of solution was assumed a priori.

By virtue of Proposition 2.2.2, it is possible to detect the class of constitutively admissible bending interactions fields since they are those that fulfil the constitutive boundary conditions (2.28). It is worth noting that statically determinate beams are those in which the linear subspace of bending interaction fields in equilibrium with vanishing loadings (self-equilibrated) is trivial. Therefore, the equilibrated bending field is uniquely defined and independent of the nonlocal parameter.

Consequently, fulfilment of the boundary conditions, for any positive value of $\lambda$, implies that reactions of kinematic constraints must vanish so that only self-equilibrated loading distributions (i.e. whose resultant and resultant momentum are both vanishing) are compatible with the strain-driven constitutive law. This kind of constraints and loadings is however not usual in engineering fields and it

is of no interest. Therefore, we can conclude that the strain-driven constitutive integral law is incompatible with the equilibrium conditions required on the bending interaction field.

An alternative proof of Proposition 2.2.2 can be got as shown below.

**Proof 2.2.3** *Let us explicitly rewrite the convolution strain-driven integral in Eq.(2.27) as follows*

$$M(x) = \frac{1}{2c}\left( \int_a^x \exp\left(\frac{\bar{x}-x}{c}\right)(k_f\,\chi^{el})(\bar{x})d\bar{x} + \int_x^b \exp\left(\frac{x-\bar{x}}{c}\right)(k_f\,\chi^{el})(\bar{x})d\bar{x}\right). \tag{2.33}$$

*Adopting the following position*

$$\begin{cases} M_1(x) = \dfrac{1}{2c}\displaystyle\int_a^x \exp\left(\frac{\bar{x}-x}{c}\right)(k_f\,\chi^{el})(\bar{x})d\bar{x}\,, \\ \\ M_2(x) = \dfrac{1}{2c}\displaystyle\int_x^b \exp\left(\frac{x-\bar{x}}{c}\right)(k_f\,\chi^{el})(\bar{x})d\bar{x}\,, \end{cases} \tag{2.34}$$

*equation (2.33) can be simply rewritten as*

$$M(x) = M_1(x) + M_2(x)\,. \tag{2.35}$$

*By taking the first derivative of $M_1$ and $M_2$ we get*

$$\begin{cases} \partial_x M_1(x) = \dfrac{1}{2c}\,(k_f\,\chi^{el})(x) - \dfrac{1}{c}M_1(x)\,, \\ \\ \partial_x M_2(x) = -\dfrac{1}{2c}\,(k_f\,\chi^{el})(x) + \dfrac{1}{c}M_2(x)\,. \end{cases} \tag{2.36}$$

*Then, first derivative of $M$ as expressed in (2.35) is*

$$\partial_x M(x) = \frac{1}{c}\,(M_2(x) - M_1(x))\,. \tag{2.37}$$

*By evaluating the expression of $\partial_x M$ at boundary points $a, b$ we get the following constitutive boundary conditions*

$$\begin{cases} \partial_x M(a) = \dfrac{1}{c}M(a)\,, \\ \partial_x M(b) = -\dfrac{1}{c}M(b)\,, \end{cases} \tag{2.38}$$

*since it can be observed that*

$$\begin{cases} M_2(a) = M(a), & M_1(a) = 0 \\ M_1(b) = M(b), & M_2(b) = 0\,. \end{cases} \tag{2.39}$$

*Finally, computing a further derivation of Eq.*(2.36) *and remembering the initial position in* (2.35) *lead to the differential equation*

$$M(x) - c^2\,\partial_x^2 M(x) = k_f(x)\,\chi^{el}(x)\,. \tag{2.40}$$

*Thus, the equivalent differential formulation of the strain-driven convolution law is proven.*

### 2.2.2 Alleged paradox of cantilever

In this section, an emblematic case-study of nonlocal elastic slender beams is presented. The paradox under question was first claimed by Peddieson in [37] and then by Challamel in [38], regarding the solution of the elastostatic problem of a nonlocal cantilever beam under concentrated loading at free end.

First, let us recall the equilibrium differential equation of a Bernoulli-Euler beam, that is

$$\partial_x^2 M = q \tag{2.41}$$

where the $x$ abscissa is taken along the beam axis. The beam length is $L$ and the applied free end force is $\mathcal{F}$. For the case under consideration $q(x) = 0$ and the natural boundary conditions are $M(L) = 0$, $\partial_x M(L) = -\mathcal{F}$.

Then, the equilibrated bending interaction field is $M(x) = \mathcal{F}(L - x)$ and it is univocally got by differential and boundary equilibrium conditions since the beam is statically determinate.

Now, let us apply the constitutive differential equation of Eringen's model expressed in (2.40). It yields

$$M(x) = k_f(x)\,\chi^{el}(x)\,. \tag{2.42}$$

It is worth noting that the nonlocal elastic constitutive law turns out to be coincident with the local one. Moreover, if we apply the integral convolution (2.27), taking into account (2.42), we get

$$M(x) = \int_0^L \phi_\lambda(x - \bar{x})\,\mathcal{F}(L - \bar{x})d\bar{x}\,. \tag{2.43}$$

Integral convolution (2.43) between the source field (2.42) and the special kernel $\phi_\lambda$ provides an output bending moment that is nonlinear, i.e.

$$M(x) = \frac{1}{2}\mathcal{F}\,L\left(\lambda \exp\left(\frac{x-L}{c}\right) - (1+\lambda)\exp\left(-\frac{x}{c}\right) + 2\left(1-\frac{x}{L}\right)\right). \quad (2.44)$$

Bending interaction field provided by (2.44) does not fulfill equilibrium requirements. This fact has been erroneously interpreted as the proof that the integral convolution (2.27) and the differential problem (2.29)-(2.28) are not equivalent.

The correct interpretation is that both the integral law and the differential constitutive formulation do not have admissible solutions. Indeed, Proposition 2.2.2 provides a tool to simply detect if a solution may be got from Eq.(2.27) depending on the fulfillment of the constitutive boundary conditions.

In the case under examination, the constitutive boundary conditions are not satisfied by the equilibrated bending interaction field since we get

$$\begin{cases} -\mathcal{F} = \dfrac{1}{c}\mathcal{F}\,L\,, \\ -\mathcal{F} = 0\,. \end{cases} \quad (2.45)$$

It is apparent that constitutive boundary conditions can be satisfied only in the case of a vanishing applied concentrated loading, that is of no applicative interest.

Thus, the nonlocal elastic equilibrium problem of a cantilever beam under concentrated loading at free end has no solution if the strain-driven nonlocal model is applied. Therefore no paradox arises since the relevant elastostatic problem is simply ill-posed. The non-existence of solution is due to the incompatibility between equilibrium requirements and the constitutive law.

For a more in-depth discussion, let us evaluate the shearing and loading fields obtained by the nonlinear bending interaction field (2.44) got by the convolution integral. That is

$$\begin{aligned} T(x) &= \frac{1}{2}\mathcal{F}\left(\exp\left(\frac{x-L}{c}\right) + \frac{c+L}{c}\exp\left(-\frac{x}{c}\right) - 2\right), \\ q(x) &= \frac{1}{2c}\mathcal{F}\left(\exp\left(\frac{x-L}{c}\right) - \frac{c+L}{c}\exp\left(-\frac{x}{c}\right)\right). \end{aligned} \quad (2.46)$$

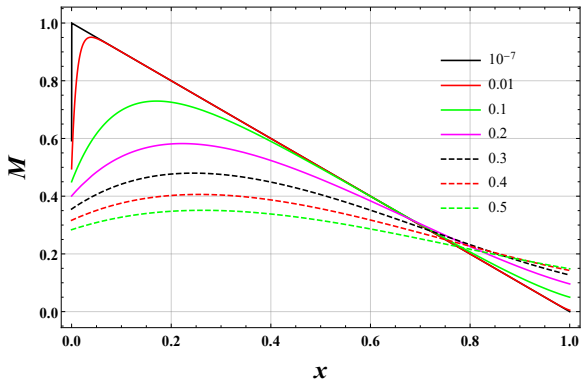


Figure 2.4: Bending interaction field (2.44) as function of $\lambda$.

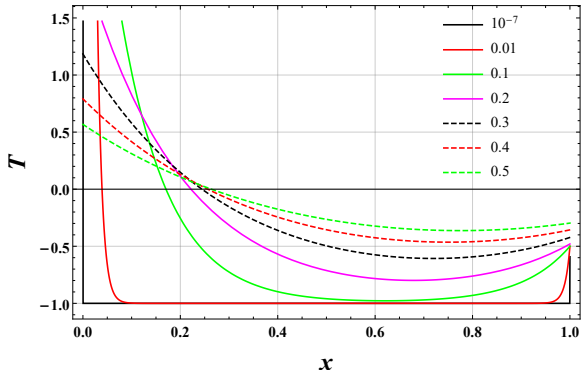


Figure 2.5: Shearing interaction field $(2.46)_1$ as function of $\lambda$.

We can notice that the bending field is not vanishing at free end (see Fig.2.4), the shearing field is not uniform (see Fig.2.5) and the loading is not vanishing (see Fig.2.6). All these aspects reveal that equilibrium conditions are significantly violated. Displacement field computed by a double integration may seem acceptable because of the integration smoothing effects, but a close look to the static fields shows the ill-posedness of the continuum problem.

This pathological issue concerns not only this specific statically determinate case-study but it deals in general with all nonlocal structural problem formulated

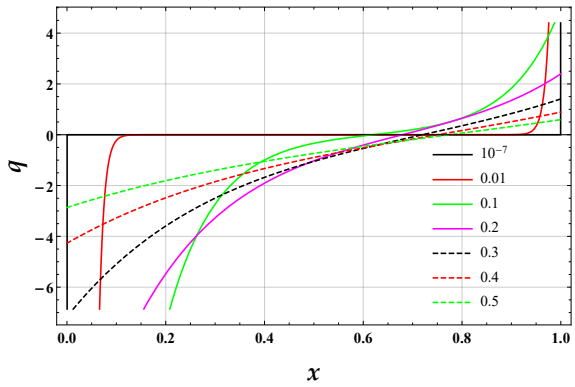


Figure 2.6: Loading field $(2.46)_2$ as function of $\lambda$.

in bounded domain [40].

To make an example concerning statically indeterminate beams, let us consider the simply structural scheme of a fully clamped beam of length $L$ under a uniformly distributed loading $q$. Our purpose is to prove that the strain-driven model provides no solution to this continuum problem.

By virtue of the equivalence expressed in Proposition 2.2.2, the differential constitutive problem can be adopted to conveniently reverse the strain-driven integral convolution.

From the differential equation of equilibrium $\partial_x^2 M = q$ the bending interaction field is got as function of $n$ integration constants, where $n = 2$ is the redundancy degree. Thus we have $M(x) = \dfrac{q\,x^2}{2} + a_1 x + a_2$ while the flexural elastic curvature $\chi^{el}$ (coincident with the total curvature $\chi$) is written in terms of transverse displacement field $v$ by taking into account the kinematic compatibility condition of Bernoulli-Euler theory, i.e. $\chi = \partial_x^2 v$.

Then, constitutive differential equation (2.40) becomes

$$\frac{q\,x^2}{2} + a_1 x + a_2 - c^2\,q = k_f\,\partial_x^2 v(x) \tag{2.47}$$

equipped with kinematic boundary conditions

$$\begin{cases} v(0) = 0\,, \quad \partial_x v(0) = 0\,, \\ v(L) = 0\,, \quad \partial_x v(L) = 0\,, \end{cases} \tag{2.48}$$

and constitutive boundary conditions

$$\begin{cases} a_1 = \dfrac{a_2}{c} \\ q\,L + a_1 = -\dfrac{q\,L^2}{2\,c} - \dfrac{a_1\,L}{c} - \dfrac{a_2}{c} \end{cases} \tag{2.49}$$

Solving system (2.49) provides the integration constants

$$\begin{cases} a_1 = -q\frac{L}{2}\,, \\ a_2 = -q\frac{L}{2}c\,, \end{cases} \tag{2.50}$$

so that the second order differential equation (2.47) with kinematic boundary conditions (2.48) can be solved only if a vanishing loading is applied to get the trivial solution in terms of transverse displacement.

Supposing to neglect the constitutive boundary conditions (2.49), as frequently done in literature, the displacement solution got by differential equation (2.47) with kinematic boundary conditions (2.48) is not the solution of Eringen's strain-driven integral model.

Moreover, the solution displacement got by the Eringen's differential model (disregarding the CBs) turns out to be coincident with the local one, i.e.

$$v(x) = \frac{q(L-x)^2\,x^2}{24\,k_f}\,. \tag{2.51}$$

If we further compute the flexural curvature kinematically compatible with the displacement field, i.e. $\chi^{el} = \chi = \partial_x^2 v$, and then insert $\chi^{el}$ as source field of the strain-driven convolution, we get a bending interaction that does not fulfill equilibrium conditions.

Pathological behaviors like the ones described in case-studies shown in this section can be observed in all structural schemes of engineering interest.

Indeed, as proven in [40] application of Eringen's strain-driven model to bounded domain leads to ill-posed structural problems. In fact, the constitutive boundary conditions of the equivalent differential formulation cannot be satisfied.

If constitutive boundary conditions are disregarded, then from the differential constitutive equation we get structural solutions that are not compatible with equilibrium requirements. Moreover, displacement solutions show contrasting scale effects for increasing nonlocal parameter $\lambda$, that is, structural behaviors can stiff or soften depending on the kind of boundary and loading conditions. In some cases, like the one observed in this section, the structural behavior exhibits no nonlocal effect at all.

# Chapter 3

# Variational nonlocal elasticity

## 3.1 Introductory remarks

Several theories have been developed during the last decades to model size-dependent mechanical behaviors and overcome the issues related to Eringen's strain driven model. Among these enriched formulations of elasticity, two phase (local/nonlocal) mixture models represent an effective tool to overcome ill-posedness of strain-driven model in bounded domains and to efficiently capture size effects. First introduced by Eringen in [35,48], strain-driven mixture model of elasticity is based on a convex combination of local and integral nonlocal responses by means of a mixture parameter. The two-phase model has been exploited by various authors [49–52] to formulate well-posed nonlocal elastic equilibrium problems, assuming that the local fraction of the constitutive law is not vanishing [53].

Difficulties and singularities of Eringen's formulations in structural mechanics can be definitely overcome if the stress-driven integral theory conceived by Romano and Barretta [54] is adopted to model size effects. This theory consists in a new nonlocal elastic law based on a stress-driven formulation providing a consistent methodology in the framework of integral elasticity to account for size-dependent mechanical behaviors. According to the stress-driven nonlocal theory, the nonlocal elastic strain field at a point of a continuum is the output of a convolution integral between the local elastic strain and a scalar averaging

kernel. Stress-driven formulation of nonlocal elasticity leads to well-posed continuum problems and thus can be efficiently adopted to model size effects due to long range interactions [55–64].

This efficient approach has been recently extended by [65] to capture both softening and stiffening elastic responses characterizing small structural scales by proposing a stress-driven two-phase (local/nonlocal) mixture model which is well-posed for any local fraction. The mixture theory based on a stress-driven formulation has been successfully applied in recent contributions such as in [41, 66, 67].

Alternatively, to account for size effects in nano-continua, mechanical responses can be assumed to depend on both elastic strain fields and gradient fields of higher-order. However, the strain gradient elasticity incorporating all the higher-order strain components is too intricate. Thus, a variety of simplified versions of strain gradient elasticity theory has been formulated in the literature to tackle a wider range of structural problems. However, different forms of strain gradient models lead to stiffening structural responses for increasing small-scale parameters [68].

Interestingly, Aifantis coupled Eringen's differential law and the strain gradient model of elasticity in [69, 70]. Then, Lim et al. [71] combined Eringen's nonlocal integral law with the strain gradient elasticity to tackle nonlocal problems of wave propagation (defined in unbounded domains). In this framework, the governing differential constitutive equation is of higher-order than the classical local one and thus Lim et al. [71] introduced higher-order boundary conditions to close the relevant problem but overlooking the constitutive boundary conditions recently established by Barretta and Marotti de Sciarra [72]. However, it is worth underlining that in the framework of wave propagation problems in unbounded domains, boundary conditions were appropriately not prescribed in [71] being tacitly verified by the fields involved in the integral convolutions since they rapidly vanish at infinity.

The aim of this chapter is to provide an in-depth investigation about the most known and recent theories of nonlocal elasticity. First, the stress-driven nonlocal model is illustrated in contraposition to the Eringen's strain-driven theory. Then, the mixture local/nonlocal strain-driven model is presented as a generalization of the Eringen's theory, and it is shown that the model exhibits some singularities for a vanishing mixture parameter. Therefore, the two-phase theory in the stress-driven formulation is illustrated as a well-posed generalization of the purely nonlocal elasticity, and its effectiveness is shown presenting an applicative exemplar case-study.

Here is the detailed outline. First, a variational approach is apply to get the

general constitutive relation of elasticity in an abstract form. Then in Section 3.3, the new stress-driven formulation of integral elasticity is investigated and size-dependent analyses of mechanical behaviors are performed. Extension of the purely nonlocal model of elasticity is then provided in Section 3.4 illustrating the two-phase (local/nonlocal) mixture theory in the strain-driven formulation. In particular, in Section 3.4.1 an in-depth discussion is performed about limiting solutions of elastic equilibrium problems based on Eringen's two-phase elasticity and then in Section 3.5 the local/nonlocal stress-driven mixture elasticity is illustrated and discussed along with exemplar case-studies.

## 3.2 Variational formulations

This section aims at formulating a general constitutive law of nonlocal elasticity in an abstract form. Then, it will be shown that all the known theories of elasticity adopted in literature can be derived as special cases of the general abstract size-dependent constitutive relation provided in the following.

To this purpose, let us introduce the source field $s : [0, L] \to \Re$ and the output field $f : [0, L] \to \Re$, being $[0, L]$ the structural interval. The abstract formulation of nonlocal elasticity is assumed to be governed by the following functional representing the elastic strain energy [73]

$$\Pi(s) := \frac{1}{2} \int_0^L \left( \alpha \, s_x^2 + (1 - \alpha)(\phi_\lambda * s)_x \, s_x \right) dx \tag{3.1}$$

where the following compact symbolism has been adopted

$$(\phi_\lambda * s)_x := (\phi_\lambda * s)(x) = \int_0^L \phi_\lambda(x - \bar{x}) \, s(\bar{x}) d\bar{x} \, , \tag{3.2}$$

being $x, \bar{x} \in [0, L]$. In Eq.(3.1), $\phi_\lambda$ is the special kernel described by the nonlocal parameter $\lambda$ as introduced in Chapter 2, while $\alpha \in [0, 1]$ is a mixture parameter introduced by Eringen [35].

In order to derive the nonlocal response $f$ at the abscissa $x$ of the domain, let us apply the following variational condition

$$< f, \delta s > = < d\Pi, \delta s > \qquad \forall \, \delta s \in C([0, L], \Re) \tag{3.3}$$

that is, the virtual work done by the output field $f$ for any virtual continuous source field $\delta s$ must be equal to the directional derivative of the functional $\Pi$ along the virtual source field $\delta s$.

It is worth noting that left-hand side of Eq.(3.3) is explicitly expressed as

$$< f, \delta s >:= \int_0^L f(x)\, \delta s(x) dx\,, \tag{3.4}$$

while the right-hand side of Eq.(3.3), i.e. $< d\Pi,\, \delta s >$, is the directional derivative of the functional $\Pi$ along a virtual source field $\delta s$ and is evaluated as follows

$$< d\Pi, \delta s >:= \int_0^L \Big( \alpha\, s_x\, \delta s_x + (1-\alpha)(\phi_\lambda * s)_x\, \delta s_x \Big) dx\,. \tag{3.5}$$

Prescription of the variational condition (3.3) along with a standard localization procedure yields the following nonlocal constitutive relation

$$f(x) = \alpha\, s(x) + (1-\alpha)\, (\phi_\lambda * s)(x) \tag{3.6}$$

that can be explicitly rewritten by taking into account the definition in (3.2), that is

$$f(x) = \alpha\, s(x) + (1-\alpha) \int_0^L \phi_\lambda(x-\bar{x})\, s(\bar{x}) d\bar{x}\,. \tag{3.7}$$

Starting from the integral equation (3.7), all theories of elasticity discussed in this chapter can be derived by properly setting source and output fields and length-scale parameters. Indeed, with reference to inflected beams, it is possible to derive the following elasticity theories as special cases of (3.7).

- **Strain-driven two-phase elasticity**

  Mixture local/nonlocal strain-driven model is got by setting $s := \chi^{el}$ and $f := k_f^{-1}\, M$ in Eq.(3.7), that is

  $$M(x) = k_f \Big( \alpha\, \chi^{el} + (1-\alpha)(\phi_\lambda * \chi^{el})(x) \Big)\,. \tag{3.8}$$

- **Purely nonlocal strain-driven elasticity**

  Eringen's strain-driven integral model is got by setting $s := \chi^{el}$, $f := k_f^{-1}\, M$ and $\alpha = 0$ in Eq.(3.7). That is

  $$M(x) = k_f\, (\phi_\lambda * \chi^{el})(x)\,, \tag{3.9}$$

  thus representing a particular case of Eq.(3.8) for $\alpha = 0$.

- **Stress-driven two-phase elasticity**

  Mixture local/nonlocal stress-driven model is got by setting $s := M$ and $f := k_f\,\chi^{el}$ in Eq.(3.7), thus obtaining

$$\chi^{el}(x) = k_f^{-1}\Big(\alpha\, M + (1-\alpha)(\phi_\lambda * M)(x)\Big)\,. \tag{3.10}$$

- **Purely nonlocal stress-driven elasticity**

  Purely stress-driven integral model is got by setting $s := M$, $f := k_f\,\chi^{el}$ and $\alpha = l = 0$ in Eq.(3.7). That is

$$\chi^{el}(x) = k_f^{-1}\,(\phi_\lambda * M)(x)\,, \tag{3.11}$$

  that represents a particular case of Eq.(3.10) for a vanishing mixture parameter.

In the following, each theory will be introduced and discussed in detail.

## 3.3 The stress-driven nonlocal model

To overcome the issues emerged from the application of the strain-driven model to bounded domains (see Chapter 2), a recent theory has been proposed by Romano and Barretta in [54] providing a consistent methodology in the framework of integral elasticity to account for size effects in nonlocal continua.

With reference to a three-dimensional continuum, the stress-driven integral law of elasticity writes as follows

$$\boldsymbol{\varepsilon}^{el}(\boldsymbol{x}) = \int_\Omega \phi_\lambda(\boldsymbol{x}-\bar{\boldsymbol{x}})\boldsymbol{C}(\bar{\boldsymbol{x}})\boldsymbol{\sigma}(\bar{\boldsymbol{x}})\,d\Omega_{\bar{\boldsymbol{x}}}\,, \tag{3.12}$$

where $\boldsymbol{C} := \boldsymbol{E}^{-1}$ is the elastic compliance tensor field and $\mathbf{x}, \bar{\mathbf{x}}$ are position vectors. It is worth recalling that $\Omega$ represents the placement of the continuum and the symbol $d\Omega_{\bar{\boldsymbol{x}}}$ denotes that integration over $\Omega$ is performed with respect to the $\bar{\boldsymbol{x}}$ variable.

The stress field $\boldsymbol{\sigma}$ must satisfy equilibrium requirements while the total strain field $\boldsymbol{\varepsilon}$, sum of non-elastic and elastic strain fields, must satisfy kinematic compatibility condition.

Equation (3.12) provides a linear elastic nonlocal relation in which the elastic strain $\boldsymbol{\varepsilon}^{el}$ at a point $\boldsymbol{x}$ of a nonlocal continuum is the output of a convolution

between the local elastic strain field and a scalar kernel $\phi_\lambda$ depending on a positive nonlocal parameter $\lambda$.

The source field of the convolution is driven by the stress $\boldsymbol{\sigma}$ and that is why this model is called stress-driven. It must be underlined that integral convolutions (2.1) and (3.12) represent two different nonlocal laws of elasticity and are not one the converse of the other. Indeed, they lead to two completely different structural problems.

Now, let us apply the stress-driven model to nonlocal elastic slender beams. In particular, we deal with the plane and linearised Bernoulli-Euler beam theory. The coordinate $x$ denotes the axial abscissa and $L := b-a$ indicates the length of the beam. The nonlocal parameter $\lambda$ is defined as the ratio $c/L$, being $c$ the internal characteristic length. The field $M$ represents the bending interaction and $\chi^{el}$ is the elastic flexural curvature field.

Hence, integral equation (3.12) applied to a one-dimensional model writes as shown below

$$\chi^{el}(x) = \int_a^b \phi_\lambda(x-\bar{x})\,(k_f^{-1}\,M)(\bar{x})d\bar{x}\,, \tag{3.13}$$

where $k_f^{-1}$ is the elastic flexural compliance.

Let us do a first comparison between the strain-driven model in Eq.(2.27) and the stress-driven law in Eq.(3.13). In Eringen's model the bending interaction field is defined by the integral convolution

$$M(x) = \Big(\phi_\lambda\, *\,(\,k_f\,\chi^{el})\Big)(x)\,, \tag{3.14}$$

where the linear operator $\phi_\lambda *$ synthetically defines the convolution by means of the special kernel. As we can see from (3.14), the strain-driven law provides an implicit definition of the unknown field $\chi^{el}$.

Thus it represents a Fredholm integral equation of the first kind in which the bending interaction field is prescribed by equilibrium requirements. This kind of integral equation is known to generally lead to no solution at all or to multiple solutions.

Conversely, the stress-driven model provides an explicit definition of the nonlocal elastic curvature, that is

$$\chi^{el}(x) = \Big(\phi_\lambda\, *\,(\,k_f^{-1}\,M)\Big)(x)\,. \tag{3.15}$$

The operator $\phi_\lambda *$ is directly applied to local elastic curvature generated by the equilibrated bending interaction so that the solution $\chi^{el}$ is the explicit output of the convolution integral.

In light of the peculiar properties shown in previous sections, the bi-exponential function in Eq.(2.4)$_1$ is chosen as averaging kernel, that is

$$\phi_\lambda(x) = \frac{1}{2c} \exp\left( - \frac{|x|}{c} \right). \tag{3.16}$$

Recalling the Proof 2.2.3, similar steps can be followed to prove the differential formulation equivalent to the stress-driven integral convolution (3.13). In fact, it is sufficient to rewrite Eq.(2.27) in an abstract formulation, that is

$$f(x) = \int_a^b \phi_\lambda(x - \bar{x})\, s(\bar{x}) d\bar{x}\,, \tag{3.17}$$

being $f$ the output field and $s$ the source (input) field. Then, the following position must be done

$$\begin{cases} f := \chi^{el}\,, \\ s := k_f^{-1}\, M\,. \end{cases} \tag{3.18}$$

Thus the following equivalence can be enunciated.

**Proposition 3.3.1** *The nonlocal elastic curvature output of the integral stress-driven law*

$$\chi^{el}(x) = \int_a^b \phi_\lambda(x - \bar{x})\, (k_f^{-1}\, M)(\bar{x}) d\bar{x} \tag{3.19}$$

*provides the unique solution of the differential problem made of the second order differential equation*

$$\chi^{el}(x) - c^2\, \partial_x^2 \chi^{el}(x) = (k_f^{-1}\, M)(x)\,, \tag{3.20}$$

*equipped with constitutive boundary conditions*

$$\begin{cases} \partial_x \chi^{el}(a) = \dfrac{1}{c} \chi^{el}(a)\,, \\ \partial_x \chi^{el}(b) = -\dfrac{1}{c} \chi^{el}(b)\,. \end{cases} \tag{3.21}$$

It is worth noting that the solution is unique since the corresponding homogeneous differential problem admits only the trivial solution.

**Remark 3.3.1** *The nonlocal elastic equilibrium problem of a slender beam can be formulated in the unknown solution of the transverse displacement field* $v : [a, b] \to \Re$ .

*To this aim, let us differentiating twice the constitutive differential equation* (3.20) *to get*

$$\partial_x^4 v - c^2 \, \partial_x^6 v = k_f^{-1} \, q \, , \tag{3.22}$$

*where kinematic compatibility and equilibrium conditions have been prescribed. For* $\lambda \to 0^+$ *the classical Bernoulli-Euler elastic equilibrium equation is recovered from the sixth-order differential equation* (3.22).

*Thus, the governing equation in case of nonlocality is of higher-order. Hence, in addition to essential and natural boundary conditions, constitutive (i.e. non classical) boundary conditions must be prescribed to close and solve the elastostatic nonlocal problem.*

*Homogeneous constitutive boundary conditions* (3.21) *in terms of displacement field write as*

$$\begin{cases} \partial_x^3 v(a) = \dfrac{1}{c} \partial_x^2 v(a) \, , \\ \partial_x^3 v(b) = -\dfrac{1}{c} \partial_x^2 v(b) \, . \end{cases} \tag{3.23}$$

Now, let us compare in detail the strain-driven model with the stress-driven theory to show the emerging differences that led to the adoption of the latest one as the most effective constitutive law to capture size effects in small-scale structures.

As deeply discussed in previous sections, the strain-driven law is generally incompatible with differential and boundary equilibrium conditions. This incompatibility leads to ill-posed nonlocal elastic structural problem.

Only in nonlocal elastic problem involving unbounded domains the strain-driven integral convolution can be efficiently replaced by a differential law equipped with boundary conditions that are tacitly satisfied since the involved fields vanish at infinity. That is why, in its original formulation the strain-driven model was conceived and efficiently applied to investigate screw dislocations and Rayleigh surface wave dispersion problems.

In the stress-driven model no issue arises since there is no incompatibility between constitutive law and kinematic compatibility conditions.

Indeed, an essential requirement for a constitutive law is its independence from prescribed kinematic constraints. That is why homogeneous boundary conditions (3.21) are of constitutive type and do not deal with kinematic or static conditions.

In respect of this requirement, no conflict arises in the stress-driven model since the constitutive boundary conditions (3.21) act on the elastic curvature field and its first derivative while the kinematic boundary conditions act on transverse displacement field and its first derivative.

### 3.3.1 Structural problems

Benchmark results are provided in this section to illustrate how the stress-driven theory can be effectively applied to capture size effects on structural behavior. Adopting the Bernoulli-Euler theory, simple exemplar schemes are solved and relative structural responses are commented upon.

- *Simply supported beam under uniformly distributed loading.* Nonlocal elastic curvature is depicted in Fig.3.1 for $\lambda \in \{10^{-7}, 0.01, 0.1, 0.2, 0.3, 0.4, 0.5\}$ showing a more and more uniform behavior as $\lambda$ increases. Limiting solution (i.e. local response) is the parabolic field got for $\lambda \to 0^+$. Plots in Fig.3.2 show the reduction of maximum displacement $v(1/2)$ as the nonlocal parameter increases.

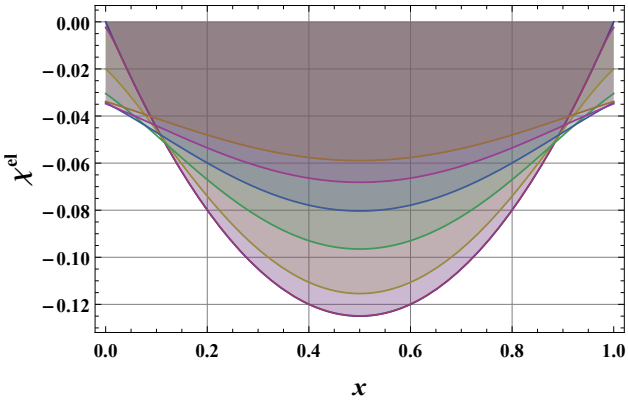


Figure 3.1: Simply supported beam: elastic flexural curvature for $\lambda \in \{10^{-7}, 0.01, 0.1, 0.2, 0.3, 0.4, 0.5\}$.

- *Cantilever beam under concentrated force at free end.* Nonlocal and linear limiting (local) elastic curvatures are depicted in Fig.3.3 for $\lambda \in \{10^{-7}, 0.01, 0.1, 0.2, 0.3, 0.4, 0.5\}$. Nonlocal elastic curvature fields become

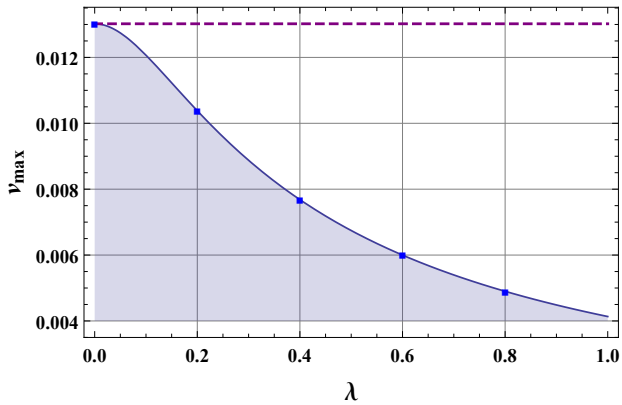


Figure 3.2: Simply supported beam: maximum elastic displacement versus $\lambda$.

lower for increasing $\lambda$. Maximum displacement $v(1)$ versus $\lambda$ is depicted in Fig.3.4.

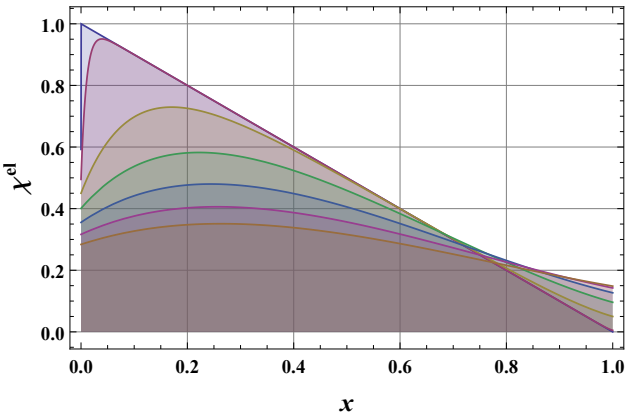


Figure 3.3: Cantilever beam: elastic flexural curvature for $\lambda \in \{10^{-7}, 0.01, 0.1, 0.2, 0.3, 0.4, 0.5\}$.

- *Doubly clamped beam under uniformly distributed loading.* As shown in Figs.3.5-3.6, stiffening effects for increasing nonlocal parameter $\lambda$ are

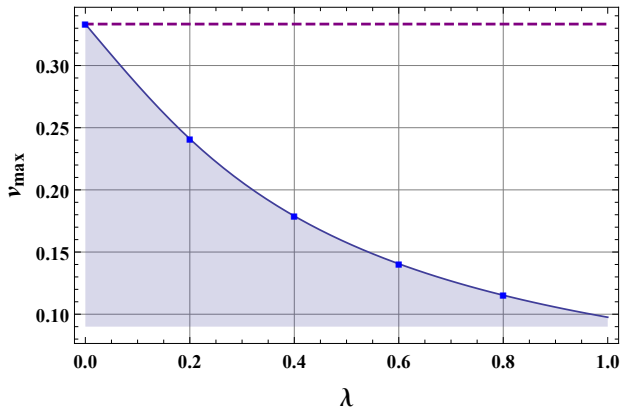


Figure 3.4: Cantilever beam: maximum elastic displacement versus $\lambda$.

greater with respect to previous cases. Maximum displacement $v(1/2)$ versus $\lambda$ is represented in Fig.3.6.

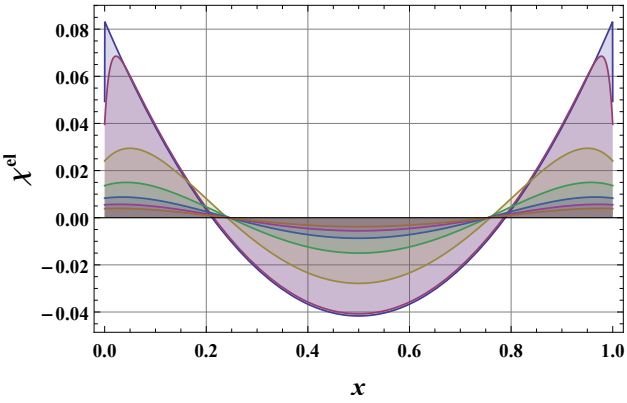


Figure 3.5: Doubly clamped beam: elastic flexural curvature for $\lambda \in \{10^{-7}, 0.01, 0.1, 0.2, 0.3, 0.4, 0.5\}$.

As shown in all the benchmark results, a stiffening behavior is predicted by the stress-driven theory for increasing nonlocal parameter. This result is in agreement with the outcomes collected in [74] and recently confirmed by [68].

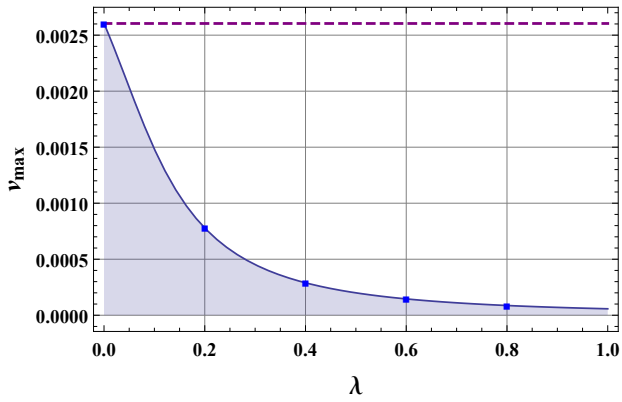


Figure 3.6: Doubly clamped beam: maximum elastic displacement versus $\lambda$.

Stiffer responses respect to the local one, are due to the peculiar properties of the special kernel. In fact, it is worth noting that the normalisation property expressed in (2.6) is the key to prove the basic property of limit impulsivity in (2.7). This peculiar feature of the special kernel $\phi_\lambda$ leads to a stiffening behavior for increasing nonlocal parameter $\lambda$.

Indeed, as $\lambda$ increases, the kernel peak reduces providing a reduction of the elastic compliance. One can observe that at the same time, the increase of $\lambda$ leads to an enlargement of the kernel's support, but the peak reduction has the predominant effect. This peculiar phenomenon affecting nonlocal structures has turned out to be a general feature in Nano-Engineering and it is referred to as "smaller-is-stiffer".

## 3.4 Strain-driven two-phase elasticity

The two-phase local/nonlocal theory, or mixture model, consists in a convex combination of local and nonlocal fractions by means of a mixture parameter, thus providing a generalization of the purely nonlocal theory. First introduced by Eringen in [35, 48] and then applied in many recent scientific contributions such as [49, 50, 65, 75], the two-phase model represents a possible strategy to overcome ill-posedness of the Eringen's model in bounded domains.

In particular, in its strain-driven formulation, the mixture model is based on a convex combination of the local phase and of the nonlocal phase provided

by the Eringen's integral convolution. Thus, the two-phase mixture model is based on two parameters, i.e. nonlocal and mixture parameters, and that is the reason why the local/nonlocal theory is able to model a wide range of structural problems.

Let us consider a Bernoulli-Euler straight beam of length $L$. The local elastic bending stiffness is denoted by $k_f$, which is defined as the second moment of the field of Euler-Young elastic moduli $E$ on beam cross-section. According to the mixture model of elasticity, the bending interaction field $M$ is the convex combination of the source field $s := k_f\,\chi^{el}$ and of the convolution between the source $s$ and the averaging kernel $\phi_\lambda$, that is

$$M(x) = \alpha\, s(x) + (1-\alpha)\int_0^L \phi_\lambda(x-\xi)\, s(\xi)\, d\xi\,, \tag{3.24}$$

where $\alpha$ is the mixture parameter that can range between $0 \leq \alpha \leq 1$. As in the purely nonlocal strain-driven law, $\lambda$ denotes the nonlocal characteristic parameter and it is required to be strictly positive.

The purely nonlocal law $M(x) = \displaystyle\int_0^L \phi_\lambda(x-\xi)\,\big(k_f\chi^{el}\big)(\xi)\, d\xi$ is got by setting $\alpha = 0$, while for $\alpha = 1$ the purely local relation $M = k_f\,\chi^{el}$ is recovered.

It is worth noting that unlike the purely nonlocal strain-driven model, the mixture law in Eq.(3.24) provides a Fredholm integral equation of the second kind in the unknown source field $s$ (see [76, 77]). The averaging kernel in Eq.(3.24) is assumed to be the bi-exponential function

$$\phi_\lambda(x) = \frac{1}{2c}\exp\!\left(-\frac{|x|}{c}\right), \tag{3.25}$$

fulfilling symmetry, positivity and limit impulsivity properties [36].

An equivalent differential formulation [40] of the two-phase model in Eq.(3.24) can be got by remembering that the special kernel in Eq.(3.25) is the Green's function of the linear differential operator $\mathcal{L}_x$ defined by

$$\mathcal{L}_x := 1 - c^2\,\partial_x^2\,. \tag{3.26}$$

Now, let us rewrite Eq.(3.24) as follows

$$\big(M - \alpha\, k_f\chi^{el}\big)(x) = (1-\alpha)\int_0^L \phi_\lambda(x-\xi)\,\big(k_f\chi^{el}\big)(\xi)\, d\xi\,. \tag{3.27}$$

Then, applying the differential operator $\mathcal{L}_x$ to Eq.(3.27) yields

$$\mathcal{L}_x\big(M - \alpha\, k_f \chi^{el}\big)(x) = (1-\alpha)\, k_f(x)\chi^{el}(x) \tag{3.28}$$

which is the differential equation equivalent to the mixture model in Eq.(3.24).

Indeed, denoting by $\delta$ the Dirac unit impulse, since $\mathcal{L}_x\phi_\lambda(x,\bar{x}) = \delta(x,\bar{x})$, we may write

$$\mathcal{L}_x\big(M-\alpha k_f\chi^{el}\big)(x) = (1-\alpha)\int_0^L \mathcal{L}_x\phi_c(x,\xi)\,\big(k_f\chi^{el}\big)(\xi)\,d\xi = (1-\alpha)k_f(x)\chi^{el}(x)\,. \tag{3.29}$$

As seen in Subsection 2.2.1, the special kernel satisfies homogeneous boundary conditions that can be rewritten as follows

$$\begin{cases} \mathcal{B}_0\phi_c\,|_0 = 0\,, \\ \mathcal{B}_L\phi_c\,|_L = 0\,, \end{cases} \tag{3.30}$$

where $\mathcal{B}_0 := 1 - c\,\partial_x$ and $\mathcal{B}_L := 1 + c\,\partial_x$ are differential operators defined at the boundary. By applying $\mathcal{B}_0$ and $\mathcal{B}_L$ to Eq.(3.27) we get

$$\begin{cases} \mathcal{B}_0\big(M - \alpha\, k_f\chi^{el}\big)\,|_0 = 0\,, \\ \mathcal{B}_L\big(M - \alpha\, k_f\chi^{el}\big)\,|_L = 0\,, \end{cases} \tag{3.31}$$

which are the constitutive boundary conditions associated with the differential equation (3.28). Finally, the equivalent differential problem in Eqs.(3.28)-(3.31) can be explicitly expressed as follows

$$\frac{M(x)}{c^2} - \partial_x^2 M(x) = \frac{(k_f\,\chi^{el})(x)}{c^2} - \alpha\,\partial_x^2(k_f\,\chi^{el})(x)\,, \tag{3.32}$$

$$\begin{cases} \partial_x M(0) - \dfrac{1}{c}\,M(0) = \alpha\left(\partial_x(k_f\,\chi^{el})(0) - \dfrac{(k_f\,\chi^{el})(0)}{c}\right), \\ \partial_x M(L) + \dfrac{1}{c}\,M(L) = \alpha\left(\partial_x(k_f\,\chi^{el})(L) + \dfrac{(k_f\,\chi^{el})(L)}{c}\right). \end{cases} \tag{3.33}$$

As deeply investigated in Section 2.2.2, for $\alpha = 0$ (i.e. in the purely nonlocal Eringen's model) constitutive boundary conditions (3.33) and equilibrium requirements turn out to be incompatible. Thus, mixture parameter of the two-phase elasticity model must be strictly positive, i.e. $\alpha > 0$. Indeed, left-hand

sides of Eq.(3.33) are known expressions (generally polynomial) unless of $n$ integration constants, with $n$ redundancy degree. Thus, for $\alpha > 0$ Eqs.(3.33) provide non-homogeneous boundary conditions imposed on the elastic curvature and its first derivative.

While, when the mixture parameter tends to zero, the two-phase strain-driven model provides ill-posed structural problems and some singularities in the mechanical behavior are expected to occur. These inconsistencies of limiting structural solutions for $\alpha \to 0$ will be deeply investigated in the following.

### 3.4.1 Elastostatic solutions

As underlined in Section 3.4, the mixture strain-driven model eliminates ill-posedness of the purely Eringen's model only for strictly positive mixture parameters [53]. If the local phase vanishes, then the purely nonlocal strain-driven law is recovered and thus inconsistencies are expected to occur for structural nonlocal solutions of the limiting elastic equilibrium problem.

Inexact conclusions are still present in scientific literature concerning limiting solutions (i.e. for $\alpha \to 0$) of the nonlocal elastic equilibrium problem based on the two-phase strain-driven theory. See for example the recent contributions [78, 79] where limiting cases of elastodynamic problems are improperly defined as solutions of free vibration problems based on the purely nonlocal Eringen's model that admits no solution [40, 45].

In this section, inconsistencies of limiting solutions of continuum problems based on Eringen's two-phase model are investigated. To this aim, closed-form solutions of the elastostatic problem of Bernoulli-Euler beams using the strain-driven mixture model are first provided and then limiting responses are analytically evaluated. Solution procedure will follow the steps summarized below

- **Step 1.** Solve the differential equilibrium equation $\partial_x^2 M = q$ with natural boundary conditions to get the bending interaction field as functions of $n$ integration constants, being $n$ the redundancy degree.
- **Step 2.** Use the constitutive differential equation (3.32) equipped with constitutive boundary conditions (3.33) to get the nonlocal elastic curvature field $\chi^{el}$; eventually compute the total curvature field $\chi = \chi^{el} + \chi^{nel}$, where $\chi^{nel}$ represents all the non-elastic curvature fields.
- **Step 3.** Solve the kinematic compatibility equation $\chi = \partial_x^2 v$ with prescription of $3 + n$ essential boundary conditions.

The described solution procedure is applied to exemplar structural schemes, i.e.: cantilever under concentrated couple at free end, cantilever under concentrated force at free end, simply supported beam under uniformly distributed loading, doubly clamped beam under uniformly distributed loading.

*Cantilever under concentrated couple at free end.* Let us consider a cantilever of length $L$ and uniform bending stiffness $k_f$ under a concentrated couple $\mathcal{M}$ applied at free end.

The bending interaction field $M$ is obtained by the differential equilibrium equation $\partial_x^2 M = 0$ equipped with standard natural boundary conditions $M(L) = \mathcal{M}$ and $\partial_x M(L) = 0$, so that Eq.(4.3) becomes

$$\frac{\mathcal{M}}{c^2} = \frac{k_f \chi^{el}(x)}{c^2} - \alpha\, k_f \partial_x^2 \chi^{el}(x)\,, \tag{3.34}$$

supplemented with the constitutive boundary conditions

$$\begin{cases} -\mathcal{M} = \alpha\, k_f \Big( c\, \partial_x \chi^{el}(0) - \chi^{el}(0) \Big)\,, \\ \mathcal{M} = \alpha\, k_f \Big( c\, \partial_x \chi^{el}(L) + \chi^{el}(L) \Big)\,. \end{cases} \tag{3.35}$$

Solving the differential problem in Eqs.(3.34)-(3.35) provides the elastic curvature $\chi^{el}$. Also, differential equation $\chi = \partial_x^2 v$ with prescription of standard essential boundary conditions $v(0) = 0$ and $\partial_x v(0) = 0$, gives the nonlocal displacement field

$$\begin{aligned} v(x) = {} & \frac{\mathcal{M} x^2}{2k_f} - \frac{\mathcal{M}}{\psi_1 k_f}\, c\,(\alpha - 1)\, e^{-\frac{x}{c\sqrt{\alpha}}} \Big( (x - c\sqrt{\alpha})\, e^{\frac{L+x}{c\sqrt{\alpha}}} + c\sqrt{\alpha}\, e^{\frac{L}{c\sqrt{\alpha}}} \\ & - e^{\frac{x}{c\sqrt{\alpha}}} (c\sqrt{\alpha} + x) + c\sqrt{\alpha} e^{\frac{2x}{c\sqrt{\alpha}}} \Big)\,, \end{aligned} \tag{3.36}$$

with

$$\psi_1 = (\sqrt{\alpha} + 1)\, e^{\frac{L}{c\sqrt{\alpha}}} + \sqrt{\alpha} - 1\,. \tag{3.37}$$

*Cantilever under concentrated force at free end.* Let us consider a cantilever of length $L$ and uniform bending stiffness $k_f$ under a concentrated force $\mathcal{F}$ applied at free end.

The equilibrated bending interaction field $M$ is defined by $\partial_x^2 M = 0$ with prescription of standard natural boundary conditions $M(L) = 0$ and $\partial_x M(L) = -\mathcal{F}$, so that Eq.(4.3) becomes

$$\frac{\mathcal{F}(L-x)}{c^2} = \frac{k_f \chi^{el}(x)}{c^2} - \alpha\, k_f \partial_x^2 \chi^{el}(x)\,, \tag{3.38}$$

equipped with the constitutive boundary conditions

$$\begin{cases} -\mathcal{F}c - \mathcal{F}L = \alpha\, k_f \Big( c\, \partial_x \chi^{el}(0) - \chi^{el}(0) \Big)\,, \\ -\mathcal{F}c = \alpha\, k_f \Big( c\, \partial_x \chi^{el}(L) + \chi^{el}(L) \Big)\,. \end{cases} \tag{3.39}$$

The unknown elastic curvature $\chi^{el}$ is obtained by solving the differential problem in Eqs.(3.38)-(3.39). Then, kinematic compatibility equation with prescription of standard essential boundary conditions provides the following nonlocal displacement field

$$\begin{aligned} v(x) = {} & \frac{\mathcal{F}x^2\,(3L-x)}{6k_f} + \frac{(\alpha-1)\,c\,\mathcal{F}}{\psi k_f}\, e^{-\frac{x}{\sqrt{\alpha}c}} \left(\sqrt{\alpha}\,\psi_1\, c^2 \left(e^{\frac{x}{\sqrt{\alpha}c}} - 1\right)\left(e^{\frac{L}{\sqrt{\alpha}c}} + e^{\frac{x}{\sqrt{\alpha}c}}\right)\right. \\ & \left. - \psi_2\, L\, x\, e^{\frac{x}{\sqrt{\alpha}c}} + \psi_3\, c\right), \end{aligned} \tag{3.40}$$

with

$$\begin{aligned} \psi &= (\sqrt{\alpha}+1)^2\, e^{\frac{2L}{\sqrt{\alpha}c}} - (\sqrt{\alpha}-1)^2 \\ \psi_2 &= \sqrt{\alpha} + (\sqrt{\alpha}+1)\, e^{\frac{2L}{\sqrt{\alpha}c}} - 1 \\ \psi_3 &= -(\sqrt{\alpha}+1)\,\sqrt{\alpha}\, L\, e^{\frac{2L}{\sqrt{\alpha}c}} + (\alpha - \sqrt{\alpha})\, L\, e^{\frac{2x}{\sqrt{\alpha}c}} - 2\sqrt{\alpha}\, x\, e^{\frac{L+x}{\sqrt{\alpha}c}} + \\ & (\sqrt{\alpha}+1)(\sqrt{\alpha}L - x)\, e^{\frac{2L+x}{\sqrt{\alpha}c}} - (\sqrt{\alpha}-1)\, e^{\frac{x}{\sqrt{\alpha}c}} (\sqrt{\alpha}L + x)\,. \end{aligned} \tag{3.41}$$

*Simply supported beam under uniformly distributed loading.* Let us consider a simply supported beam of length $L$ and uniform bending stiffness $k_f$ under uniformly distributed loading $q$.

Bending interaction field $M$ is determined by differential equilibrium equation $\partial_x^2 M = q$ equipped with natural boundary conditions $M(0) = 0$ and $M(L) = 0$, so that Eq.(4.3) becomes

$$\frac{qx(x-L)}{2c^2} - q = \frac{k_f \chi^{el}}{c^2} - \alpha\, k_f \partial_x^2 \chi^{el}\,, \tag{3.42}$$

supplemented with constitutive boundary conditions

$$\begin{cases} -c\,\dfrac{qL}{2} = \alpha\, k_f \left( c\,\partial_x \chi^{el}(0) - \chi^{el}(0) \right), \\ c\,\dfrac{qL}{2} = \alpha\, k_f \left( c\,\partial_x \chi^{el}(L) + \chi^{el}(L) \right). \end{cases} \tag{3.43}$$

The elastic curvature $\chi^{el}$ is obtained from Eqs.(3.42)-(3.43); then, kinematic compatibility equation together with essential boundary conditions $v(0) = 0$ and $v(L) = 0$, provides the nonlocal displacement field

$$\begin{aligned} v(x) = {} & \frac{qx\,(L^3 - 2Lx^2 + x^3)}{24 k_f} - \frac{(\alpha - 1)\,c^2\,q}{2\psi_1 k_f}\, e^{-\frac{x}{\sqrt{\alpha}\,c}} \left( -e^{\frac{x}{\sqrt{\alpha}\,c}} \left( 2\,\alpha^{3/2}\,c^2 + L\left( \sqrt{\alpha} c \right.\right.\right. \\ & \left. - \sqrt{\alpha}\,x + x \right) + \left( \sqrt{\alpha} - 1 \right) x^2 \Big) + e^{\frac{L+x}{\sqrt{\alpha}c}} \left( -2\,\alpha^{3/2}\,c^2 + L\left( -\sqrt{\alpha}\,c + \sqrt{\alpha}\,x \right.\right. \\ & \left. \left. + x \right) - \left( \sqrt{\alpha} + 1 \right) x^2 \Big) + \sqrt{\alpha}\,c\, e^{\frac{L}{\sqrt{\alpha}c}} \left( 2\,\alpha\,c + L \right) + \sqrt{\alpha}\,c\,(2\,\alpha\,c + L)\, e^{\frac{2x}{\sqrt{\alpha}\,c}} \right). \end{aligned} \tag{3.44}$$

*Doubly clamped beam under uniformly distributed loading.* Let us consider a doubly clamped beam of length $L$ and uniform bending stiffness $k_f$ under uniformly distributed loading $q$.

The bending interaction field $M$ obtained by the differential equilibrium equation $\partial_x^2 M = q$ is a function of two integration constants, $a_1$ and $a_2$. Hence, Eq.(4.3) in terms of displacement field $v$ becomes

$$\frac{qx^2}{2} + a_1 x + a_2 - c^2 q = k_f \partial_x^2 v - \alpha\, c^2\, k_f \partial_x^4 v\,, \tag{3.45}$$

supplemented with constitutive and kinematic boundary conditions

$$\begin{cases} c\,a_1 - a_2 = \alpha k_f \left( c\,\partial_x^3 v(0) - \partial_x^2 v(0) \right), \\ c\,(qL + a_1) + \dfrac{qL^2}{2} + a_1 L + a_2 = \alpha k_f \left( c\,\partial_x^3 v(L) + \partial_x^2 v(L) \right), \\ v(0) = 0\,, \\ \partial_x v(0) = 0\,, \\ v(L) = 0\,, \\ \partial_x v(L) = 0\,. \end{cases} \tag{3.46}$$

By solving the differential problem in Eqs.(3.45)-(3.46) the nonlocal displacement field is given by

$$v(x) = \frac{q\,x^2\,(L-x)^2}{24k_f} + \frac{c\,(\alpha-1)\,q}{12\,\psi_4\,k_f}(12\,c^2 + 6c\,L + L^2)\,e^{-\frac{x}{\sqrt{\alpha}c}}(\sqrt{\alpha}\,c\,L\,e^{\frac{L}{\sqrt{\alpha}c}} - e^{\frac{L+x}{\sqrt{\alpha}c}}(\sqrt{\alpha}\,cL - Lx + x^2) + e^{\frac{x}{\sqrt{\alpha}c}}(-\sqrt{\alpha}\,cL - Lx + x^2) + \sqrt{\alpha}\,c\,L\,e^{\frac{2x}{\sqrt{\alpha}c}})\,, \tag{3.47}$$

with

$$\psi_4 = L\,(-\sqrt{\alpha} - (\sqrt{\alpha}+1)\,e^{\frac{L}{\sqrt{\alpha}c}} + 1) + 2\,(\alpha-1)\,c\,(e^{\frac{L}{\sqrt{\alpha}c}} - 1)\,. \tag{3.48}$$

### 3.4.2 Inconsistency of limiting solutions

As enlightened in detail, no solution can be found to Eq.(3.24) for a vanishing mixture parameter. Indeed, for any value $c > 0$, constitutive boundary conditions in Eq.(3.33) can be satisfied by equilibrated bending moments only for a strictly positive mixture parameter $\alpha$. Hence, inconsistencies of two-phase solutions are expected to occur as $\alpha \to 0$.

In the following, analytical limiting responses of case-studies in Section 3.4.1 are provided. Non-dimensional variables are adopted in parametric plots by introducing the non-dimensional abscissa $\xi = x/L$, the nonlocal parameter $\lambda = c/L$ and the following non-dimensional limiting displacement fields

$$\bar{v_l} = v_l \frac{k_f}{FL^3} \quad or \quad \bar{v_l} = v_l \frac{k_f}{\mathcal{M}L^2} \quad or \quad \bar{v_l} = v_l \frac{k_f}{qL^4}\,. \tag{3.49}$$

*Cantilever under concentrated couple at free end.* Computing the limit as $\alpha \to 0$ of Eq.(3.36), we get the following limiting displacement field

$$v_l(x) = \frac{\mathcal{M}}{k_f}\left(\frac{x^2}{2} + c\,x\right). \tag{3.50}$$

The displacement field in Eq.(3.50) is clearly in contrast with essential boundary conditions prescribed by constraints. Indeed, except for the local case $\lambda = 0^+$, kinematic inconsistency is apparent in parametric plots of displacement (Fig.3.7) and rotation fields (Fig.3.8) obtained from derivation of Eq.(3.50).

Double derivation of Eq.(3.50) leads to the limiting elastic bending curvature $\chi_l$ that inserted into the integral convolution in Eq.(3.24), with $\alpha = 0$,

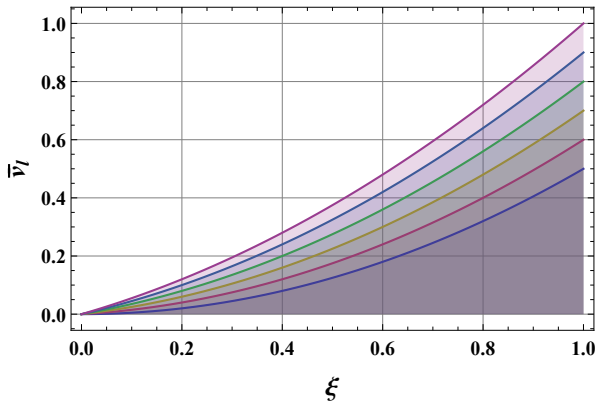


Figure 3.7: Cantilever under concentrated couple at free end: displacement $\bar{v}_l$ versus $\xi$ for $\lambda \in \{0^+, 0.1, 0.2, 0.3, 0.4, 0.5\}$.

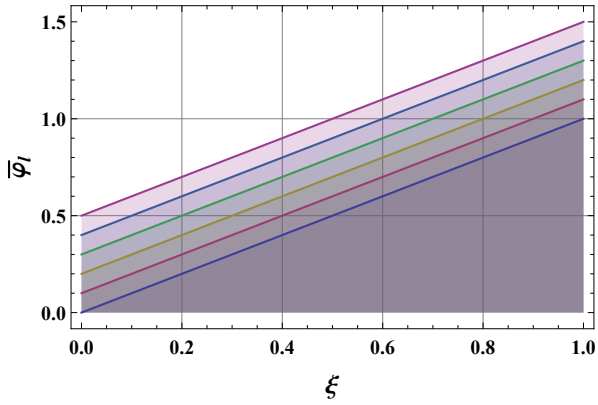


Figure 3.8: Cantilever under concentrated couple at free end: rotation $\bar{\varphi}_l$ versus $\xi$ for $\lambda \in \{0^+, 0.1, 0.2, 0.3, 0.4, 0.5\}$.

should provide the equilibrated bending interaction field. Moreover, since the redundancy degree is zero, equilibrated bending interaction is the uniform field univocally determined by equilibrium conditions. As clearly shown by parametric plots in Fig.3.9, the limiting elastic nonlocal curvature $\chi_l$ provides a bending moment which is not equilibrated; indeed, it is not uniform and not equal to

the applied couple, except for the asymptotic local bending moment which is equilibrated for $\xi \in ]0,1[$. A further derivation leads to shear force field which is not vanishing (see Fig.3.10), except for $\lambda = 0^+$ with $\xi \in ]0,1[$.

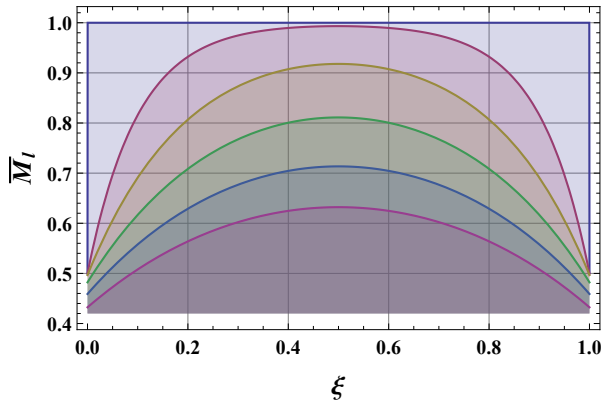


Figure 3.9: Cantilever under concentrated couple at free end: bending moment $\bar{M}_l$ versus $\xi$ for $\lambda \in \{0^+, 0.1, 0.2, 0.3, 0.4, 0.5\}$.

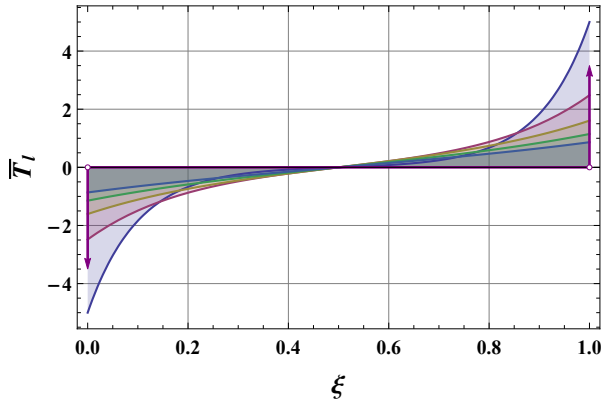


Figure 3.10: Cantilever under concentrated couple at free end: shear force $\bar{T}_l$ versus $\xi$ for $\lambda \in \{0^+, 0.1, 0.2, 0.3, 0.4, 0.5\}$.

*Cantilever under concentrated force at free end.* Computing the limit as

$\alpha \to 0$ of Eq.(5.3), we get the following limiting displacement field

$$v_l(x) = \frac{\mathcal{F}}{k_f}\left(L\,\frac{x^2}{2} - \frac{x^3}{6} + c^2\,x + L\,c\,x\right). \tag{3.51}$$

Kinematic inconsistencies are clearly shown in parametric plots of displacement and rotation fields as a function of $c$, except for the local case $\lambda = 0^+$ (see Figs.3.11-3.12). Double derivation of Eq.(3.51) leads to the limiting bending curvature that inserted into the integral convolution in Eq.(3.24), for $\alpha = 0$, provides a bending moment field which is not compatible with differential and boundary equilibrium requirements.

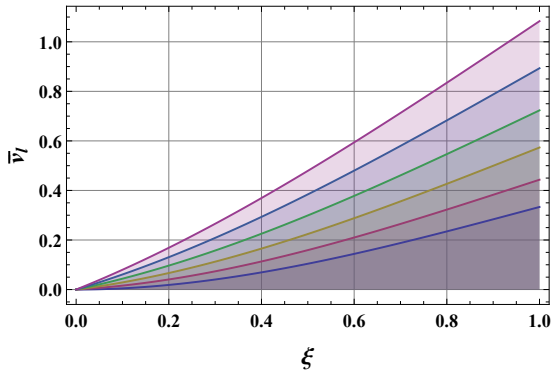


Figure 3.11: Cantilever under concentrated force at free end: displacement $\bar{v}_l$ versus $\xi$ for $\lambda \in \{0^+, 0.1, 0.2, 0.3, 0.4, 0.5\}$.

Indeed, since the redundancy degree is zero, the equilibrated bending moment is the linear field univocally determined by equilibrium conditions. Instead, as clearly shown by parametric plots in Fig.3.13, the limiting nonlocal elastic bending curvature $\chi_l$ provides a bending moment which is not equilibrated since it is not linear and does not vanish at free end of the cantilever, except for the asymptotic local bending interaction field which is equilibrated for $\xi \in ]0, 1]$. A further derivation leads to the shear force field which is not equal to the value of the applied force (see Fig.3.14) and hence, it is not uniform (except for $\lambda = 0^+$ with $\xi \in ]0, 1[$), i.e.: the emerging distributed loading is not vanishing.

*Simply supported beam under uniformly distributed loading.* Computing the

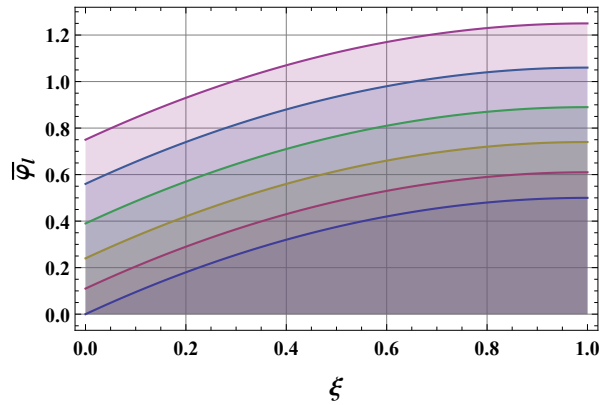


Figure 3.12: Cantilever under concentrated force at free end: rotation $\bar{\varphi}_l$ versus $\xi$ for $\lambda \in \{0^+, 0.1, 0.2, 0.3, 0.4, 0.5\}$.

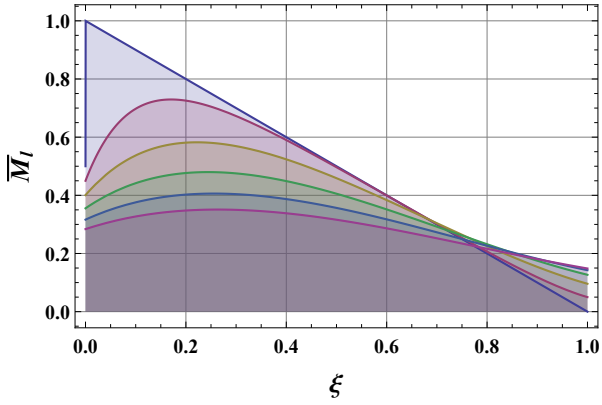


Figure 3.13: Cantilever under concentrated force at free end: bending moment $\bar{M}_l$ versus $\xi$ for $\lambda \in \{0^+, 0.1, 0.2, 0.3, 0.4, 0.5\}$.

limit as $\alpha \to 0$ of Eq.(3.44), we get the following limiting displacement

$$v_l(x) = \frac{q}{k_f}\left(\frac{x^4}{24} - \frac{Lx^3}{12} - \frac{c^2x^2}{2} + \frac{L^3x}{24}(12\lambda^2 + 1)\right). \tag{3.52}$$

Parametric plots of displacement and rotation fields as functions of $\lambda$ are

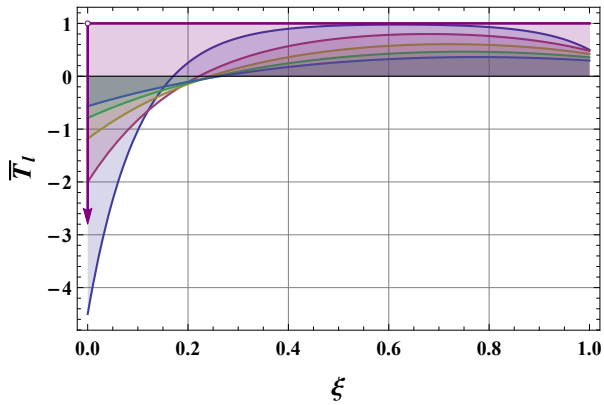


Figure 3.14: Cantilever under concentrated force at free end: shear force $\bar{T}_l$ versus $\xi$ for $\lambda \in \{0^+, 0.1, 0.2, 0.3, 0.4, 0.5\}$.

shown in Figs.3.15-3.16. Double derivation of Eq.(3.52) leads to the limiting nonlocal bending curvature that inserted into the integral convolution in Eq.(3.24) (for $\alpha = 0$) provides the static fields shown in Figs.3.17-3.18. The bending moment field is clearly incompatible with natural boundary conditions and the shear force field is not linear, i.e.: the emerging distributed loading is not uniform (see Fig.3.19). Hence, the interaction fields for $\lambda > 0$ are not compatible with differential and boundary equilibrium requirements.

*Doubly clamped beam under uniformly distributed loading.* The limiting displacement field as $\alpha \to 0$ of Eq.(5.5) is given by

$$v_l(x) = \frac{q}{k_f}\left(\frac{x^4}{24} - \frac{Lx^3}{12} - \frac{c^2x^2}{2} + \frac{c\left(12\lambda^2+6\lambda+1\right)L^2x}{12(2\lambda+1)} + \frac{L^2x^2}{24(2\lambda+1)}\right). \tag{3.53}$$

The displacement field in Eq.(3.53) is in contrast with essential boundary conditions prescribed by constraints. These kinematic inconsistencies are clearly shown in parametric plots of displacement and rotation fields (see Figs.3.20-3.21). Double derivation of Eq.(3.51) leads to the limiting nonlocal elastic curvature that is used to compute the integral convolution in Eq.(3.24), for $\alpha = 0$, to get the bending interaction field depicted in Fig.3.22. A further derivation leads to shear force field which is not linear (see Fig.3.23) and the emerging distributed loading is not uniform and not equal to the applied one (see Fig.3.24).

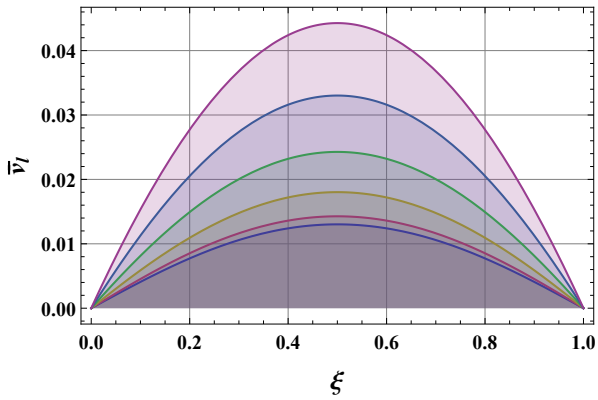


Figure 3.15: Simply supported beam under uniformly distributed loading: displacement $\bar{v}_l$ versus $\xi$ for $\lambda \in \{0^+, 0.1, 0.2, 0.3, 0.4, 0.5\}$.

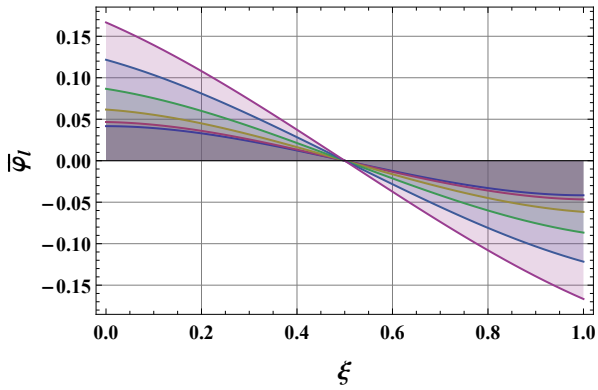


Figure 3.16: Simply supported beam under uniformly distributed loading: rotation $\bar{\varphi}_l$ versus $\xi$ for $\lambda \in \{0^+, 0.1, 0.2, 0.3, 0.4, 0.5\}$.

Hence, limiting solutions of the elastostatic problem do not satisfy kinematic compatibility and equilibrium requirements, except for the asymptotic local displacement and rotation fields $\forall \xi \in [0, 1]$ and for the asymptotic local bending and shearing interaction fields for $\xi \in ]0, 1[$.

Thus, it has been proven that the asymptotic solution fields of Eringen's two-phase structural problems are in contrast with kinematic boundary conditions

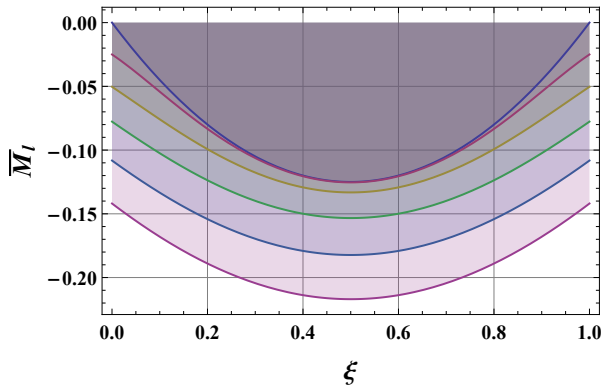


Figure 3.17: Simply supported beam under uniformly distributed loading: bending moment $\bar{M}_l$ versus $\xi$ for $\lambda \in \{0^+, 0.1, 0.2, 0.3, 0.4, 0.5\}$.

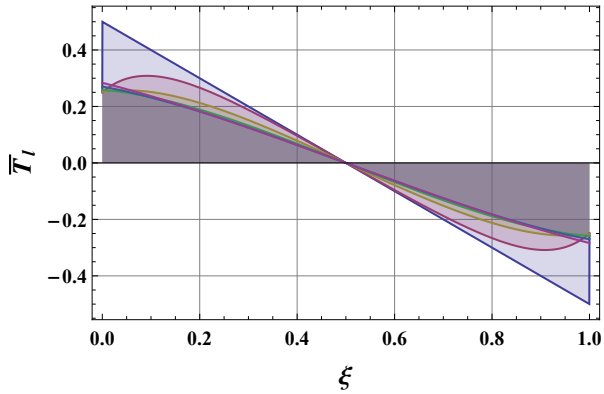


Figure 3.18: Simply supported beam under uniformly distributed loading: shear force $\bar{T}_l$ versus $\xi$ for $\lambda \in \{0^+, 0.1, 0.2, 0.3, 0.4, 0.5\}$.

and equilibrium requirements for any value of $\lambda$.

Accordingly, these limiting responses cannot be used as solutions of ill-posed purely nonlocal strain-driven structural problems.

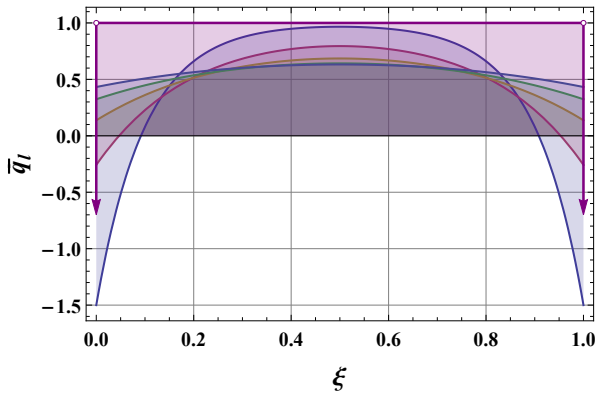


Figure 3.19: Simply supported beam under uniformly distributed loading: emerging loading $\bar{q}_l$ versus $\xi$ for $\lambda \in \{0^+, 0.1, 0.2, 0.3, 0.4, 0.5\}$.

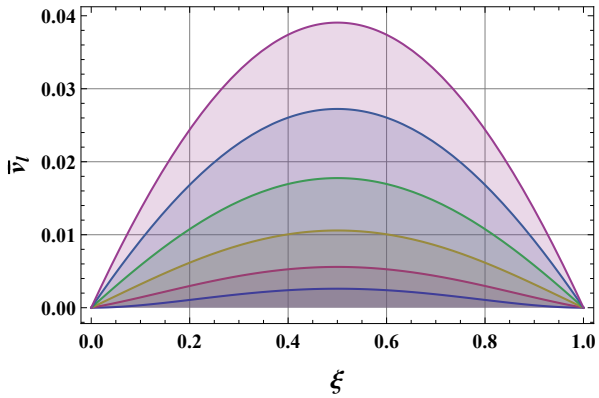


Figure 3.20: Doubly clamped beam under uniformly distributed loading: displacement $\bar{v}_l$ versus $\xi$ for $\lambda \in \{0^+, 0.1, 0.2, 0.3, 0.4, 0.5\}$.

## 3.5 Stress-driven two-phase elasticity

All issues discussed in Section 3.4 concerning the strain-driven two-phase elasticity can be completely overcome if a mixture local/nonlocal stress-driven theory is formulated. This two-phase model represents an extension of the purely nonlocal stress-driven elasticity and provides well-posed nonlocal continuum problems

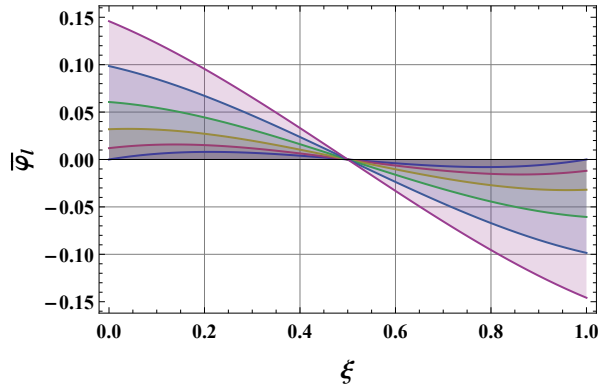


Figure 3.21: Doubly clamped beam under uniformly distributed loading: rotation $\bar{\varphi}_l$ versus $\xi$ for $\lambda \in \{0^+, 0.1, 0.2, 0.3, 0.4, 0.5\}$.

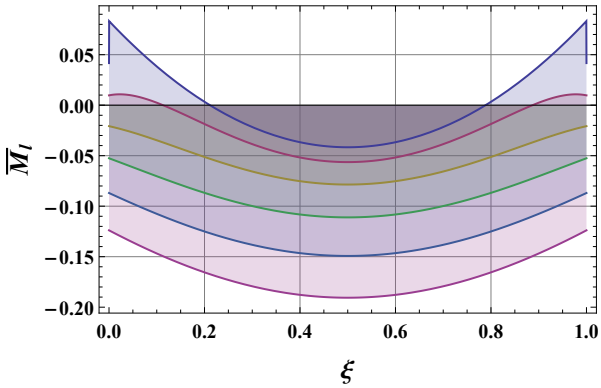


Figure 3.22: Doubly clamped beam under uniformly distributed loading: bending moment $\bar{M}_l$ versus $\xi$ for $\lambda \in \{0^+, 0.1, 0.2, 0.3, 0.4, 0.5\}$.

for any mixture parameter.

According to the stress-driven two-phase elasticity [65] with reference to a Bernoulli-Euler beam, the elastic curvature $\chi^{el}$ is the convex combination, by means of the mixture parameter $\alpha$, of the source field $s := k_f^{-1} M$ and of the

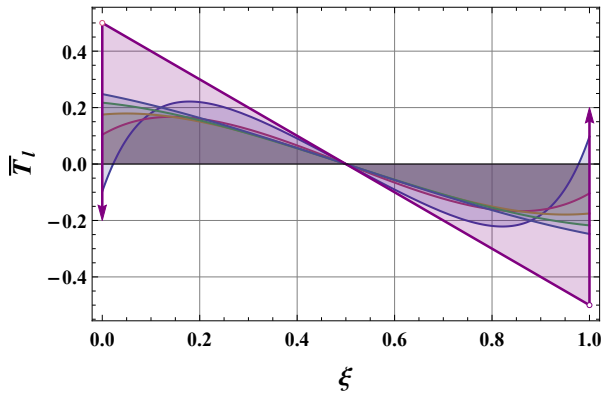


Figure 3.23: Doubly clamped beam under uniformly distributed loading: shear force $\bar{T}_l$ versus $\xi$ for $\lambda \in \{0^+, 0.1, 0.2, 0.3, 0.4, 0.5\}$.

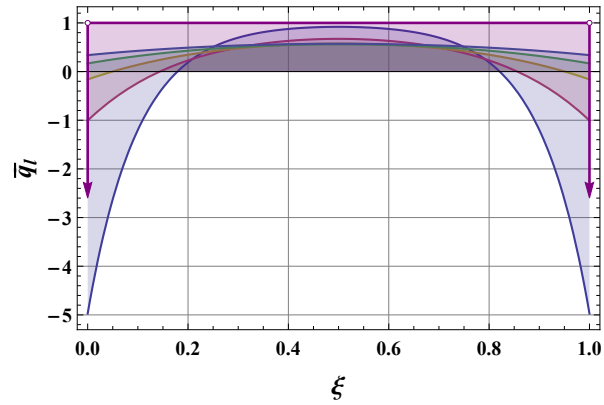


Figure 3.24: Doubly clamped beam under uniformly distributed loading: emerging loading $\bar{q}_l$ versus $\xi$ for $\lambda \in \{0^+, 0.1, 0.2, 0.3, 0.4, 0.5\}$.

convolution between the source $s$ and the averaging kernel $\phi_\lambda$, that is

$$\chi^{el}(x) = \alpha\,(k_f^{-1}\,M)(x) + (1-\alpha)\int_0^L \phi_\lambda(x-\xi)\,(k_f^{-1}\,M)(\xi)\,d\xi\,, \tag{3.54}$$

where $0 \le \alpha \le 1$ and $\lambda > 0$ is the nonlocal parameter.

Purely nonlocal stress-driven elasticity is recovered for a vanishing mixture parameter, that is $\chi^{el}(x) = \int_0^L \phi_\lambda(x-\xi)\,(k_f^{-1}M)(\xi)\,d\xi$. While by setting $\alpha = 1$ the purely local elastic law $\chi^{el} = k_f^{-1}\,M$ is recovered.

Thanks to the choice of the special kernel $\phi_\lambda$ as averaging function of the integral convolution in Eq.(3.54), the equivalent differential formulation can be derived, as expressed by the following mixture equivalence.

**Proposition 3.5.1** *The convex combination in* (3.54)*, for* $0 \le \alpha \le 1$ *and* $\lambda > 0$*, is equivalent to the differential equation*

$$\frac{\chi^{el}(x)}{c^2} - \partial_x^2\chi^{el}(x) = \frac{(k_f^{-1}\,M)(x)}{c^2} - \alpha\,\partial_x^2(k_f^{-1}\,M)(x) \tag{3.55}$$

*equipped with constitutive boundary conditions*

$$\begin{cases} \partial_x\chi^{el}(0) - \dfrac{1}{c}\,\chi^{el}(0) = \alpha\left(\partial_x(k_f^{-1}\,M)(0) - \dfrac{(k_f^{-1}\,M)(0)}{c}\right), \\ \partial_x\chi^{el}(L) + \dfrac{1}{c}\,\chi^{el}(L) = \alpha\left(\partial_x(k_f^{-1}\,M)(L) + \dfrac{(k_f^{-1}\,M)(L)}{c}\right). \end{cases} \tag{3.56}$$

Unlike the two-phase strain-driven elasticity, mixture stress-driven formulation is well-posed for any mixture parameter $\alpha$.

Moreover, being described by two parameters, the mixture elastic law has been proven to be able to simulate both softening and stiffening structural behaviors and thus is advantageously apply to model and design size-dependent nonlocal behaviours of a wide class of small-scale technological devices.

In the following, elastostatic problems of slender beams based on the purely stress-driven model illustrated in 3.3.1 are now solved adopting the mixture stress-driven elasticity. A parametric study is performed to analyse structural responses as function of nonlocal and mixture parameters.

Denoting by $v_{loc}$ the corresponding local solution, non-dimensional maximum displacement $\bar{v}_{max} := v_{max}/v_{loc}$ is depicted in Fig.3.25 for a simply supported beam under uniformly distributed loading. For a fixed nonlocal parameter, a softening behavior can be observed for increasing mixture parameter. On the contrary, for a fixed mixture parameter, the response stiffens for increasing nonlocal parameter. Similar trends can be observed for structural responses in Figs.3.26-3.27.

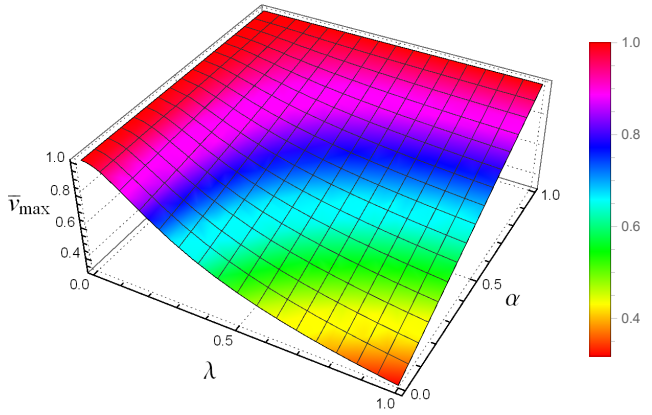


Figure 3.25: Simply supported beam under uniformly distributed loading: non-dimensional maximum displacement $\bar{v}_{max}$ versus nonlocal parameter $\lambda$ and mixture parameter $\alpha$.

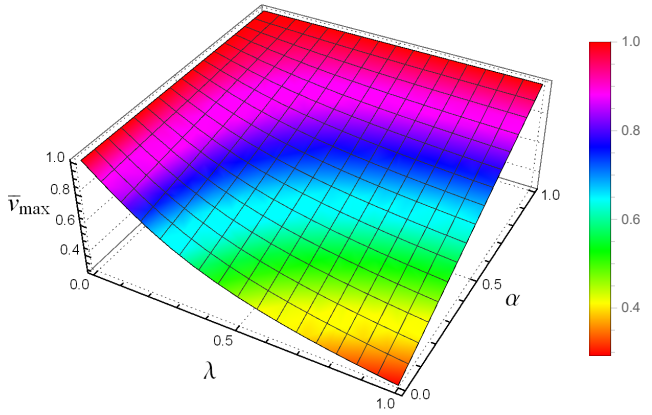


Figure 3.26: Cantilever under concentrated force: non-dimensional maximum displacement $\bar{v}_{max}$ versus nonlocal parameter $\lambda$ and mixture parameter $\alpha$.

### 3.5.1 Structural problems

Potentialities of the stress-driven two-phase elasticity theory are here investigated with reference to an applicative case-study. For the sake of generality, a

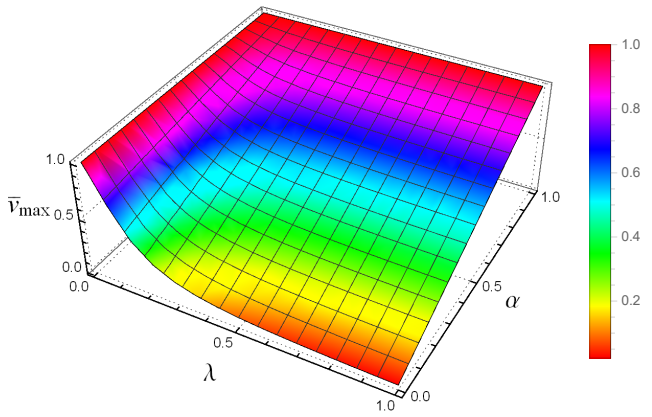


Figure 3.27: Doubly clamped beam under uniformly distributed loading: non-dimensional maximum displacement $\bar{v}_{max}$ versus nonlocal parameter $\lambda$ and mixture parameter $\alpha$.

curved Timoshenko beam is considered so that the elastostatic problems that will be discussed in Sections 5 and 6 can be derived as particular cases.

Let us consider a Timoshenko curved beam of length $L$ whose axis is a regular planar curve $\mathbf{\Gamma}$ parameterized by the curvilinear abscissa $s \in [0, L]$. A coordinate-free intrinsic formulation is adopted introducing the tangent unit vectors field, defined as follows

$$\mathbf{t} := \partial_s \mathbf{\Gamma} \,. \tag{3.57}$$

By applying the orthogonal linear transformation $\mathbf{R}$ (performing the rotation by $\pi/2$ counterclockwise in the plane) the transversal unit vectors field is obtained as $\mathbf{t}_\perp := \mathbf{R}\mathbf{t}$. Finally, we define the uniform unit vectors field $\mathbf{k} := \mathbf{t} \times \mathbf{t}_\perp$. According to Timoshenko theory of thick beams, cross-sections are hinged to the beam axis. Thus, kinematics is described by the following independent parameters: the velocity $\mathbf{v} : [0, L] \to V$ of the beam axis and the angular velocity of cross-sections $\varphi : [0, L] \to \Re$, being $V$ the linear space of translations.

The tangent deformation field kinematically compatible with $\{\mathbf{v}, \omega\}$ is de-

fined as

$$\begin{vmatrix} \varepsilon \\ \gamma \\ \chi \end{vmatrix} = \begin{vmatrix} \partial_s \mathbf{v} \cdot \mathbf{t} \\ \partial_s \mathbf{v} \cdot \mathbf{t}_\perp - \varphi \\ \partial_s \varphi \end{vmatrix} \tag{3.58}$$

where $\{\varepsilon, \gamma, \chi\} : [0, L] \mapsto \Re$ are the axial strain, shear strain and flexural curvature scalar fields, respectively. By duality with the tangent deformation field, the stress in a Timoshenko beam is composed of axial force, shear force and bending moment scalar fields, that is $\{N, T, M\} : [0, L] \mapsto \Re$, satisfying the following differential equations of equilibrium, that is

$$\begin{cases} \partial_s N - T\, \mathbf{t}_\perp \cdot \partial_s \mathbf{t} = -\mathbf{p} \cdot \mathbf{t}\,, \\ \partial_s T - N\, \mathbf{t} \cdot \partial_s \mathbf{t}_\perp = -\mathbf{p} \cdot \mathbf{t}_\perp\,, \\ T + \partial_s M = -m\,, \end{cases} \tag{3.59}$$

equipped with boundary conditions at $\partial\mathbf{\Gamma}$

$$\begin{cases} -(N\mathbf{t} + T\mathbf{t}_\perp)(0) \cdot \delta\mathbf{v}(0) = \mathbf{F}_0 \cdot \delta\mathbf{v}(0)\,, \\ (N\mathbf{t} + T\mathbf{t}_\perp)(L) \cdot \delta\mathbf{v}(L) = \mathbf{F}_L \cdot \delta\mathbf{v}(L)\,, \\ -M(0)\ \delta\omega(0) = \mathcal{M}_0\ \delta\omega(0)\,, \\ M(L)\ \delta\omega(L) = \mathcal{M}_L\ \delta\omega(L)\,, \end{cases} \tag{3.60}$$

where $\{\delta\mathbf{v},\ \delta\omega\}$ represent any virtual translation velocity and angular velocity fulfilling homogeneous kinematic boundary conditions. The external force system in Eqs.(3.59)-(3.60) is composed of a distributed vector loading $\mathbf{p} : [0, L] \to V$, distributed bending couples $m : [0, L] \to \Re$, boundary concentrated forces $\mathbf{F}_0 \in V$ and $\mathbf{F}_L \in V$ and boundary concentrated bending couples $\mathcal{M}_0 \in \Re$ and $\mathcal{M}_L \in \Re$. It is worth noting that in the framework of linearised Timoshenko beam theory, $\{\mathbf{v}, \varphi\}$ will denote displacement and rotation fields, respectively.

Now let us denote by $E$ and $G$, the Euler-Young and shear moduli, respectively, by $A$ the cross-sectional area and by $J_r$ the moment of inertia along the bending axis $\eta$ identified by transversal unit vector $\mathbf{t}_\perp$, that is:

$$J_r = \int_\Omega \eta^2 \frac{r}{r - \eta\,(\mathbf{n} \cdot \mathbf{t}_\perp)}\, dA\,, \tag{3.61}$$

where $r$ is the curvature radius and the vector $\mathbf{n}$ is related to $\mathbf{t}_\perp$ by the relation $\mathbf{n} = (\mathbf{t}_\perp \cdot \mathbf{n})\, \mathbf{t}_\perp$ provided in [80]. Local elastic constitutive equations of curved

planar beams are expressed as follows

$$\begin{cases} \varepsilon_l^{el}(s) = \dfrac{1}{EA}\left[N + \dfrac{M}{r\,\mathbf{n}\cdot\mathbf{t}_\perp}\right](s)\,, \\ \chi_l^{el}(s) = \dfrac{M}{EJ_r}(s) + (\mathbf{n}\cdot\mathbf{t}_\perp)\dfrac{1}{r\,EA}\left[N + \dfrac{M}{r\,\mathbf{n}\cdot\mathbf{t}_\perp}\right](s)\,, \\ \gamma_l^{el}(s) = \left[\dfrac{T}{GK_r}\right](s)\,, \end{cases} \tag{3.62}$$

where vanishing distributed bending couples have been assumed. In Eq. $(3.62)_3$, $K_r$ is the shear stiffness for curved beams defined as follows

$$K_r^{-1} := \int_\Omega \frac{r^2}{\left[r - \eta(\mathbf{n}\cdot\mathbf{t}_\perp)\right]^2 b^2}\left[\frac{S_r}{J_r} - \frac{A^*}{(\mathbf{n}\cdot\mathbf{t}_\perp)rA}\right]^2 dA\,, \tag{3.63}$$

where $S_r$ is the static moment of $A^*$, that is

$$S_r := \int_{\Omega^*} \frac{r\,\eta}{r - \eta\,(\mathbf{n}\cdot\mathbf{t}_\perp)}\,dA^*\,. \tag{3.64}$$

In order to apply the local/nonlocal stress-driven theory of elasticity, let us introduce the vectors $\mathbf{i}$ and $\mathbf{f}$ respectively collecting source and output fields, i.e.: $\mathbf{i} = \{\varepsilon_l^{el}, \chi_l^{el}, \gamma_l^{el}\}$; $\mathbf{f} = \{\varepsilon^{el}, \chi^{el}, \gamma^{el}\}$. Then, the stress-driven mixture law of elasticity as formulated in Section 3.5 is expressed as follows

$$\mathbf{f}(s) = \alpha\,\mathbf{i}(s) + (1-\alpha)\int_0^L \phi_\lambda(s-\xi)\,\mathbf{i}(\xi)\,d\xi\,. \tag{3.65}$$

By extending to Timoshenko curved beams the *Mixture equivalence* provided in Section 3.5 the integral convolutions in Eq. (3.65) is equivalent to the following differential equation

$$\frac{\mathbf{f}(s)}{c^2} - \partial_s^2\mathbf{f}(s) = \frac{\mathbf{i}(s)}{c^2} - \alpha\,\partial_s^2\mathbf{i}(s) \tag{3.66}$$

equipped with the constitutive boundary conditions

$$\begin{cases} \partial_s\mathbf{f}(0) = \dfrac{1}{c}\,\mathbf{f}(0) + \alpha\left(\partial_s\mathbf{i}(0) - \dfrac{\mathbf{i}(0)}{c}\right), \\ \partial_s\mathbf{f}(L) = -\dfrac{1}{c}\,\mathbf{f}(L) + \alpha\left(\partial_s\mathbf{i}(L) + \dfrac{s(L)}{c}\right). \end{cases} \tag{3.67}$$

Nonlocal elastic equilibrium problems based on the formulation illustrated above are solved for thick silicon carbide nanobeams. A Cartesian coordinate system $(x, y)$ is also introduced. Euler-Young modulus and Poisson ratio are $E = 427$ [GPa] and $\nu = 0.2$. The beam axis is assumed to be a circle arc of radius $r = 10$ [nm] so that the beam length is $L = r\,\pi/2$. Base and height of the rectangular cross-section are $b = 5$ [nm] and $h = 2L/3$.

Tables 3.1-3.3 collect numerical results of transverse displacements $v_{t_\perp} := \mathbf{v} \cdot \mathbf{t}_\perp$, axial displacements $v_t := \mathbf{v} \cdot \mathbf{t}$ and bending rotations $\varphi$ of the following case-studies: cantilever beam under point-force $F = 10\,[nN]$ at free end; slider and roller supported beam under uniformly distributed loading $q = 2\,[nN/nm]$ (along $x$-direction) and directed upwards; clamped and roller supported beam under uniformly distributed loading $q = 5\,[nN/nm]$ (along $x$-direction) and directed upwards.

| $\lambda$ | $v_\perp(L)\,[10^{-2}nm]$ | | $v_t(L)\,[10^{-2}nm]$ | | $\varphi(L)\,[10^{-3}]$ | | $v^{tot}_{max}(L)\,[10^{-2}nm]$ | |
|---|---|---|---|---|---|---|---|---|
| | $\alpha = 0.3$ | $\alpha = 0.6$ | $\alpha = 0.3$ | $\alpha = 0.6$ | $\alpha = 0.3$ | $\alpha = 0.6$ | $\alpha = 0.3$ | $\alpha = 0.6$ |
| 0.1 | 4.131 | 4.289 | -2.633 | -2.732 | 3.808 | 3.916 | 4.899 | 5.085 |
| 0.2 | 3.744 | 4.068 | -2.406 | -2.602 | 3.528 | 3.756 | 4.450 | 4.829 |
| 0.3 | 3.414 | 3.879 | -2.209 | -2.490 | 3.264 | 3.605 | 4.066 | 4.609 |
| 0.4 | 3.149 | 3.728 | -2.048 | -2.398 | 3.037 | 3.475 | 3.756 | 4.432 |
| 0.5 | 2.939 | 3.608 | -1.916 | -2.323 | 2.847 | 3.367 | 3.509 | 4.291 |
| 0.6 | 2.770 | 3.511 | -1.809 | -2.261 | 2.690 | 3.277 | 3.308 | 4.176 |
| 0.7 | 2.632 | 3.432 | -1.721 | -2.211 | 2.558 | 3.202 | 3.145 | 4.083 |
| 0.8 | 2.518 | 3.367 | -1.647 | -2.169 | 2.447 | 3.138 | 3.008 | 4.005 |
| 0.9 | 2.422 | 3.312 | -1.584 | -2.133 | 2.352 | 3.084 | 2.894 | 3.939 |

Table 3.1: Cantilever thick nanobeam: numerical outcomes.

It is important to remark that for statically indeterminate beams, static interaction fields are function of the scale parameters governing the two-phase elasticity model. Thus, for the third case-study (i.e. clamped and roller supported beam), static fields of axial force $\mathbf{R}N\mathbf{t} = N\mathbf{t}_\perp$, shear force $T\mathbf{t}_\perp$ and bending moment $\mathbf{R}M\mathbf{k} = -M\mathbf{t}_\perp$, parameterized in terms of the arch length $s$, are graphically represented in Figs.3.28-3.30 for a fixed pair $\{\lambda, \alpha\}$.

From the collected results, it is apparent that stiffening or softening structural responses can be obtained for increasing nonlocal parameter $\lambda$ or mixture parameter $\alpha$, respectively.

Thus, the new methodology recently provided in [66] and here briefly discussed, extending the stress-driven mixture formulation to curved thick beams can be efficiently applied for design and optimization of a wide class of new-

| $\lambda$ | $v_\perp(0)$ $[10^{-2}nm]$ | | $v_\perp(L)$ $[10^{-2}nm]$ | | $\varphi(L)$ $[10^{-3}]$ | | $v^{tot}_{max}(0)$ $[10^{-2}nm]$ | |
|---|---|---|---|---|---|---|---|---|
| | $\alpha = 0.3$ | $\alpha = 0.6$ | $\alpha = 0.3$ | $\alpha = 0.6$ | $\alpha = 0.3$ | $\alpha = 0.6$ | $\alpha = 0.3$ | $\alpha = 0.6$ |
| 0.1 | 3.665 | 3.809 | -3.527 | -3.652 | -3.945 | -4.073 | 3.665 | 3.809 |
| 0.2 | 3.321 | 3.613 | -3.196 | -3.463 | -3.652 | -3.905 | 3.321 | 3.613 |
| 0.3 | 3.030 | 3.447 | -2.911 | -3.300 | -3.383 | -3.751 | 3.030 | 3.447 |
| 0.4 | 2.798 | 3.314 | -2.683 | -3.170 | -3.152 | -3.619 | 2.798 | 3.314 |
| 0.5 | 2.613 | 3.208 | -2.502 | -3.067 | -2.959 | -3.509 | 2.613 | 3.208 |
| 0.6 | 2.464 | 3.123 | -2.357 | -2.984 | -2.797 | -3.417 | 2.464 | 3.123 |
| 0.7 | 2.342 | 3.054 | -2.239 | -2.916 | -2.662 | -3.339 | 2.342 | 3.054 |
| 0.8 | 2.241 | 2.996 | -2.141 | -2.860 | -2.547 | -3.274 | 2.241 | 2.996 |
| 0.9 | 2.156 | 2.947 | -2.058 | -2.813 | -2.450 | -3.218 | 2.156 | 2.947 |

Table 3.2: Slider and roller supported thick nanobeam: numerical outcomes.

| $\lambda$ | $v_\perp(L)$ $[10^{-2}nm]$ | | $\varphi(L)$ $[10^{-3}]$ | | $v^{tot}_{max}(s^*)$ $[10^{-2}nm]$ | | $v^{tot}_{max}(s^*)$ $[10^{-2}nm]$ | |
|---|---|---|---|---|---|---|---|---|
| | $\alpha = 0.3$ | $\alpha = 0.6$ | $\alpha = 0.3$ | $\alpha = 0.6$ | $\alpha = 0.3$ | | $\alpha = 0.6$ | |
| 0.1 | -1.036 | -1.135 | -1.658 | -1.751 | 1.136 | $s^* = 5.892$ | 1.241 | $s^* = 5.738$ |
| 0.2 | -0.815 | -1.010 | -1.474 | -1.648 | 0.921 | $s^* = 6.041$ | 1.117 | $s^* = 5.788$ |
| 0.3 | -0.667 | -0.926 | -1.330 | -1.568 | 0.787 | $s^* = 6.063$ | 1.041 | $s^* = 5.774$ |
| 0.4 | -0.574 | -0.874 | -1.221 | -1.506 | 0.703 | $s^* = 6.042$ | 0.993 | $s^* = 5.750$ |
| 0.5 | -0.515 | -0.840 | -1.137 | -1.458 | 0.648 | $s^* = 6.009$ | 0.962 | $s^* = 5.727$ |
| 0.6 | -0.477 | -0.818 | -1.072 | -1.421 | 0.609 | $s^* = 5.974$ | 0.940 | $s^* = 5.707$ |
| 0.7 | -0.450 | -0.802 | -1.020 | -1.391 | 0.580 | $s^* = 5.940$ | 0.923 | $s^* = 5.691$ |
| 0.8 | -0.431 | -0.791 | -0.977 | -1.366 | 0.559 | $s^* = 5.910$ | 0.911 | $s^* = 5.678$ |
| 0.9 | -0.418 | -0.784 | -0.942 | -1.346 | 0.542 | $s^* = 5.884$ | 0.902 | $s^* = 5.667$ |

Table 3.3: Clamped and roller supported thick nanobeam: numerical outcomes.

generation smart devices based on curved nanobeams. Further details about the adopted solutions procedure, investigated case-studies and obtained results can be found in [66].

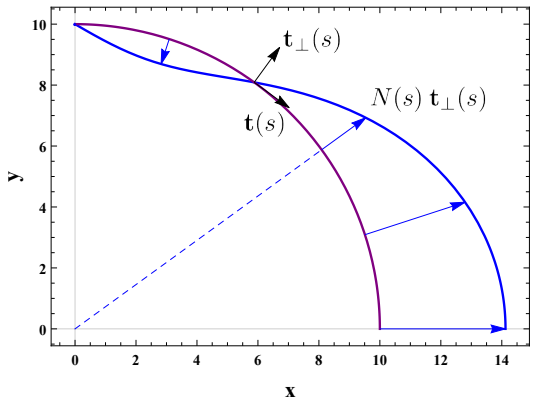


Figure 3.28: Clamped and roller supported beam: plot of the vector field $\mathbf{R}N\mathbf{t} = N\mathbf{t}_\perp$ $[5\,nN]$ in the Cartesian plane $x[nm], y[nm]$ for $\lambda = 0.5$ and $\alpha = 0.3$.

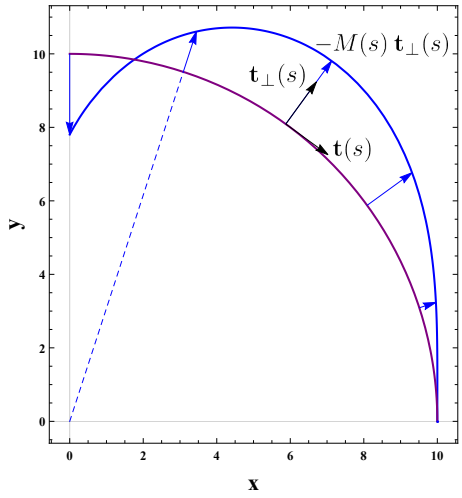


Figure 3.29: Clamped and roller supported beam: plot of the vector field $\mathbf{R}M\mathbf{k} = -M\mathbf{t}_\perp$ $[20\,nN\,nm]$ in the Cartesian plane $x[nm], y[nm]$ for $\lambda = 0.5$ and $\alpha = 0.3$.

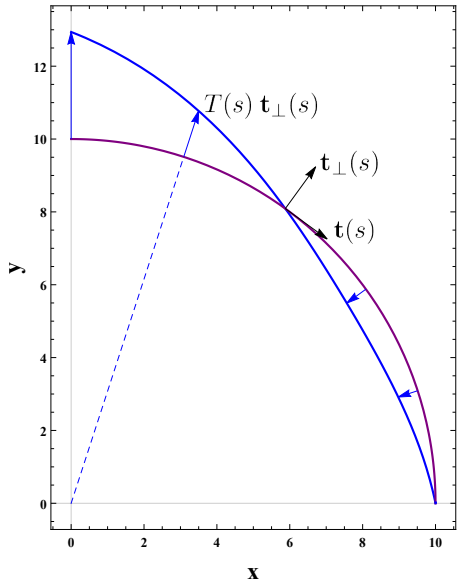


Figure 3.30: Clamped and roller supported beam: plot of the vector field $T\mathbf{t}_\perp$ $[10\,nN]$ in the Cartesian plane $x[nm], y[nm]$ for $\lambda = 0.5$ and $\alpha = 0.3$.

# Chapter 4

# Case-study: a nanocomposite actuator

## 4.1 Introduction

Small-scale electromechanical devices, such as switches, actuators and storage systems, are based on structural components designed to undergo large displacements in order to absolve their function. Thus, geometrically nonlinear analyses must be performed for modeling and optimization of micro- and nano-electromechanical systems. Moreover, smart and advanced small-scale devices are nowadays involving the use of nanofillers to enhance mechanical properties.

In light of this growing interest, nonlocal theories of elasticity illustrated in Chapter 2 are here exploited to assess effective elastic properties of nanofillers and to capture the size-dependent mechanical behavior of a CNTs reinforced microcantilever conceived as a basic component of a nanocomposite actuator [81]. During the working mechanism, the microbeam undergoes large displacements and thus an iterative solution procedure is conceived and put into operation to perform geometrically nonlinear analyses.

Here is the outline. In Section 4.2, a novel approach is proposed for the assessment of the effective Euler-Young modulus of nanofillers. Then, the rule of mixtures is applied to evaluate homogenized elastic properties of nanocomposites. In Section 4.3, the stress-driven nonlocal elasticity is exploited to model the size-dependent mechanical behavior of a nanocomposite inflected microbeam. Section 4.4 is devoted to the formulation of the elastostatic problem of a beam

undergoing large displacements. An iterative procedure is then conceived and put into operation with reference to a CNTs reinforced microcantilever. In Section 4.5, geometrically nonlinear parametric analyses are performed and numerical results are commented upon. Convergence of the adopted algorithm is finally discussed.

## 4.2 Elastic properties of nanofillers

Small-scale phenomena that significantly affect elastic properties of nanofillers can be conveniently modeled by adopting a continuum mechanics based approach. In particular, the two-phase local/nonlocal strain driven theory of elasticity is here applied in order to capture size effects on Euler-Young modulus of carbon nanotubes.

On this purpose, the CNT can be regarded as a nonlocal elastic rod of length $L_{cnt}$ and thus, according to the mixture model, the axial interaction field $N$ is expressed as the output of a convex combination of the local response $s := K_a \varepsilon^{el}$ and the convolution between the local response field $s$ and the scalar attenuation kernel $\phi_{c_{cnt}}$, that is

$$N(x) = \alpha\, K_a \varepsilon^{el}(x) + (1-\alpha) \int_0^{L_{cnt}} \phi_{c_{cnt}}(x-\xi)\, K_a \varepsilon^{el}(\xi)\, d\xi\,, \tag{4.1}$$

where $N$ and $\varepsilon^{el}$ denote the axial interaction and the elastic axial strain fields, respectively, and $K_a := E\,A$ denotes the elastic axial stiffness of the rod, being $E$ the local Euler-Young modulus and $A$ the cross-sectional area. In Eq.(4.1), $\alpha \in [0,1]$ is the mixture parameter and $\phi_{c_{cnt}}$ is a scalar averaging kernel described by a nonlocal characteristic length $c_{cnt} > 0$, as introduced in Section 3.4. The averaging kernel is assumed to be the Helmholtz's function as adopted in [36], i.e.:

$$\phi_{c_{cnt}}(x) = \frac{1}{2c_{cnt}} \exp\left(-\frac{|x|}{c_{cnt}}\right). \tag{4.2}$$

Thanks to the choice of the special kernel, the following equivalent constitutive problem can be formulated (see Section 3.4), made of the differential equation

$$\frac{N(x)}{c_{cnt}^2} - \partial_x^2 N(x) = K_a \left(\frac{\varepsilon^{el}(x)}{c_{cnt}^2} - \alpha\, \partial_x^2 \varepsilon^{el}(x)\right), \tag{4.3}$$

equipped with the constitutive boundary conditions

$$\begin{cases} \partial_x N(0) - \dfrac{1}{c_{cnt}} N(0) = K_a \alpha \left( \partial_x \varepsilon^{el}(0) - \dfrac{\varepsilon^{el}(0)}{c_{cnt}} \right), \\ \partial_x N(L_{cnt}) + \dfrac{1}{c_{cnt}} N(L_{cnt}) = K_a \alpha \left( \partial_x \varepsilon^{el}(L_{cnt}) + \dfrac{\varepsilon^{el}(L_{cnt})}{c_{cnt}} \right). \end{cases} \tag{4.4}$$

By solving the differential problem Eqs.(4.3)-(4.4) we get the constitutive relation

$$\varepsilon^{el}(x) = \frac{N}{E(x)A}, \tag{4.5}$$

where

$$\begin{aligned} E(x)^{-1} = e^{-\frac{x}{c_{cnt}\sqrt{\alpha}}} \left( (-e^{\frac{L_{cnt}}{c_{cnt}\sqrt{\alpha}}} - e^{\frac{2x}{c_{cnt}\sqrt{\alpha}}})(-1+\alpha) + e^{\frac{x}{c_{cnt}\sqrt{\alpha}}}(-\sqrt{\alpha}+\alpha) \right. \\ \left. + e^{\frac{L_{cnt}+x}{c_{cnt}\sqrt{\alpha}}}(\sqrt{\alpha}+\alpha) \right) / E(-1 + e^{\frac{L_{cnt}}{c_{cnt}\sqrt{\alpha}}}(1+\sqrt{\alpha}) + \sqrt{\alpha})\sqrt{\alpha}. \end{aligned} \tag{4.6}$$

Thus, the nonlocal elastic constitutive relation can be formulated as done in Eq.(4.5) leading to an axial elastic heterogeneity $E(x)$ affecting the rod. Therefore, Homogenization theory can be exploited to evaluate the effective Euler-Young modulus of carbon nanotubes $E_{cnt}$ according to the boundary schemes of Uniform Tractions (UT) and Uniform Displacements (UD) [82].

*Uniform tractions boundary condition (UT).* Traction forces $N$ are applied at the rod boundary as shown in Fig.4.1. The average of the elastic axial strain

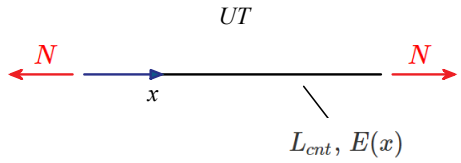


Figure 4.1: Uniform tractions ($UT$) boundary condition scheme.

in the domain $[0, L_{cnt}]$ is defined as follows

$$< \varepsilon > := \frac{\int_0^{L_{cnt}} \varepsilon^{el}(x)\, dx}{L_{cnt}}. \tag{4.7}$$

Then, let us introduce Eq.(4.5) in Eq.(4.7) to obtain the effective elastic compliance $(A\,E_{cnt})^{-1}$ as the ratio between the averages of elastic axial strain $<\varepsilon>$ and axial force $N$, that is

$$\frac{<\varepsilon>}{N} = \frac{1}{A}\frac{\int_0^{L_{cnt}} \frac{1}{E(x)}\,dx}{L_{cnt}} = \frac{1}{A\,E_{cnt}}\,. \tag{4.8}$$

Finally, from Eq.(4.8) the effective elastic modulus $E_{cnt}$ can be got as follows

$$E_{cnt} = \frac{E\,L_{cnt}(-1+e^{\frac{L_{cnt}}{c_{cnt}\sqrt{\alpha}}}(1+\sqrt{\alpha})+\sqrt{\alpha})}{L_{cnt}(-1+e^{\frac{L_{cnt}}{c_{cnt}\sqrt{\alpha}}}(1+\sqrt{\alpha})+\sqrt{\alpha})-2(-1+e^{\frac{L_{cnt}}{c_{cnt}\sqrt{\alpha}}})c_{cnt}(-1+\alpha)}\,. \tag{4.9}$$

It is worth noting that, as shown by Eq.(4.8), the effective elastic axial compliance is the average of the elastic compliance field $\big(E(x)A\big)^{-1}$ in the domain $[0, L_{cnt}]$. Moreover, it can be observed from Eq.(4.9) that the effective Euler-Young modulus $E_{cnt}$ is function of the length $L_{cnt}$ and of the local Euler-Young modulus $E$ of the carbon nanotube. Characteristic length $c_{cnt}$ and mixture parameter $\alpha$ in Eq.(4.9) have to be properly tuned to reproduce results provided by molecular dynamics simulation.

*Uniform displacements boundary condition (UD).* An axial displacement $u(L) = \varepsilon_0 L_{cnt}$ is prescribed to the rod end as shown in Fig.4.2. Since there are

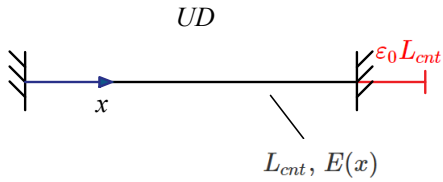


Figure 4.2: Uniform displacements $(UD)$ boundary condition scheme.

not inelastic axial strains, the average of the elastic axial strain in the domain $[0, L_{cnt}]$ writes as shown below

$$<\varepsilon> = \frac{\int_0^{L_{cnt}} u'(x)\,dx}{L_{cnt}} = \varepsilon_0\,. \tag{4.10}$$

Then, kinematic compatibility is expressed by the condition that the external virtual power is equal to the internal virtual power for a unit self-equilibrated

virtual axial interaction field, that is:

$$\int_0^{L_{cnt}} 1 \cdot \frac{N}{AE(x)}\, dx = 1 \cdot \varepsilon_0\, L_{cnt}\ . \tag{4.11}$$

Finally, from Eqs.(4.11) and (4.10) we get

$$\frac{N}{<\varepsilon>} = A \frac{L_{cnt}}{\displaystyle\int_0^{L_{cnt}} \frac{1}{E(x)}\, dx} = A\, E_{cnt} \tag{4.12}$$

showing that the effective elastic axial stiffness $A\,E_{cnt}$ in Eq.(4.12) is exactly the reverse of the effective elastic axial compliance in Eq.(4.8).

**Homogenized Euler-Young modulus of nanocomposites**

In this section, the homogenized Euler-Young modulus of a carbon nanotube reinforced matrix is provided. The rule of mixtures is applied, according to which the effective elastic modulus of nanocomposite is convex combination of Euler-Young moduli of carbon nanotubes $E_{cnt}$ (Eq.(4.9)) and matrix $E_{mat}$, id est

$$E_h = E_{cnt}V_{cnt} + E_{mat}(1 - V_{cnt})\,, \tag{4.13}$$

where $V_{cnt}$ is the volume fraction of CNTs and $1 - V_{cnt}$ is the volume fraction $V_{mat}$ of the matrix.

Expression of $V_{cnt}$ depends on the distribution pattern of CNTs in the matrix. Denoting by $\bar{y}$ the principal axis of geometric inertia originating at geometric centre $O$ of cross-section, the following distribution patterns are investigated

$$\begin{cases} V_{cnt} = V^* & \text{U-D} \\ V_{cnt} = 4\, V^* |\bar{y}|/h_0 & \text{X-D} \end{cases} \tag{4.14}$$

corresponding to Uniform Distribution (U-D) and X-shaped Distribution (X-D). In Eq.(4.14), $h_0$ denotes thickness of the distribution layer and $V^*$ is expressed as shown below

$$V^* = \frac{m_{cnt}}{m_{cnt} + \frac{\rho_{cnt}}{\rho_{mat}} - \frac{\rho_{cnt}}{\rho_{mat}} m_{cnt}}\,, \tag{4.15}$$

where $\rho_{cnt}$ and $\rho_{mat}$ are the carbon nanotube and the matrix densities, respectively, and $m_{cnt}$ is the CNTs mass fraction (see [83–85]).

Then, the effective elastic bending stiffness is given by the second moment of Euler-Young modulus (4.13) on the beam cross-section, that is

$$K_f := \int_\Omega E_h(y)\, y^2\, dA\,, \tag{4.16}$$

where $\Omega$ is the two-dimensional domain modeling cross-section. In Eq.(4.16), the coordinate $y$ is defined as $y := \bar{y} - \bar{y}_C$, where $\bar{y}_C$ is the $\bar{y}$-coordinate of the elastic centre $C$ of the Euler-Young moduli distribution, that is

$$\bar{y}_C = \frac{\displaystyle\int_\Omega E_h(\bar{y})\, \bar{y}\, dA}{\displaystyle\int_\Omega E_h(\bar{y})\, dA}\,. \tag{4.17}$$

## 4.3 Stress-driven nonlocal viscoelasticity

Let us consider a nanocomposite small-scale beam of length $L$. A linearised theory is preliminary recalled in this section before formulating geometrically nonlinear problems.

A general nonlocal law of viscoelasticity is derived in the sequel since matrices adopted in composite materials are usually of polymeric type. Notably, for inflected beams, according to nonlocal viscoelasticity theory based on the stress-driven formulation, the nonlocal viscoelastic flexural curvature $\chi^{ve}$ is expressed as the output field of the convolution integral between the special kernel described by a nonlocal characteristic length $c$, that is

$$\phi_c(x) = \frac{1}{2c} \exp\left( - \frac{|x|}{c} \right), \tag{4.18}$$

and the local viscoelastic curvature, i.e.:

$$\chi_l^{ve}(x,t) = \int_0^t J(t-\tau)\, \partial_\tau M(x,\tau)\, d\tau \tag{4.19}$$

where $J(t)$ is the creep compliance and $t$ the time variable. Thus, the stress-driven nonlocal viscoelastic curvature writes as follows

$$\chi^{ve}(x,t) = \int_0^L \phi_c(x-\xi)\, \chi_l^{ve}(\xi,t)\, d\xi\,. \tag{4.20}$$

Extending the equivalence property illustrated in Section 3.3, the integral law (4.20) is equivalent to the second order differential equation

$$\frac{1}{c^2}\chi^{ve}(x,t) - \partial_x^2\chi^{ve}(x,t) = \frac{1}{c^2}\chi_l^{ve}(x,t)\,, \tag{4.21}$$

equipped with the constitutive boundary conditions

$$\begin{cases} \partial_x\chi^{ve}(0,t) = \dfrac{1}{c}\,\chi^{ve}(0,t)\,, \\ \\ \partial_x\chi^{ve}(L,t) = -\dfrac{1}{c}\,\chi^{ve}(L,t)\,. \end{cases} \tag{4.22}$$

In the next sections, a preliminary study will be performed in the framework of geometrically nonlinear continuum mechanics assuming a stress-driven nonlocal purely elastic constitutive law.

## 4.4 Geometrically nonlinear analysis

Let us consider a nonlocal elastic cantilever inflected by a concentrated force $\mathcal{F}$ at free end (see Fig.4.3). This simple structural scheme represents a common basic element of miniaturized electromechanical systems like actuators, switches and storage devices. In the undeformed configuration the beam axis is assumed to be a straight line as depicted in Fig.4.3, that is, the initial geometric flexural curvature is zero.

Let us introduce the curvilinear abscissa $s \in [0, L]$ and the position vector $\mathbf{r}$ of a generic point belonging to the curve. Then, the unknown deformed configuration of the beam axis is a curve of the bending plane that can be parameterized as follows

$$\mathbf{r} = \begin{vmatrix} x(s) \\ y(s) \end{vmatrix} = \begin{vmatrix} x \\ y(x) \end{vmatrix}\,. \tag{4.23}$$

It is worth noting that the unit tangent vector field is defined as $\mathbf{t} := \partial_s\mathbf{r}$ and $|\partial_s\mathbf{t}|$ provides the exact (not linearised) geometric flexural curvature of the beam axis, i.e.:

$$\chi(x) = \frac{\partial_x^2 y(x)}{\left[1 + \left(\partial_x y(x)\right)^2\right]^{3/2}}\,. \tag{4.24}$$

Assuming a purely elastic behavior, the geometric flexural curvature is equal to the elastic one. Then, according to the stress-driven nonlocal model, the

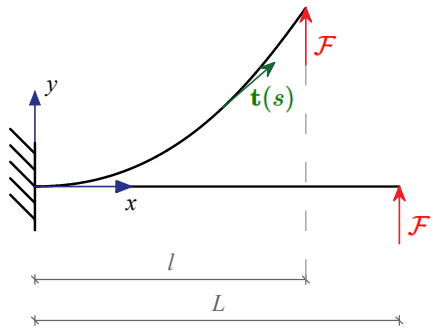


Figure 4.3: Cantilever beam undergoing large displacements.

flexural curvature $\chi$ is expressed by

$$\chi(x) = \int_0^l \phi_c(x-\xi) \left(\frac{M}{K_f}\right)(\xi)\, d\xi\,, \tag{4.25}$$

where $l$ is the projective length on the $x$-axis. Moreover, the equilibrated bending interaction field $M$ in Eq.(4.25) is expressed as

$$M(x) = \mathcal{F}(l-x)\,. \tag{4.26}$$

By integrating Eq.(4.24) with the positions $z := \partial_x y$ and $G := \dfrac{z}{\sqrt{1+z^2}}$, we get the following equation

$$G(x) = \int_0^x \chi(\eta) d\eta\,, \tag{4.27}$$

where the boundary condition $z(0) = 0$ has been prescribed. Then, by noting that $G := \partial_s y$ and $|\mathbf{t}| = \sqrt{(\partial_s x)^2 + G^2} = 1$, the following differential equation is got

$$\partial_x s(x) = \frac{1}{\sqrt{1-G^2(x)}}\,, \tag{4.28}$$

equipped with the boundary condition $s(0) = 0$. The unknown length $l$ is obtained prescribing that the relation $s(l) = L$ is satisfied. Finally, the deformed

configuration $y(x)$ of the beam axis is got from the differential equation

$$\partial_x y(x) = \frac{G(x)}{\sqrt{1 - G^2(x)}}\,, \tag{4.29}$$

equipped with the boundary condition $y(0) = 0$. An effective iterative procedure is conceived to solve the nonlinear elastostatic problem here formulated. Steps of the solution procedure are explained in the next Section.

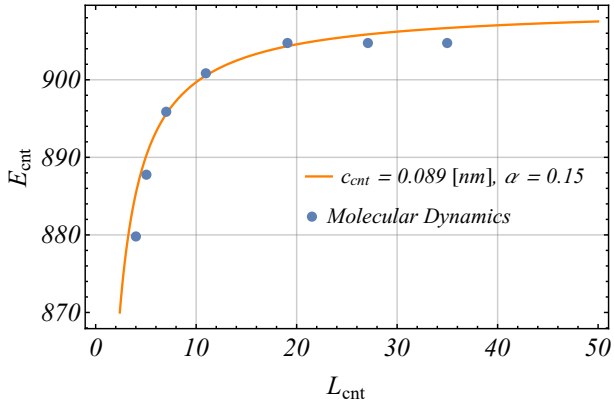


Figure 4.4: CNT effective Euler-Young modulus $E_{cnt}\,[GPa]$ (Eq.(4.9)) versus carbon nanotube length $L_{cnt}\,[nm]$, compared to Molecular Dynamics results.

## 4.5 Numerical results

The geometrically nonlinear flexural behavior of a carbon nanotubes reinforced microcantilever is numerically analyzed. The nanofillers are assumed to be (10, 10) armchair single-walled CNTs with effective diameter $d = 1.356\,[nm]$, thickness $t = 0.34\,[nm]$ and local Euler-Young modulus $E = 909.5\,[GPa]$ (see [86, 87]). Uniform and X-shaped distribution patterns of CNTs in a polymer matrix of Euler-Young modulus $E_{mat} = 2.5\,[GPa]$ are considered.

Characteristic length $c_{cnt}$ and mixture parameter $\alpha$ in Eq.(4.9) have been properly tuned as shown in Fig.4.4 in order to reproduce results of molecular dynamics simulations [87].

The length of CNTs is assumed to be $L_{cnt} = 10\,[nm]$, and thus, from Eq.(4.9) we get $E_{cnt} = 899.7\,[GPa]$. Carbon nanotubes and matrix densities

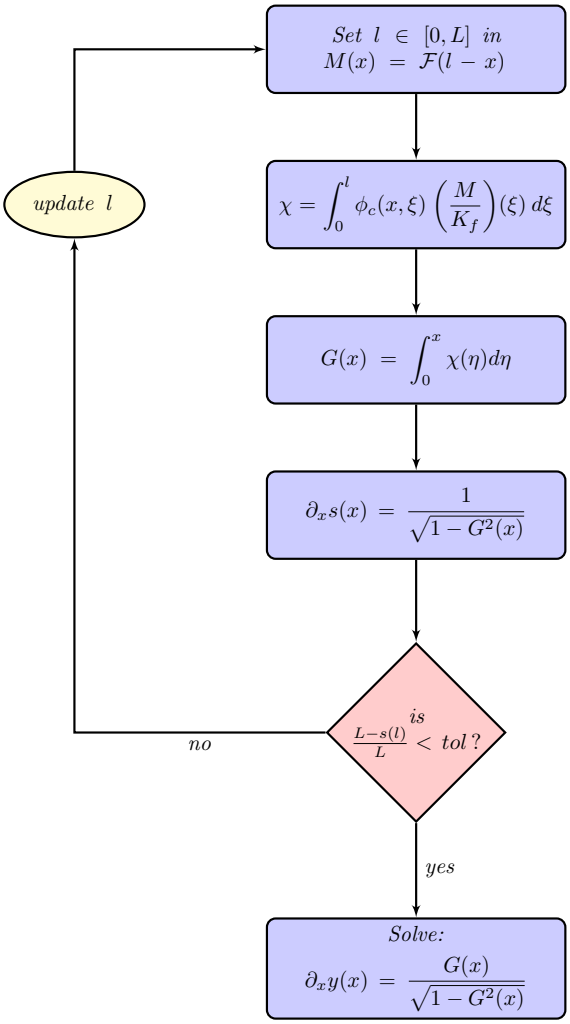


Figure 4.5: Flow chart of the iterative solution procedure.

are $\rho_{cnt} = 1400\,[kg/m^3]$ and $\rho_{mat} = 1190\,[kg/m^3]$, respectively. Geometric parameters of the microbeam are: length $L = 100\,[\mu m]$, height $h = 5\,[\mu m]$ and base $b = 3.5\,[\mu m]$.

The iterative solution procedure explained in Fig.4.5 is put into operation using the Mathematica software, fixing a suitable tolerance $tol$ as discussed in subsection 4.5.1. Effects of scale parameter, CNTs mass fraction and distribution pattern on structural responses are investigated performing a parametric study. The deformed configuration $y(x)$ is got for increasing values of the applied force $\mathcal{F}$ and for different CNTs mass fractions $m_{cnt}$ and nonlocal parameters $\lambda := c/L$, in the case of a CNTs uniform distribution pattern (see Figs.4.6-4.7) and of a X-shaped distribution pattern (see Figs.4.8-4.9).

Structural responses for increasing nonlocal parameter show an agreement with the "smaller-is-stiffer" phenomenon evidenced by [74]. Moreover, a stiffening behavior is shown for increasing CNTs mass fraction since increasing $m_{cnt}$ increases the volume fraction $V_{cnt}$ which is the coefficient of the Euler-Young modulus $E_{cnt}$ in the convex combination in Eq. (4.13). Finally, a comparison shows that the X-shaped distribution pattern of CNTs leads to a stiffer response with respect to the uniform one.

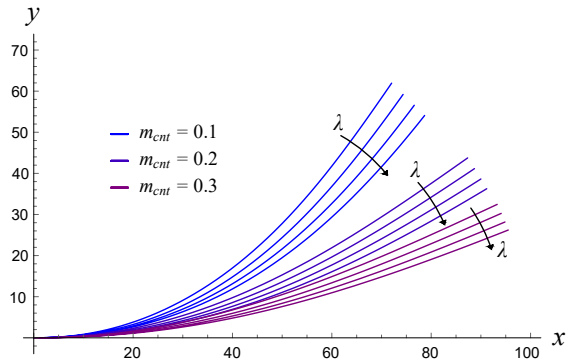


Figure 4.6: CNTs uniform distribution pattern: deformed configuration $y\,[\mu m]$ versus $x\,[\mu m]$ for $\lambda = \{0.05, 0.10, 0.15, 0.20\}$ and $F = 1000\,[\mu N]$.

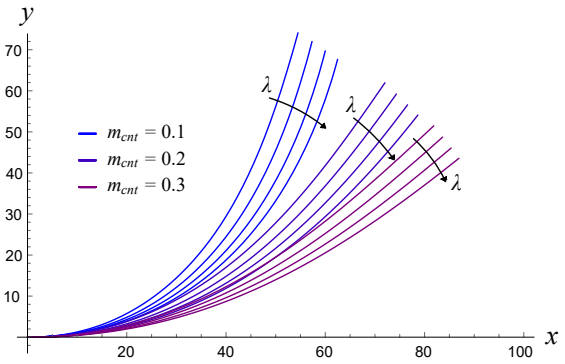


Figure 4.7: CNTs uniform distribution pattern: deformed configuration $y\,[\mu m]$ versus $x\,[\mu m]$ for $\lambda = \{0.05, 0.10, 0.15, 0.20\}$ and $F = 2000\,[\mu N]$.

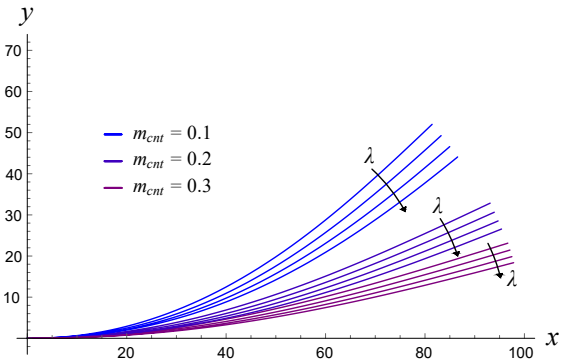


Figure 4.8: CNTs X-shaped distribution pattern: deformed configuration $y\,[\mu m]$ versus $x\,[\mu m]$ for $\lambda = \{0.05, 0.10, 0.15, 0.20\}$ and $F = 1000\,[\mu N]$.

### 4.5.1 Convergence of the algorithm

Results obtained exploiting the iterative procedure illustrated by the flow chart (Fig.4.5) are here analysed to show convergence of the algorithm. To this purpose, numerical solutions are evaluated for the nanocomposite cantilever of Section 4.5 under a concentrated force $F = 2000\,[\mu N]$ assuming a uniform distri-

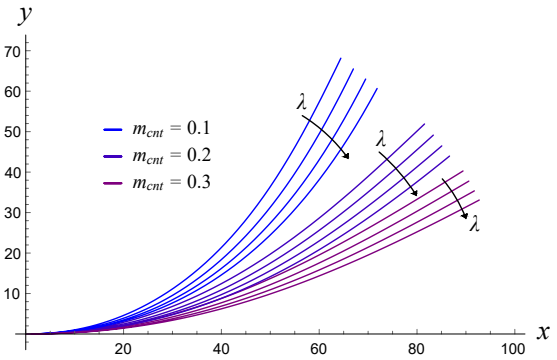


Figure 4.9: CNTs X-shaped distribution pattern: deformed configuration $y\,[\mu m]$ versus $x\,[\mu m]$ for $\lambda = \{0.05, 0.10, 0.15, 0.20\}$ and $F = 2000\,[\mu N]$.

bution pattern of carbon nanotubes and a mass fraction $m_{cnt} = \{0.1, 0.2, 0.3\}$, with a nonlocal parameter $\lambda = 0.2$. Table 6.2 shows numerical results obtained for decreasing value of tolerance $tol$.

Notably, symbol $u_L$ represents modulus of displacement vector at free end, i.e. $u_L := \sqrt{\big(y(l)\big)^2 + \big(L - l\big)^2}$, being $l$ the projective length on the $x$-axis and $L = 100\,\mu m$ the beam length. Trial length at $i$-th iteration is got as $l_i = l_{i-1} + \Delta l$, being $\Delta l$ the analysis step. The iteration number in Tab.6.2 is denoted by $n$ while relative error is defined as $e_r := \dfrac{L - s(l)}{L} < tol$. Moreover, results in Tab.6.2 are referred to first trial lengths $l_0 = \{60, 70, 80\}\,[\mu m]$ respectively for $m_{cnt} = \{0.1, 0.2, 0.3\}$. For decreasing values of tolerance, results $l$ and $u_L$ of the $n$th iteration converge to $l = \{63.627, 79.721, 87.744\}\,[\mu m]$ and $u_L = \{76.148, 56.674, 44.006\}\,[\mu m]$, got by setting $tol =$ E-06, respectively for $m_{cnt} = \{0.1, 0.2, 0.3\}$.

It is worth noting that the iteration number increases for decreasing prescribed $tol$ since a smaller step $\Delta l$ is required, starting from the same first trial length $l_0$. Tab.6.1 shows decreasing relative error percentages $e_{r_{\%}}$ for trial lengths $l_i$ at iteration $i = \{1, ..., 5\}$, showing convergence of the algorithm.

Table 4.1: Numerical results for $F = 2000\,[\mu N]$ with nonlocal parameter $\lambda = 0.2$ and a uniform distribution pattern of carbon nanotubes.

| $m_{cnt} = 0.1$ | | | | | | |
|---|---|---|---|---|---|---|
| *tol* | $\Delta l\,[\mu m]$ | $n$ | $l\,[\mu m]$ | $s(l)\,[\mu m]$ | $e_r\,[-]$ | $u_L\,[\mu m]$ |
| E-01 | 1 | 4 | 63.00 | 92.8058 | 7.19E-02 | 69.784 |
| E-02 | 0.1 | 36 | 63.60 | 99.6203 | 3.80E-03 | 75.806 |
| E-03 | 0.02 | 181 | 63.62 | 99.9049 | 9.51E-04 | 76.062 |
| $m_{cnt} = 0.2$ | | | | | | |
| *tol* | $\Delta l\,[\mu m]$ | $n$ | $l\,[\mu m]$ | $s(l)\,[\mu m]$ | $e_r\,[-]$ | $u_L\,[\mu m]$ |
| E-01 | 1 | 8 | 77.00 | 91.8015 | 9.49E-02 | 49.533 |
| E-02 | 0.5 | 20 | 79.50 | 99.2443 | 7.56E-03 | 55.972 |
| E-03 | 0.1 | 97 | 79.70 | 99.9286 | 7.14E-04 | 56.608 |
| E-04 | 0.05 | 216 | 79.72 | 99.9979 | 2.10E-05 | 56.672 |
| $m_{cnt} = 0.3$ | | | | | | |
| *tol* | $\Delta l\,[\mu m]$ | $n$ | $l\,[\mu m]$ | $s(l)\,[\mu m]$ | $e_r\,[-]$ | $u_L\,[\mu m]$ |
| E-01 | 1 | 4 | 83.00 | 91.2071 | 9.46E-02 | 37.419 |
| E-02 | 0.5 | 16 | 87.50 | 99.5024 | 9.01E-03 | 43.576 |
| E-03 | 0.1 | 77 | 87.70 | 99.9094 | 9.06E-04 | 43.927 |
| E-04 | 0.05 | 172 | 87.74 | 99.9913 | 8.70E-05 | 43.998 |

Table 4.2: Relative error percentages $e_{r_\%}\,[\%]$ for trial lengths $l_i\,[\mu m]$ at iteration $i = \{1, ..., 5\}$.

| $m_{cnt} = 0.1$ | | | | | |
|---|---|---|---|---|---|
| $l_i$ | 25.00 | 45.00 | 60.00 | 63.60 | 63.63 |
| $e_{r_\%}$ | 74.96 | 53.24 | 24.16 | 3.80E-01 | 5.25E-05 |
| $m_{cnt} = 0.2$ | | | | | |
| $l_i$ | 45.00 | 65.00 | 75.00 | 79.70 | 79.72 |
| $e_{r_\%}$ | 54.59 | 30.75 | 13.09 | 7.14E-02 | 1.71E-05 |
| $m_{cnt} = 0.3$ | | | | | |
| $l_i$ | 50.00 | 70.00 | 80.00 | 87.70 | 87.74 |
| $e_{r_\%}$ | 49.66 | 27.31 | 13.62 | 9.06E-02 | 8.92E-05 |

# Chapter 5

# Nonlocal elasticity for structural assemblages

## 5.1 Main contents

In the present chapter, stress-driven elastostatic problems of slender nonlocal elastic beams are analysed in the case of piecewise smooth local elastic curvature fields. Thus, a new stress-driven methodology is proposed to investigate size-dependent behaviors of nonlocal elastic beams involving discontinuous and concentrated loadings, internal kinematic constraints, non-smooth elastic and geometric properties. In particular, we focus on source fields of stress-driven integral convolutions that are piecewise smooth functions and it will be proven that convolution outputs are continuously differentiable nonlocal elastic curvatures, a property that plays a fundamental role in reversing the integral law of elasticity.

Indeed as shown in the following, if Helmholtz's special kernel is adopted as averaging function, the stress-driven integral convolution with piecewise smooth source fields can be inverted by providing an equivalent differential formulation. It is shown that the differential constitutive law is made of a differential system of constitutive equations equipped with constitutive conditions at the exterior points of the domain and interface conditions at the interior discontinuity points.

Size effects in the elastic behavior can be thus taken into account in constitutive equations also in case of non-smooth source fields by means of a new stress-driven methodology [59] that will be discussed in detail. Moreover, other

size-dependent behaviors associated with non-elastic phenomena (i.e. thermal, plastic, electro-magnetic) on small-scale structures will be also investigated.

## 5.2 Nonlocal elastostatics

Let us consider a planar and straight Bernoulli-Euler beam. Adopting the usual notation, $x$ is the axial abscissa while the flexural axis is denoted by $y$.

The slender beam is bent by distributed and concentrated loadings and, for the sake of simplicity, the assemblage domain is partitioned in two parts $[0, L] = [0, x_d] \cup [x_d, L]$, being $x_d$ the discontinuity abscissa. The schematic view of the investigated structural problem is illustrated in Fig.5.1.

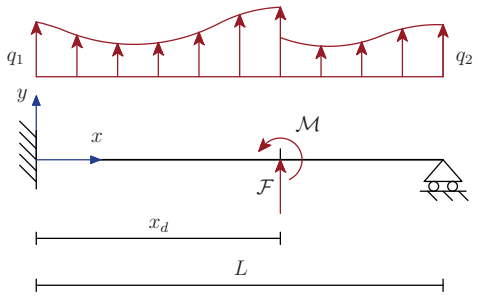


Figure 5.1: Nonlocal beam under concentrated force and couple and distributed transverse loadings.

1. **Equilibrium.** According to Bernoulli-Euler beam theory, stress field is described by bending interaction $M$ which is a piecewise regular scalar function due to discontinuities occurring at abscissa $x_d$. Bending field $M : [0, L] - \{x_d\} \mapsto \Re$ is expressed by

$$M(x) = \begin{cases} M_1(x)\,, & x \in [0, x_d[\,, \\ M_2(x)\,, & x \in ]x_d, L]\,, \end{cases} \tag{5.1}$$

with $M_1$ and $M_2$ regular scalar functions, fulfilling standard natural (static) boundary conditions depending on prescribed kinematic constraints,

solution fields of the differential equations of equilibrium

$$\begin{cases} \partial_x^2 M_1 = q_1 \,, \\ \partial_x^2 M_2 = q_2 \,. \end{cases} \tag{5.2}$$

The scalar functions $q_1 : [0, x_d] \mapsto \Re$ and $q_2 : [x_d, L] \mapsto \Re$ denote regular intensities of the distributed transverse loading.

2. **Nonlocal Elasticity.** According to the stress-driven nonlocal model [54], elastic curvature $\chi^{el}$ is the convolution integral between bending field $M$ Eq.(5.1) and a smoothing kernel $\phi$

$$\begin{aligned} \chi^{el}(x) &= \left(\phi * \frac{M}{k_f}\right)(x) \\ &= \int_0^L \phi(x - \xi, c) \cdot \frac{M}{k_f}(\xi)\, d\xi \,, \end{aligned} \tag{5.3}$$

where $c > 0$ stands for nonlocal length-scale parameter and $k_f := I_E$ is the local elastic bending stiffness, i.e. second moment of the field of Euler-Young elastic moduli $E$ on beam cross-sections. The averaging kernel $\phi$ involved in the integral convolution Eq.(5.3) is assumed to fulfill positivity, symmetry, normalisation and impulsivity properties on the real axis $\Re$.

3. **Kinematic compatibility.** According to Bernoulli-Euler theory, geometric nonlocal strain field is described by the regular total flexural curvature $\chi : [0, L] \mapsto \Re$

$$\chi(x) = \begin{cases} \chi_1(x) = \partial_x^2 v_1(x) \,, & x \in [0, x_d] \,, \\ \chi_2(x) = \partial_x^2 v_2(x) \,, & x \in [x_d, L] \,, \end{cases} \tag{5.4}$$

with $v_1 : [0, x_d] \mapsto \Re$ and $v_2 : [x_d, L] \mapsto \Re$ regular transverse displacements fulfilling standard essential (kinematic) boundary conditions.

**Remark 5.2.1** *It is worth noting that Eq.(5.4) holds for strictly positive nonlocal length-scale parameter. Indeed, as will be proven in the following,* $\chi \in \mathrm{C}^1([0, L]; \Re)$ *for* $c > 0$ *.*

## 5.3 Differential formulation

The integral elastic law in Eq.(5.3) can be equivalently reformulated in differential terms by adopting the special bi-exponential averaging kernel

$$\phi_c(x) := \frac{1}{2\,c}\,\exp\left(-\frac{|x|}{c}\right). \tag{5.5}$$

Next two propositions play a key role in deriving the equivalent differential formulation of the stress-driven integral elastic law in Eq.(5.3) equipped with the special kernel in Eq.(5.5).

**Proposition 5.3.1** *Elastic curvatures generated by the stress-driven convolution integral Eq.(5.3) with the special kernel Eq.(5.5) are continuously differentiable fields $\chi^{el} \in \mathrm{C}^1([0,L];\Re)$ in the whole domain, for any piecewise smooth source field of local elastic curvature.*

**Proof 5.3.1** *Stress-driven integral convolution Eq.(5.3) along with the adoption of the special kernel Eq.(5.5), leads to the following definition of the nonlocal elastic curvature $\chi^{el}$*

$$\begin{aligned}
\chi^{el}(x) &= \begin{cases} \chi_1^{el}(x)\,, & x \in [0, x_d] \\ \chi_2^{el}(x)\,, & x \in [x_d, L] \end{cases} \\
&= \begin{cases} \dfrac{1}{2c}\displaystyle\int_0^x exp\left(\frac{t-x}{c}\right)\frac{M_1}{I_{E1}}(t)dt + \frac{1}{2c}\int_x^{x_d} exp\left(\frac{x-t}{c}\right)\frac{M_1}{I_{E1}}(t)dt \\ \quad + \dfrac{1}{2c}\displaystyle\int_{x_d}^L exp\left(\frac{x-t}{c}\right)\frac{M_2}{I_{E2}}(t)dt, \qquad x \in [0, x_d]\,, \\ \dfrac{1}{2c}\displaystyle\int_0^{x_d} exp\left(\frac{t-x}{c}\right)\frac{M_1}{I_{E1}}(t)dt + \frac{1}{2c}\int_{x_d}^x exp\left(\frac{t-x}{c}\right)\frac{M_2}{I_{E2}}(t)dt \\ \quad + \dfrac{1}{2c}\displaystyle\int_x^L exp\left(\frac{x-t}{c}\right)\frac{M_2}{I_{E2}}(t)dt, \qquad x \in [x_d, L]\,. \end{cases}
\end{aligned} \tag{5.6}$$

*Elastic curvature field in Eq.(5.6) is continuously differentiable in the domain*

$[0, L]$ *; indeed, its first derivative is given by*

$$\partial_x \chi^{el}(x) = \begin{cases} \dfrac{1}{2c^2}\left( -\displaystyle\int_0^x exp\left(\frac{t-x}{c}\right)\frac{M_1}{I_{E1}}(t)dt + \int_x^{x_d} exp\left(\frac{x-t}{c}\right)\frac{M_1}{I_{E1}}(t)dt \right. \\ \left. + \displaystyle\int_{x_d}^L exp\left(\frac{x-t}{c}\right)\frac{M_2}{I_{E2}}(t)dt\right), \qquad x \in [0, x_d]\,, \\ \dfrac{1}{2c^2}\left( -\displaystyle\int_0^{x_d} exp\left(\frac{t-x}{c}\right)\frac{M_1}{I_{E1}}(t)dt - \int_{x_d}^x exp\left(\frac{t-x}{c}\right)\frac{M_2}{I_{E2}}(t)dt \right. \\ \left. + \displaystyle\int_x^L exp\left(\frac{x-t}{c}\right)\frac{M_2}{I_{E2}}(t)dt\right), \qquad x \in [x_d, L]\,. \end{cases} \tag{5.7}$$

Derivative of nonlocal elastic curvature in Eq.(5.6) can be expressed in other equivalent ways. For instance, by combining Eq.(5.6) and Eq.(5.7), the following expression can be derived

$$\partial_x \chi^{el}(x) = \begin{cases} \dfrac{1}{c}\left( \chi^{el}(x) - \dfrac{1}{c}\displaystyle\int_0^x exp\left(\frac{t-x}{c}\right)\frac{M_1}{I_{E1}}(t)dt\right), \qquad x \in [0, x_d]\,, \\ \dfrac{1}{c}\left( -\chi^{el}(x) + \dfrac{1}{c}\displaystyle\int_x^L exp\left(\frac{x-t}{c}\right)\frac{M_2}{I_{E2}}(t)dt\right), \quad x \in [x_d, L]\,. \end{cases} \tag{5.8}$$

It is worth noting that evaluation of Eq.(5.8) at the abscissa $x_d$ provides the interface conditions in [88], Eqs.$(13)_2$ and $(14)_1$.

**Proposition 5.3.2** *Higher-order derivatives of nonlocal elastic curvature field* $\chi^{el}$ *defined by integral convolutions in* (5.6)*, are given by*

$$\partial_x^{(2+n)} \chi^{el}(x) = \begin{cases} \dfrac{1}{c^2}\left( \partial_x^n \chi_1^{el}(x) - \partial_x^n \dfrac{M_1}{I_{E1}}(x)\right), \qquad x \in [0, x_d[\,, \\ \dfrac{1}{c^2}\left( \partial_x^n \chi_2^{el}(x) - \partial_x^n \dfrac{M_2}{I_{E2}}(x)\right), \qquad x \in ]x_d, L]\,, \end{cases} \tag{5.9}$$

*with* $n \in \{0, 1, 2, ...\}$ *and* $\partial_x^0$ *identity operator.*

**Proof 5.3.2** *Second derivative of the nonlocal elastic curvature* $\chi^{el}$ *in Eq.*(5.6)

*is given by*

$$\partial_x^2\chi^{el}(x) = \begin{cases} \frac{1}{2c^3}\left(\int_0^x exp\left(\frac{t-x}{c}\right)\frac{M_1}{I_{E1}}(t)dt + \int_x^{x_d} exp\left(\frac{x-t}{c}\right)\frac{M_1}{I_{E1}}(t)dt + \right. \\ \left. + \int_{x_d}^{L} exp\left(\frac{x-t}{c}\right)\frac{M_2}{I_{E2}}(t)dt\right) - \frac{1}{c^2}\frac{M_1}{I_{E1}}(x), \qquad x \in [0, x_d[\,, \\ \frac{1}{2c^3}\left(\int_0^{x_d} exp\left(\frac{t-x}{c}\right)\frac{M_1}{I_{E1}}(t)dt + \int_{x_d}^{x} exp\left(\frac{t-x}{c}\right)\frac{M_2}{I_{E2}}(t)dt + \right. \\ \left. + \int_{x}^{L} exp\left(\frac{x-t}{c}\right)\frac{M_2}{I_{E2}}(t)dt\right) - \frac{1}{c^2}\frac{M_2}{I_{E2}}(x), \qquad x \in ]x_d, L]\,. \end{cases} \tag{5.10}$$

*Using Eq.(5.6) in Eq.(5.10), we infer Eq.(5.9) for* $n = 0$*. For* $n \geq 1$ *the proof of Eq.(5.9) is got by n-times differentiating Eq.(5.10).*

Table 5.1 summarizes regularity properties of the elastic curvature field got by the stress-driven convolution. Proof of properties collected in Tab.5.1 can be

Table 5.1: Regularity properties of elastic curvature field.

| | $\frac{M}{I_E}$ Continuous (C) | $\frac{M}{I_E}$ Discontinuous (D) | $\partial_x\frac{M}{I_E}$ Continuous (C) | $\partial_x\frac{M}{I_E}$ Discontinuous (D) |
|---|---|---|---|---|
| $\chi^{el}$ | C | C | – | – |
| $\partial_x\chi^{el}$ | C | C | – | – |
| $\partial_x^2\chi^{el}$ | C | D | – | – |
| $\partial_x^3\chi^{el}$ | – | – | $C$ | $D$ |

inferred from Propositions 5.3.1 and 5.3.2.

By virtue of the propositions listed above, nonlocal elastic curvature $\chi^{el}$ in Eq.(5.6) is the unique solution of a differential equivalent problem made of second order differential constitutive equations, boundary condition at $\partial[0, L]$ and interface conditions at $x_d$.

Constitutive system of differential equations can be got from Eq.(5.9) setting

$n = 0$ , that is

$$\begin{cases} \dfrac{1}{c^2}\chi_1^{el}(x) - \partial_x^2\chi_1^{el}(x) = \dfrac{1}{c^2}\dfrac{M_1}{I_{E1}}(x)\,, & x \in [0, x_d]\,, \\ \dfrac{1}{c^2}\chi_2^{el}(x) - \partial_x^2\chi_2^{el}(x) = \dfrac{1}{c^2}\dfrac{M_2}{I_{E2}}(x)\,, & x \in [x_d, L]\,, \end{cases} \tag{5.11}$$

each one pertaining to a regularity domain for the source field $M/k_f$ . Boundary condition at $\partial[0, L]$ is given by

$$\begin{cases} \partial_x\chi_1^{el}(0) = \dfrac{1}{c}\,\chi_1^{el}(0)\,, \\ \partial_x\chi_2^{el}(L) = -\dfrac{1}{c}\,\chi_2^{el}(L)\,. \end{cases} \tag{5.12}$$

Proof of Eqs.(5.12) is got by evaluating and comparing the expressions in Eqs.(5.6), (5.7) at boundary $\partial[0, L]$ . Interface (continuity) conditions at $x_d$ write as

$$\begin{cases} \chi_1^{el}(x_d) = \chi_2^{el}(x_d)\,, \\ \partial_x\chi_1^{el}(x_d) = \partial_x\chi_2^{el}(x_d)\,. \end{cases} \tag{5.13}$$

Proof of Eqs.(5.13) is got by evaluating elastic curvature in Eq.(5.6) and its first derivative in Eq.(5.7) at abscissa $x_d$ .

Constitutive interface conditions in Eqs.(5.13) can be replaced by alternative conditions expressing continuity of higher-order derivatives of elastic curvature. These continuity conditions can be chosen from the synoptic table 5.1, depending on regularity properties of the source field $M/k_f$ considered in the stress-driven law of nonlocal elasticity Eq.(5.6).

## 5.4 Solution methods

Nonlocal solution fields of a bent beam under inelastic curvature distortions and distributed and concentrated loadings are got by following three steps.

1. Detection of parametric representation of equilibrated bending fields $M$ Eq.(5.1) by solving the differential problem Eq.(5.2) supplemented with (standard) natural boundary conditions. The number of involved static parameters is the redundancy degree. For statically determinate beams,

the redundancy degree is zero and a single bending solution field is obtained by equilibrium.

2. Computation of the corresponding parametric nonlocal elastic curvature field $\chi^{el}$ using the stress-driven convolution Eq.(5.3) and evaluation of the ensuing parametric total flexural curvature field $\chi$.

3. Detection of nonlocal displacement field $v = \{ v_1, v_2 \}$ by double integration of total flexural parametric curvature $\chi = \{ \chi_1, \chi_2 \}$ Eq.(5.4) and prescription of (standard) essential boundary conditions.

**Remark 5.4.1** *The above illustrated mathematical formulation and solution procedure are independent of the averaging kernel expression adopted in the stress-driven nonlocal integral convolution Eq.*(5.3)*. Closure of the nonlocal structural problem of an inflected beam with a piecewise regular source field is performed by enforcing only standard essential and natural boundary conditions.*

Nonlocal solution fields can be also got adopting the equivalent differential constitutive formulation. In this case, the solution technique presented above can be still adopted modifying the second item. Specifically, computation of nonlocal elastic parametric curvatures $\chi^{el}$ is carried out solving the differential problem Eqs.(5.11), (5.12) and (5.13), instead of using the stress-driven convolution Eq.(5.3).

Alternatively, the structural problem can be formulated in terms of regular nonlocal displacement functions $v_1 : [0, x_d] \mapsto \Re$ and $v_2 : [x_d, L] \mapsto \Re$ by differentiating twice the nonlocal laws (5.11) and enforcing equilibrium Eq.(5.2) and kinematic compatibility Eq.(5.4), that is

$$\begin{cases} \dfrac{\partial_x^4 v_1(x)}{c^2} - \partial_x^6 v_1(x) = \dfrac{1}{c^2}\left(\dfrac{q_1(x)}{k_f} + \partial_x^2 \chi_1^{nel}(x)\right) - \partial_x^4 \chi_1^{nel}(x)\,, \quad x \in [0, x_d]\,, \\ \dfrac{\partial_x^4 v_2(x)}{c^2} - \partial_x^6 v_2(x) = \dfrac{1}{c^2}\left(\dfrac{q_2(x)}{k_f} + \partial_x^2 \chi_2^{nel}(x)\right) - \partial_x^4 \chi_2^{nel}(x)\,, \quad x \in [x_d, L]\,. \end{cases} \tag{5.14}$$

The set $\{ v_1, v_2 \}$ of functions, within an additional rigid body motion, are evaluated by integrating the differential problem Eq.(5.14) and enforcing standard (essential) kinematic and (natural) static boundary conditions, non-standard constitutive (5.12) and continuity (5.13) boundary conditions. Using Eq.(5.4), non-standard boundary conditions Eqs.(5.12) and (5.13) are respec-

tively expressed in terms of displacement fields by

$$\begin{cases} \partial_x^3 v_1(0) - \partial_x \chi_1^{nel}(0) = \dfrac{1}{c}\left(\partial_x^2 v_1(0) - \chi_1^{nel}(0)\right), \\ \partial_x^3 v_2(L) - \partial_x \chi_2^{nel}(L) = -\dfrac{1}{c}\left(\partial_x^2 v_2(L) - \chi_2^{nel}(L)\right), \end{cases} \tag{5.15}$$

and

$$\begin{cases} \partial_x^2 v_1(x_d) - \chi_1^{nel}(x_d) = \partial_x^2 v_2(x_d) - \chi_2^{nel}(x_d), \\ \partial_x^3 v_1(x_d) - \partial_x \chi_1^{nel}(x_d) = \partial_x^3 v_2(x_d) - \partial_x \chi_2^{nel}(x_d). \end{cases} \tag{5.16}$$

## 5.5 Asymptotic nonlocal responses

In this section, limit nonlocal elastic curvature in Eq.(5.6) for $c \to 0^+$ is examined. Specifically, asymptotic behaviors are investigated at boundary $\partial[0, L]$, at interface abscissa $x = x_d$ and at regularity internal points $x \in ]0, x_d[ \cup ]x_d, L[$.

For this purpose, let us recall from Section 2.2.1 the impulsivity property of the special kernel $\phi_c$ as formulated in (2.10). Specifically, Eq.(2.10) clarifies that the asymptotic behavior of the averaging kernel $\phi_c$ for $c \to 0^+$ depends on the location of the evaluation abscissa in the domain, that is

$$\lim_{c \to 0^+} \phi_c = \begin{cases} \delta, & x \in ]0, L[, \\ \dfrac{\delta}{2}, & x \in \partial[0, L]. \end{cases} \tag{5.17}$$

The halved Dirac impulse $\dfrac{\delta}{2}$ is due to the fact that, at a boundary point, half of the kernel's support falls out of the integration domain.

Now, let us evaluate the elastic curvature in Eq.(5.6) at the interface abscissa $x = x_d$. That is,

$$\begin{aligned} \chi^{el}(x_d) &= \left(\phi_c * \frac{M}{I_E}\right)(x_d) = \int_0^L \phi_c(x_d - \xi, c) \frac{M}{I_E}(\xi)\, d\xi \\ &= \int_0^{x_d} \phi_c(x_d - \xi, c) \frac{M_1}{I_{E1}}(\xi)\, d\xi + \int_{x_d}^L \phi_c(x_d - \xi, c) \frac{M_2}{I_{E2}}(\xi)\, d\xi. \end{aligned} \tag{5.18}$$

It is worth noting that from the split done in Eq.(5.18), it is evident that abscissa $x_d$ is the boundary point of both the integration domains. Therefore,

taking into account Eq.(5.17), nonlocal elastic curvature at $x = x_d$ for $c \to 0^+$ is the average of local elastic curvatures $\dfrac{M_1}{I_{E1}}(x_d)$ and $\dfrac{M_2}{I_{E2}}(x_d)$.

The following synoptic system summarizes asymptotic behaviors of nonlocal elastic curvature $\chi^{el}$ in Eq.(5.6), id est

$$\chi^{el}_{0^+}(x) := \lim_{c\to 0^+} \chi^{el}(x) = \begin{cases} \dfrac{M_1}{2I_{E1}}(0)\,, & x = 0\,, \\ \dfrac{M_1}{I_{E1}}(x)\,, & x \in ]0, x_d[\,, \\ \dfrac{1}{2}\Big(\dfrac{M_1}{I_{E1}}(x_d) + \dfrac{M_2}{I_{E2}}(x_d)\Big)\,, & x = x_d\,, \\ \dfrac{M_2}{I_{E2}}(x)\,, & x \in ]x_d, L[\,, \\ \dfrac{M_2}{2I_{E2}}(L)\,, & x = L\,. \end{cases} \tag{5.19}$$

**Remark 5.5.1** *As evidenced in Eq.(5.19), except for null measure sets, the asymptotic behaviour of nonlocal elastic curvature fields coincides with local response fields. Accordingly, limit displacement solutions for $c \to 0^+$ of the relevant nonlocal structural problems are coincident with local ones in the whole structural domain.*

## 5.6 Preliminary case-studies

Theoretical outcomes provided in Section 5.5 are confirmed in the sequel by analysing the static behavior of slender nonlocal beams under concentrated loadings. For this purpose, a nonlocal elastic beam of length $L$ and bending stiffness $I_E$ is considered, with the beam axis coinciding with the $x$-coordinate as shown in Fig.5.1. Exact nonlocal solution fields will be provided by following the methodologies illustrated in Section 5.4.

Parametric solutions will be provided as functions of the nonlocal parameter $\lambda = c/L$. Denoting by $\bar{x} = x/L \in [0, 1]$ the non-dimensional abscissa, the following non-dimensional fields of transverse displacement, flexural curvature and bending interaction will be adopted in the plots

$$\bar{v}(\bar{x}) = v(x)\frac{I_E}{\mathcal{M}L^2}, \qquad \bar{\chi}(\bar{x}) = \chi(x)\frac{I_E}{\mathcal{M}}, \qquad \bar{M}(\bar{x}) = M(x)\frac{1}{\mathcal{M}}. \tag{5.20}$$

**Case 1**. A simply supported nonlocal beam is subjected to a concentrated couple $\mathcal{M}$ at mid-span $x_d = L/2$. Essential boundary conditions are

$$\begin{cases} v_1(0) = 0, \\ v_1(L/2) = v_2(L/2), \\ \partial_x v_1(L/2) = \partial_x v_2(L/2), \\ v_2(L) = 0. \end{cases} \tag{5.21}$$

Thus, natural boundary conditions are

$$\begin{cases} M_1(0) = 0, \\ -M_1(L/2) + M_2(L/2) + \mathcal{M} = 0, \\ T_1(L/2) = T_2(L/2), \\ M_2(L) = 0. \end{cases} \tag{5.22}$$

Solving the differential equilibrium problem (5.2)-(5.22) leads to the equilibrated bending interaction fields. Then, from Eq.(5.3) the corresponding nonlocal elastic curvature field is

$$\begin{aligned} \chi_1^{el}(x) &= -\frac{\mathcal{M}(Le^{-\frac{L-2x}{2c}} + c(e^{\frac{x-L}{c}} - e^{-\frac{x}{c}}) - 2x)}{2I_E L}, \\ \chi_2^{el}(x) &= -\frac{\mathcal{M}(L(2 - e^{\frac{L-2x}{2c}}) + c(e^{\frac{x-L}{c}} - e^{-\frac{x}{c}}) - 2x)}{2I_E L}. \end{aligned} \tag{5.23}$$

Double integration of total flexural curvature $\chi = \chi^{el} + \chi^{in} = \{\chi_1^{el}, \chi_2^{el}\}$ Eq.(5.4) with the essential boundary conditions (5.21) leads to the following nonlocal displacement field $v = \{v_1, v_2\}$

$$
\begin{aligned}
v_1(x) = &-\frac{\mathcal{M}e^{-\frac{L+x}{c}}}{24I_E L^2}(x(L^3-4Lx^2)e^{\frac{L+x}{c}}+12c^3(Le^{\frac{2x}{c}}+(2x-L)e^{\frac{x}{c}}\\
&+(L-2x)e^{\frac{L+x}{c}}-Le^{\frac{L}{c}})+12Lc^2e^{\frac{L+2x}{2c}}(L(e^{\frac{x}{c}}-1)-2x(e^{\frac{L}{2c}}-1))),\\
v_2(x) = &-\frac{\mathcal{M}e^{-\frac{L+x}{c}}}{24I_E L^2}(L(3L^3-11L^2x+12Lx^2-4x^3)e^{\frac{L+x}{c}}+12c^3(Le^{\frac{2x}{c}}\\
&+(2x-L)e^{\frac{x}{c}}+(L-2x)e^{\frac{L+x}{c}}-Le^{\frac{L}{c}})-12Lc^2e^{\frac{L}{2c}}(-2(L-x)e^{\frac{L+2x}{2c}}\\
&+(L-2x)e^{\frac{x}{c}}+Le^{\frac{L}{c}})).
\end{aligned}
\tag{5.24}
$$

Alternatively, the nonlocal displacement field can be obtained by solving differential Eqs.(5.14) with non-standard and standard boundary conditions, respectively Eqs.(5.15)-(5.16) and Eqs.(5.21)-(5.22). Non-dimensional plots of the obtained results are presented in the following.

As it is shown in Fig.5.2, nonlocal elastic curvatures become lower and uniform for increasing nonlocal parameter, while for $\lambda = 0^+$ the local elastic curvature is recovered $\forall \bar{x} \in [0,1]-\{\bar{x}_d\}$. Indeed, at middle abscissa $x_d$ the asymptotic behavior yields $\chi^{el}_{0^+}(x_d) = \dfrac{M_1(x_d)+M_2(x_d)}{2I_E} = 0$ as predicted by theoretical outcomes contributed in Sec.5.5. Non-dimensional transverse displacements $\bar{v}$ illustrated in Fig.5.3 exhibit a stiffening behavior for increasing values of $\lambda$.

**Case 2**. A slender nonlocal beam with clamped and simply supported ends is subjected to a concentrated couple $\mathcal{M}$ at mid-span $x_d = L/2$. Essential boundary conditions are expressed as

$$
\begin{cases}
v_1(0) = 0,\\
\partial_x v_1(0) = 0,\\
v_1(L/2) = v_2(L/2),\\
\partial_x v_1(L/2) = \partial_x v_2(L/2),\\
v_2(L) = 0.
\end{cases}
\tag{5.25}
$$

Hence, natural boundary conditions take the form

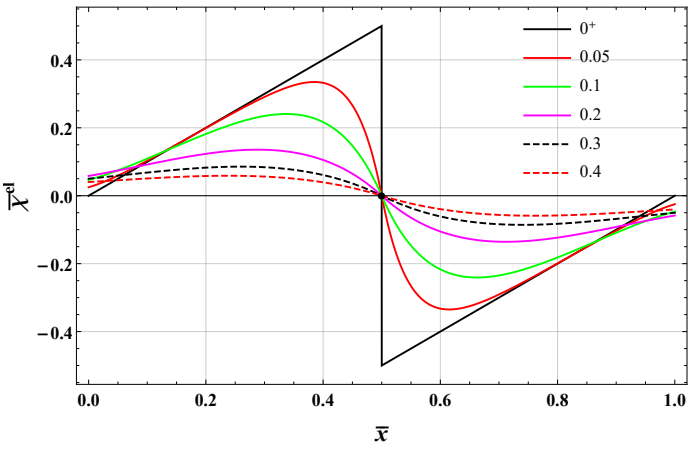


Figure 5.2: Simply supported beam under concentrated couple $\mathcal{M}$ at mid-span $\bar{x} = 1/2$: elastic curvature $\bar{\chi}^{el}$ versus $\bar{x}$ for increasing nonlocal parameter.

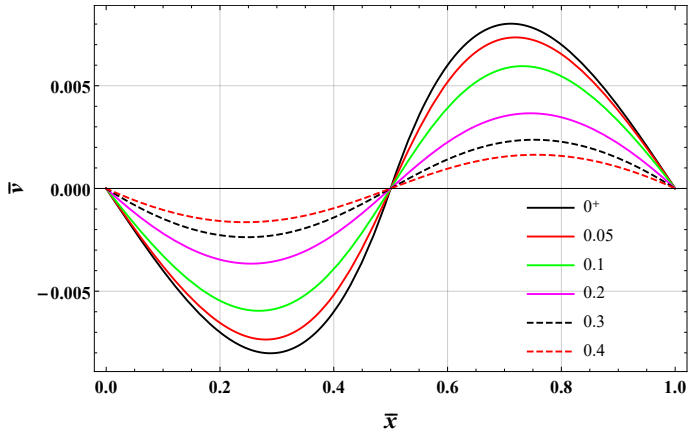


Figure 5.3: Simply supported beam under concentrated couple $\mathcal{M}$ at mid-span $\bar{x} = 1/2$: transverse displacement $\bar{v}$ versus $\bar{x}$ for increasing nonlocal parameter.

$$\begin{cases} -M_1(L/2) + M_2(L/2) + \mathcal{M} = 0, \\ T_1(L/2) = T_2(L/2), \\ M_2(L) = 0. \end{cases} \tag{5.26}$$

Bending interaction fields $M$ (5.1) solutions of the differential equilibrium problem Eqs.(5.2)-(5.26) are expressed in terms of $n = 1$ integration constant and then introduced into the integral convolution in Eq.(5.3) to obtain the corresponding parametric nonlocal elastic curvature $\chi^{el} = \{\chi_1^{el}, \chi_2^{el}\}$. Double integration of Eq.(5.4) (where $\chi = \chi^{el} + \chi^{in} = \chi^{el}$) and prescription of essential boundary conditions (5.25) lead to the nonlocal displacement field $v = \{v_1, v_2\}$. Same nonlocal results can be obtained by following the differential methodology explained in Sec.5.4. Non-dimensional plots of nonlocal fields are shown in the following. Analytical expressions of solutions are omitted for brevity. Fig.5.4 shows that the nonlocal elastic curvature becomes lower and uniform as $\lambda$ increases and for $\lambda = 0^+$ the local elastic curvature is recovered for $\bar{x} \in ]0, 1] - \{\bar{x}_d\}$. Non-dimensional transverse displacements $\bar{v}$ become smaller in modulus for increasing values of the nonlocal parameter (see Fig.5.5).

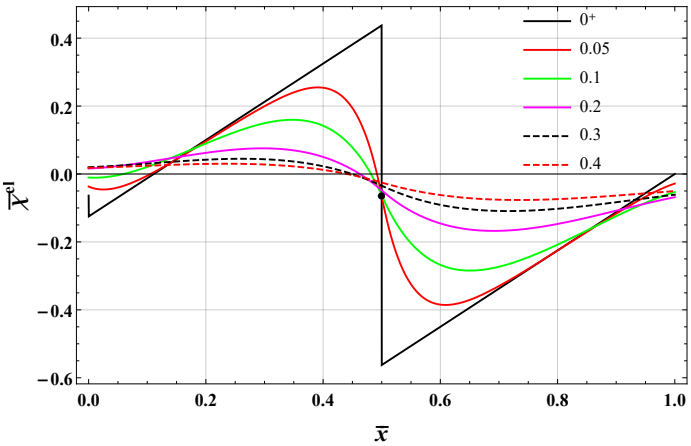


Figure 5.4: Beam with clamped and simply supported ends under concentrated couple $\mathcal{M}$ at mid-span $\bar{x} = 1/2$: elastic curvature $\bar{\chi}^{el}$ versus $\bar{x}$ for increasing nonlocal parameter $\lambda$.

## 5.7 Assembled structural problem

Let us apply the proposed stress-driven nonlocal methodology to an articulated assemblage of slender elastic beams under concentrated couple and piecewise smooth distributed loading and thermal distortion (see Fig.5.6).

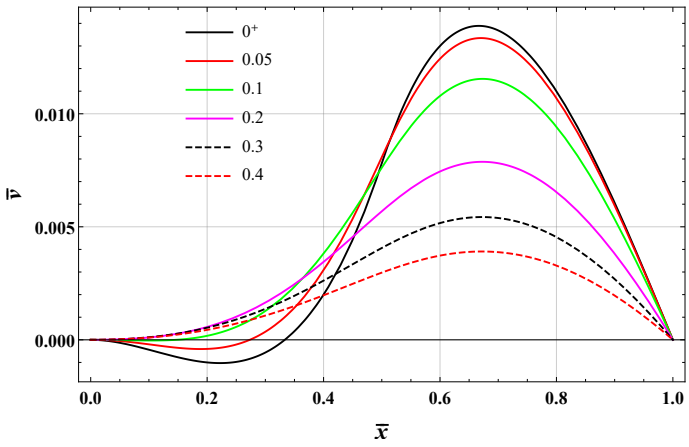


Figure 5.5: Beam with clamped and simply supported ends under concentrated couple $\mathcal{M}$ at mid-span $\bar{x} = 1/2$: transverse displacement $\bar{v}$ versus $\bar{x}$ for increasing nonlocal parameter $\lambda$.

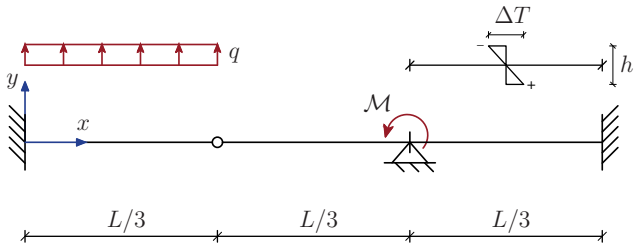


Figure 5.6: Assemblage of beams under concentrated couple, piecewise smooth distributed loading and thermal distortion.

The beam domain $[0, L]$ is partitioned in three subdomains. Accordingly, the relevant nonlocal elastic equilibrium problem can be formulated in terms of transverse displacement field $v = \{ v_1, v_2, v_3 \}$. Constitutive law (5.11) (rewritten in the three intervals) is differentiated twice; then, equilibrium is enforced, that is $\partial_x^2 M = \partial_x^2 \{ M_1, M_2, M_3 \} = \{ q, 0, 0 \}$; finally, kinematic compatibility conditions are prescribed.

Following these steps, the resulting differential problem of nonlocal elastic

equilibrium is thus formulated

$$\begin{cases} \dfrac{1}{c^2}\partial_x^4 v_1(x) - \partial_x^6 v_1(x) = \dfrac{1}{c^2}\left(\dfrac{q}{I_{E1}} + \partial_x^2 \chi^{nel}(x)\right) - \partial_x^4 \chi^{nel}(x)\,, & x \in \left[0, \dfrac{L}{3}\right], \\ \dfrac{1}{c^2}\partial_x^4 v_2(x) - \partial_x^6 v_2(x) = \dfrac{1}{c^2}\,\partial_x^2 \chi^{nel}(x) - \partial_x^4 \chi^{nel}(x)\,, & x \in \left[\dfrac{L}{3}, \dfrac{2L}{3}\right], \\ \dfrac{1}{c^2}\partial_x^4 v_3(x) - \partial_x^6 v_3(x) = \dfrac{1}{c^2}\,\partial_x^2 \chi^{nel}(x) - \partial_x^4 \chi^{nel}(x)\,, & x \in \left[\dfrac{2L}{3}, L\right]. \end{cases} \tag{5.27}$$

Solution field of transverse displacement $\{ v_1, v_2, v_3 \}$ is evaluated by integrating the differential system (5.27) along with prescription of essential and natural boundary conditions, and constitutive and interface boundary conditions. Last set of boundary conditions (BC), i.e. non-standard and continuity BC, are respectively expressed in terms of displacements by

$$\begin{cases} \partial_x^3 v_1(0) - \partial_x \chi^{nel}(0) = \dfrac{1}{c}\left(\partial_x^2 v_1(0) - \chi^{nel}(0)\right), \\ \partial_x^3 v_3(L) - \partial_x \chi^{nel}(L) = -\dfrac{1}{c}\left(\partial_x^2 v_3(L) - \chi^{nel}(L)\right), \end{cases} \tag{5.28}$$

and

$$\begin{cases} \partial_x^2 v_1(L/3) = \partial_x^2 v_2(L/3)\,, \\ \partial_x^3 v_1(L/3) = \partial_x^3 v_2(L/3)\,, \\ \partial_x^2 v_2(2L/3) = \partial_x^2 v_3(2L/3)\,, \\ \partial_x^3 v_2(2L/3) = \partial_x^3 v_3(2L/3)\,. \end{cases} \tag{5.29}$$

**Remark 5.7.1** *Nonlocal non-elastic curvature* $\chi^{nel}$ *is defined as the integral convolution between the averaging kernel* $\phi_c$ *and the prescribed local non-elastic curvature* $\chi^* : [a, b] \to \Re$. *That is*

$$\chi^{nel}(x) := \int_a^b \phi_c(x - \xi)\, \chi^*(x)\, d\xi \tag{5.30}$$

As depicted in Fig.5.6, a thermal distortion is applied in the interval $[\frac{2L}{3}, L]$; specifically, a butterfly shaped distortion with gradient $g_{\Delta T} := \frac{\Delta T}{h}$. Nonlocal non-elastic effects related to the applied thermal distortion are then provided

by the convolution integral in Eq.(5.30), that is

$$\chi^{nel}(x) = \chi^{th}(x) := \int_{\frac{2L}{3}}^{L} \phi_c(x-\xi)\,\alpha\, g_{\Delta T}\, d\xi\,, \qquad x \in [0, L]\,, \tag{5.31}$$

where $\alpha$ is the coefficient of linear isotropic thermal expansion. It is worth noting that although the butterfly shaped thermal distortion is vanishing in the interval $[0, \frac{2L}{3}]$ and only defined in $[\frac{2L}{3}, L]$, the corresponding nonlocal thermal curvature is defined on the whole structural domain $[0, L]$ due to long range effects modeled by integral convolution in Eq.(5.31).

The nonlocal elastic equilibrium problem is solved using the Mathematica software. In order to provide numerical values to the solver, we set $I_E = I_{E1} = I_{E2} = I_{E3}\,,\ L = 1$ and

$$\frac{qL^3}{I_E} = \frac{\mathcal{M}L}{I_E} = \frac{\alpha\Delta T}{h}L = 1\,. \tag{5.32}$$

Figure 5.7 shows nonlocal thermal curvatures for increasing nonlocal parameter $\lambda = c/L$. It is worth noting that convolution integral (5.31) has a smoothing effect on the applied thermal distortion. Moreover, the local ther-

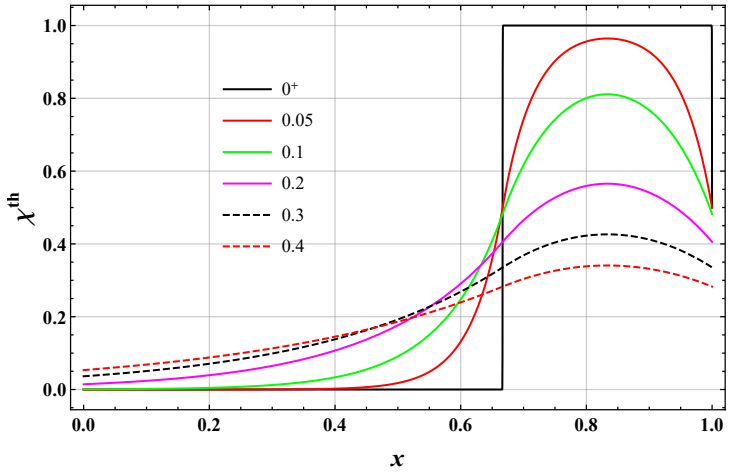


Figure 5.7: Thermal curvature $\chi^{th}$ versus $x$ for $\lambda \in \{0^+, 0.05, 0.1, 0.2, 0.3, 0.4\}$.

mal curvature is recovered for $x \in [0, L[-\{\frac{2L}{3}\}$ when the nonlocal parameter

tends to zero, $\lambda \to 0^+$. Nonlocal elastic curvature field $\chi^{el}$ for increasing $\lambda$ is depicted in Fig.5.8. As predicted by theoretical outcomes, nonlocal elastic curvatures are smooth functions for strictly positive values of nonlocal parameter. Limiting elastic curvature for $\lambda \to 0^+$ is coincident with the local one except

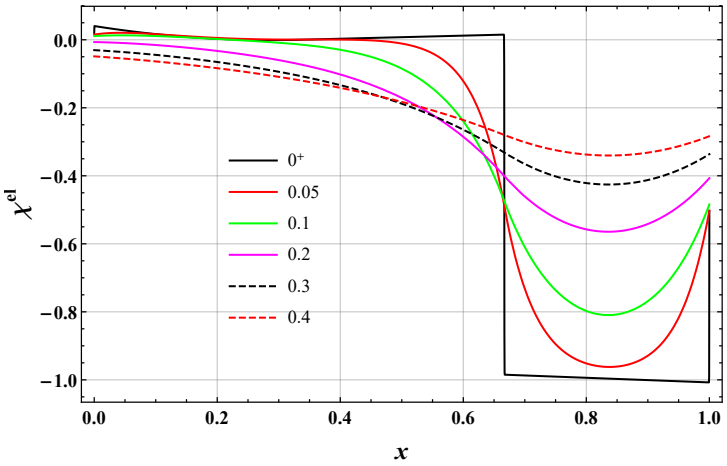


Figure 5.8: Elastic curvature $\chi^{el}$ versus $x$ for $\lambda \in \{0^+, 0.05, 0.1, 0.2, 0.3, 0.4\}$.

for the external boundaries $\{\,0,\,L\,\}$ and for the interface abscissa $\{\,\frac{2L}{3}\,\}$ where we get the asymptotic behaviors predicted in Eq.(5.19).

Total curvature fields $\chi$ are shown in Fig.5.9. It is apparent that for increasing $\lambda$ total curvatures become lower and uniform. For $\lambda \to 0^+$, the local total curvature is recovered $\forall x \in ]0, L[$. Finally, transverse displacement field $v$ as function of nonlocal parameter $\lambda$ is depicted in Fig.5.10 showing a stiffening behavior for increasing $\lambda$, in agreement with the smaller-is-stiffer phenomenon [74].

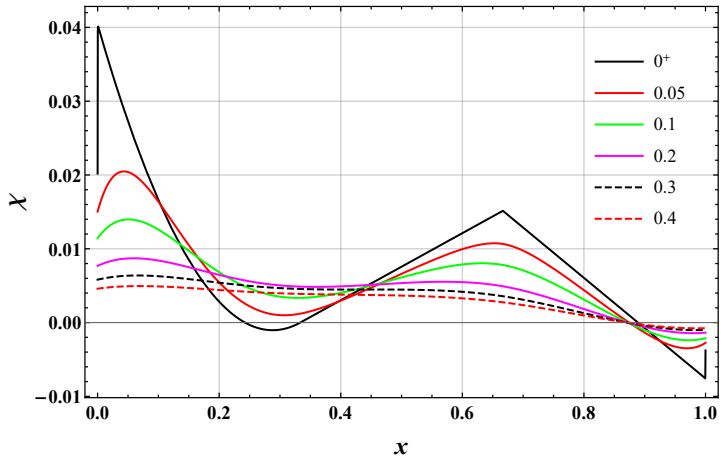


Figure 5.9: Total curvature $\chi$ versus $x$ for $\lambda \in \{0^+, 0.05, 0.1, 0.2, 0.3, 0.4\}$.

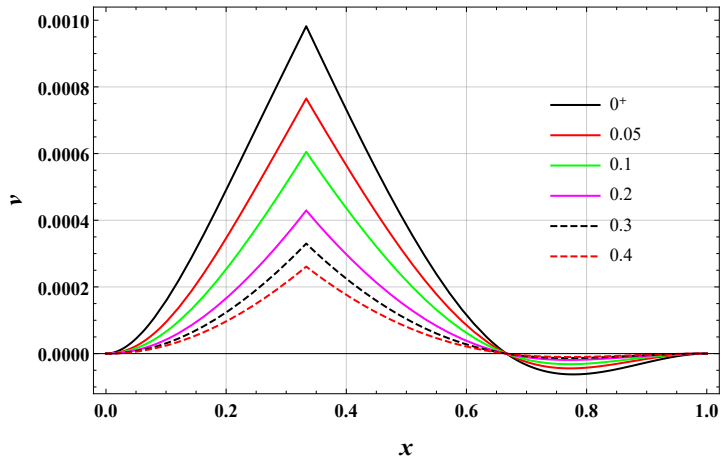


Figure 5.10: Displacement $v$ versus $x$ for $\lambda \in \{0^+, 0.05, 0.1, 0.2, 0.3, 0.4\}$.

# Chapter 6

# Nonlocal finite element formulation

## 6.1 Introductory remarks

By virtue of their exceptional mechanical, chemical and electrical properties, micro- and nano-structures have attracted lots of attention in the last decades [89–92]. As highlighted in Section 2, when dealing with small-scale continua the classical (local) elasticity theory leads to inaccurate results and thus, nonlocal continuum theories must be exploited to account for long range interaction forces and size-dependent mechanical behaviors in micro- and nano-structures.

Differential formulations of nonlocal elasticity have been widely applied for nanobeams [93, 94], nanoplates [95, 96] and nanoshells [97, 98], since they provide the possibility to reverse the constitutive laws of integral nonlocal elasticity. Among the most used methodologies for solving the governing differential equations, the Finite Element Method (FEM) is successfully applied to handle complex geometries, material properties and loading conditions in Structural Mechanics.

Thus, in scientific literature considerable attention is given to development of nonlocal finite element formulations. A two-noded nonlocal finite element with six degrees of freedom is provided in [99] to solve free vibration problems of functionally graded (FG) nanobeams. A nonlocal finite element formulation based on a five-noded finite element with ten degrees of freedom is provided in [100] to study free vibration and buckling behaviors of FG Timoshenko

nanobeams. A nonlocal finite element approach is proposed in [101] to analyse Reddy third-order plates. Nonlocal finite element nonlinear formulation for laminated composite plates is provided in [102]. Nonlocal finite element approach for free vibration analysis of axial rods embedded in elastic medium is performed in [103]. Mechanical behavior of thin laminated nanoplates is analysed in [104] by a FEM approach. A nonlinear finite element method is applied to investigate vibrations of nano-hetero-structures in thermal and magnetic fields in [105]. A nonlocal FE formulation of hereditary fractional-order Timoshenko beams is performed in [106].

In this chapter, a nonlocal finite element formulation based on the stress-driven (SD) integral model is illustrated by following the novel formulation developed in [107]. Long range interactions and size effects are introduced into the finite element methodology thanks to the differential formulation recently proposed in [59] where the stress-driven model is conceived to solve elastostatic problems involving articulated assemblage of nonlocal elastic beams, as deeply discussed in Section 5.

As shown in the following, the nonlocal finite element method based on the stress-driven approach is formulated in differential terms, by virtue of the constitutive boundary conditions and continuity conditions derived in [59]. This FE formulation is based on a two-noded element with two degrees of freedom for each node and the obtained nonlocal shape functions are $4N$ being $N$ the number of elements. A direct procedure to get the nonlocal stiffness matrix and nodal force vector of a single finite element is provided. Then, the global nonlocal stiffness matrix is derived by applying an assemblage procedure.

Benefits and novelties of the proposed approach rely on the fact that, unlike previous nonlocal finite element formulations, in the SD-FE methodology developed in [107] long range effects are not confined into the single finite element but they involve instead the entire structural assemblage. Moreover, SD-FEM provides the exact stress-driven nonlocal elastic solution, by considering a unique finite element or any other mesh involving a different number of FE. In agreement with the smaller-is-stiffer feature, the SD-FEM provides a stiffer structural response with respect to the classical (local) one, independently of prescribed kinematic boundary conditions and applied loadings.

## 6.2 Assemblage of nonlocal elastic beams

Let us consider a planar and straight slender beam of length $L$. The $x$- and $y$-coordinates are taken along beam and flexural axis, respectively. According

to the geometrically linearised theory of Bernoulli-Euler beam, cross-sections are clamped to the beam axis and thus kinematics is uniquely described by the transverse displacement field $v$. Indeed, rotation field of cross-sections are provided by the differential equation

$$\varphi := \partial_x v \tag{6.1}$$

where the symbol $\partial_x^n$ denotes $n-$differentiation along the beam axis $x$. Kinematic compatibility equation is expressed by the condition that the total flexural curvature $\chi$ must be equal to the geometric curvature, that is

$$\chi = \chi^{el} + \chi^{nel} = \partial_x^2 v \tag{6.2}$$

where $\chi^{nel}$ represents non-elastic curvature fields. By duality with the flexural curvature, the stress in the slender beam is the bending interaction field $M$ satisfying the equilibrium conditions specified below. For this purpose, let us denote by $q_y$ transverse distributed loading and by $\{\mathcal{F}_0, \mathcal{M}_0, \mathcal{F}_L, \mathcal{M}_L\}$ boundary concentrated forces and couples. Equilibrium conditions are expressed by the equation $\partial_x^2 M = q_y$ in $[0, L]$ equipped with the boundary conditions: $-T(0)\,\delta v(0) = \mathcal{F}_0\,\delta v(0)\,,\ -M(0)\,\partial_x \delta v(0) = \mathcal{M}_0\,\partial_x \delta v(0)\,,\ T(L)\,\delta v(L) = \mathcal{F}_L\,\delta v(L)\,,\ M(L)\,\partial_x \delta v(L) = \mathcal{M}_L\,\partial_x \delta v(L)$, where $T := -\partial_x M$ is the shearing interaction field and $\delta v$ represents any transverse virtual displacement field fulfilling homogeneous kinematic boundary conditions.

Now, let us partition the domain $\Omega = [0, L]$ in $N$ homogeneous subdomains $\Omega_i = [x_{i-1}, x_i] \subset \Omega$, with $i \in \{1, \ldots, N\}$ and end points $x_0 = 0$ and $x_N = L$, fulfilling the conditions $\cup_{i=1}^N \Omega_i = \Omega$ and $\mathring{\Omega}_i \cap \mathring{\Omega}_j = \varnothing$ for any element with $i \neq j$. Thus we have $N-1$ internal boundaries given by abscissae $x_1$, $x_2$, …, $x_{N-1}$. On each subdomain it is defined a smooth elastic curvature

$$\chi_i^{el} = \frac{M_i\,(x)}{I_{Ei}} : [x_{i-1}, x_i] \to \Re \tag{6.3}$$

where $M_i\,(x)$ is the bending interaction field pertaining to the $i-$th element $\Omega_i$ of the nanobeam and $I_{Ei}$ is the elastic bending stiffness, i.e. second moment of Euler-Young elastic moduli $E$ on cross-section $A_i$

$$I_{Ei} = \int_{A_i} E\,(y)\,y^2 dA\,. \tag{6.4}$$

Hereinafter the symbolism $\chi := \chi^{el}$ will be adopted, since no non-elastic effect will be considered.

Following the nonlocal stress-driven integral model (SD), flexural curvature is got in terms of the following convolution

$$\chi(x) = \left(\phi * \frac{M}{I_E}\right)(x) := \int_0^L \phi(x-t,c)\frac{M\,(t)}{I_E}dt \tag{6.5}$$

where $\phi$ is a scalar kernel described by a nonlocal length-scale parameter $c > 0$. The piecewise regular bending curvature $\chi(x) = \{\chi_1\,(x), \ldots, \chi_N\,(x)\}$ in Eq. (6.5) can be explicitly rewritten as follows [59]

$$\chi\,(x) = \begin{cases} \displaystyle\int_{x_0}^{x_1} \exp\left(-\frac{|x-t|}{c}\right)\frac{M_1\,(t)}{2cI_{E1}}dt + \sum_{i=2}^{N}\int_{x_{i-1}}^{x_i} \exp\left(\frac{x-t}{c}\right)\frac{M_i\,(t)}{2cI_{Ei}}dt \\ \ldots \\ \displaystyle\sum_{i=1}^{\bar{i}-1}\int_{x_{i-1}}^{x_i} \exp\left(\frac{t-x}{c}\right)\frac{M_i\,(t)}{2cI_{Ei}}dt + \int_{x_{\bar{i}-1}}^{x_{\bar{i}}} \exp\left(-\frac{|x-t|}{c}\frac{M_{\bar{i}}\,(t)}{2cI_{E\bar{i}}}dt\right) \\ \displaystyle + \sum_{i=\bar{i}+1}^{N}\int_{x_{i-1}}^{x_i} \exp\left(\frac{x-t}{c}\right)\frac{M_i\,(t)}{2cI_{Ei}}dt \\ \ldots \\ \displaystyle\sum_{i=1}^{N-1}\int_{x_{i-1}}^{x_i} \exp\left(\frac{t-x}{c}\right)\frac{M_i\,(t)}{2cI_{Ei}}dt + \int_{x_{N-1}}^{x_N} \exp\left(-\frac{|x-t|}{c}\right)\frac{M_N\,(t)}{2cI_{EN}}dt \end{cases} \tag{6.6}$$

where the special averaging kernel given by the bi-exponential Helmholtz's function has been adopted, that is

$$\phi\,(x,c) := \frac{1}{2c}\exp\left(-\frac{|x|}{c}\right). \tag{6.7}$$

Indeed, choice of the special kernel in Eq.(6.7) leads to an equivalent differential constitutive problem. Specifically, the nonlocal elastic curvature $\chi$ is the unique solution of the following set of $N$ differential equations [59]

$$\frac{1}{c^2}\chi_i(x) - \partial_x^2\chi_i(x) = \frac{1}{c^2}\frac{M_i}{I_{Ei}}\,(x) \qquad x \in \Omega_i \tag{6.8}$$

with $i \in \{1, \ldots, N\}$, equipped with two constitutive boundary conditions (CBCs) at $\partial[0, L]$

$$\begin{cases} \partial_x \chi_1 (0) - \dfrac{1}{c} \chi_1 (0) = 0 \\ \partial_x \chi_N (L) + \dfrac{1}{c} \chi_N (L) = 0 \end{cases} \tag{6.9}$$

and $2(N-1)$ constitutive continuity conditions (CCCs), or interface conditions, at internal abscissae $x_i$

$$\begin{cases} \chi_i (x_i) - \chi_{i+1} (x_i) = 0 \\ \partial_x \chi_i (x_i) - \partial_x \chi_{i+1} (x_i) = 0 \end{cases} \qquad i \in \{1, \ldots, N-1\} . \tag{6.10}$$

The relevant nonlocal elastic problem of equilibrium can be also formulated in the unknown piecewise smooth field of transverse displacement $v(x) = \{v_1 (x), \ldots, v_i (x), \ \ldots, v_N (x)\}$, each one defined as

$$v_i : \Omega_i \to \Re . \tag{6.11}$$

For this purpose, equation (6.8) is differentiated twice to prescribe the differential equilibrium condition $\partial_x^2 M_i = q_{yi}$ with $i \in \{1, \ldots, N\}$, being $q_{yi}$ the distributed transverse loading on the element $\Omega_i$. Kinematic compatibility condition $\partial_x^2 v_i = \chi_i$ with $i \in \{1, \ldots, N\}$ is also taken into account. Following these steps, we get the set of six-order differential equations, that is

$$\frac{1}{c^2} \partial_x^4 v_i(x) - \partial_x^6 v_i(x) = \frac{1}{c^2} \frac{q_{yi}}{I_{Ei}} (x) \qquad x \in \Omega_{\ i} . \tag{6.12}$$

Thus, transverse displacement field $v(x) = \{v_1 (x), \ldots, v_i (x), \ldots, v_N (x)\}$ is got by solving the differential problem given by the $N$ sixth-order differential equations (6.12) equipped with $4N$ standard essential and/or natural boundary conditions, two constitutive boundary conditions in Eq.(6.9) and $2(N-1)$ constitutive continuity conditions in Eq.(6.10). Standard BCs, CBCs and CCCc

can be expressed in terms of transverse displacements $v_i$ as follows

$$\begin{cases} \left.\begin{array}{l} \{v\,(x)\,,\partial_x v\,(x)\,, \\ \quad I_{Ei}\partial_x^2 v_i(x) - c^2 I_{Ei}\partial_x^4 v_i(x), \\ \quad -I_{Ei}\partial_x^3 v_i(x) + c^2 I_{Ei}\partial_x^5 v_i(x)\}_{x=\{x_{i-1},x_i\}} \end{array}\right\} & \text{Essential and natural BCs} \\ & \text{with } i \in \{1,\ldots,N\} \\ \left.\begin{array}{l} \partial_x^3 v_1\,(0) - \dfrac{1}{c}\partial_x^2 v_1\,(0) = 0 \\ \partial_x^3 v_N\,(L) + \dfrac{1}{c}\partial_x^2 v_N\,(L) = 0 \end{array}\right\} & \text{CBCs} \\ \left.\begin{array}{l} \partial_x^2 v_i\,(x_i) - \partial_x^2 v_{i+1}\,(x_i) = 0 \\ \partial_x^3 v_i\,(x_i) - \partial_x^3 v_{i+1}\,(x_i) = 0 \end{array}\right\} & \text{CCCs} \\ & \text{with } i \in \{1,\ldots,N-1\}\,. \end{cases} \tag{6.13}$$

Finally, taking into account Eq.(6.8), bending interaction field $M_i$ on the generic element $\Omega_i = [x_{i-1}, x_i]$, writes as

$$M_i(x) = I_{Ei}\partial_x^2 v_i(x) - c^2 I_{Ei}\partial_x^4 v_i(x), \tag{6.14}$$

with $i \in \{1,\ldots,N\}$. Shearing interaction field $T_i$ follows from the definition $T := -\partial_x M$ , that is

$$T_i(x) = -I_{Ei}\partial_x^3 v_i(x) + c^2 I_{Ei}\partial_x^5 v_i(x). \tag{6.15}$$

## 6.3 Two-noded finite element

In this section, a nonlocal finite element methodology based on the stress-driven approach is formulated. Hereinafter, the proposed nonlocal FEM approach will be referred to as SD-FEM. The two-noded finite element pertaining to the $i-$th domain $\Omega_i = [x_{i-1}, x_i]$ is represented in Fig.6.1 along with the nodal degrees of freedom $\{u_{i1}, u_{i2}\}$, $\{u_{i3}, u_{i4}\}$, representing transverse displacements and rotations at each node, respectively.

The interpolated displacement field $v_i^h$ defined on the $i-$th element $\Omega_i$ is sum of the solution $\bar{v}_i$ of the homogeneous equation associated with Eq.(6.12) and a particular solution $\hat{v}$ for an assigned distributed loading $q_{yi}(x)$ . That is

$$v_i^h\,(x) = \bar{v}_i\,(x) + \hat{v}_i\,(x) \tag{6.16}$$

with $i \in \{1,\ldots,N\}$.

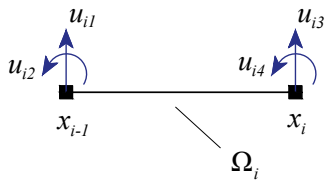


Figure 6.1: Beam element $\Omega_i$ with nodal degrees of freedom.

The integral $\bar{v}_i(x)$ of the homogeneous differential equation associated with Eq.(6.12) is given by

$$\bar{v}_i(x) = \sum_{j=1}^{4} a_{ij} x^{j-1} + \sum_{j=1}^{2} d_{ij} \exp\left((-1)^j \frac{x}{c}\right) \tag{6.17}$$

where $a_{ij}$, with $j \in \{1, \ldots, 4\}$, and $d_{ij}$, with $j \in \{1, 2\}$, are unknown real, dimensional constants for any element $\Omega_i$. Matrix form of Eq.(6.17) writes as

$$\bar{v}_i(x) = \mathbf{h}_0^T(x)\mathbf{a}_i + \mathbf{k}_0^T(x)\mathbf{d}_i \tag{6.18}$$

where (4,1) vectors $\mathbf{h}_0(x)$ and $\mathbf{a}_i$ and (2, 1) vectors $\mathbf{k}_0(x)$ and $\mathbf{d}_i$ are

$$\mathbf{h}_0(x) = \begin{bmatrix} 1 \\ x \\ x^2 \\ x^3 \end{bmatrix}, \quad \mathbf{k}_0(x) = \begin{bmatrix} \exp\left(-\frac{x}{c}\right) \\ \exp\left(\frac{x}{c}\right) \end{bmatrix}, \quad \mathbf{a}_i = \begin{bmatrix} a_{i1} \\ a_{i2} \\ a_{i3} \\ a_{i4} \end{bmatrix}, \quad \mathbf{d}_i = \begin{bmatrix} d_{i1} \\ d_{i2} \end{bmatrix}. \tag{6.19}$$

Without loss of generality, a linear variation of the external loading on the $i-$th element $\Omega_i$ is assumed. Thus, the transverse distributed loading $q_{yi}(x)$ is given by

$$q_{yi}(x) = q_{i,i-1} + \frac{q_{i,i} - q_{i,i-1}}{x_i - x_{i-1}}(x - x_{i-1}) \tag{6.20}$$

where $q_{i,i-1}$, $q_{i,i}$ are the values of the distributed loading $q_{yi}$ at the ends of the element $\Omega_i = [x_{i-1}, x_i]$, respectively. Accordingly, the complementary integral $\hat{v}_i(x)$ is given by

$$\hat{v}_i(x) = \frac{q_{i,i} - q_{i,i-1}}{120 I_{Ei}(x_i - x_{i-1})} x^5 - \frac{q_{i,i} x_{i-1} - q_{i,i-1} x_i}{24 I_{Ei}(x_i - x_{i-1})} x^4. \tag{6.21}$$

Moreover, it is useful to introduce the (4,1) and (2,1) vectors

$$\mathbf{h}_j(x) = \partial_x \mathbf{h}_{j-1}(x), \quad \mathbf{k}_j(x) = \partial_x \mathbf{k}_{j-1}(x) \quad j = \{1, 2, 3, \ldots\} \tag{6.22}$$

so that the following equalities hold

$$\begin{aligned} &\mathbf{h}_j(x) = 0 \quad j \geq 4, \\ &\mathbf{k}_j(x) = \frac{1}{c^j}\mathbf{k}_0(x) \quad j = \{2, 4, 6, \ldots\}, \\ &\mathbf{k}_l(x) = \frac{1}{c^l}\mathbf{k}_1(x) \quad l = \{3, 5, 7, \ldots\}. \end{aligned} \tag{6.23}$$

Then, the interpolated displacement field $v_i^h$ on the $i-$th element $\Omega_i$ can be written as

$$v_i^h(x) = \mathbf{h}_0^T(x)\mathbf{a}_i + \mathbf{k}_0^T(x)\mathbf{d}_i + \hat{v}_i(x) \tag{6.24}$$

so that the two CBCs, at the end points $x_0 = 0$ and $x_N = L$, and the $2(N-1)$ CCCs, at the $N-1$ internal points $x_i$, see Eqs.(6.13)$_{2-3}$, are expressed in terms of the parameter vectors $\mathbf{a}_i$, $\mathbf{d}_i$ in the following form

$$\begin{cases} \left(\mathbf{h}_3^T(0) - \dfrac{1}{c}\mathbf{h}_2^T(0)\right)\mathbf{a}_1 + \left(\mathbf{k}_3^T(0) - \dfrac{1}{c}\mathbf{k}_2^T(0)\right)\mathbf{d}_1 = \dfrac{1}{c}\partial_x^2\hat{v}_1(0) - \partial_x^3\hat{v}_1(0) \\ \ldots \\ \mathbf{h}_2^T(x_i)\mathbf{a}_i + \mathbf{k}_2^T(x_i)\mathbf{d}_i - \mathbf{h}_2^T(x_i)\mathbf{a}_{i+1} - \mathbf{k}_2^T(x_i)\mathbf{d}_{i+1} = \partial_x^2\hat{v}_{i+1}(x_i) - \partial_x^2\hat{v}_i(x_i) \\ \mathbf{h}_3^T(x_i)\mathbf{a}_i + \mathbf{k}_3^T(x_i)\mathbf{d}_i - \mathbf{h}_3^T(x_i)\mathbf{a}_{i+1} - \mathbf{k}_3^T(x_i)\mathbf{d}_{i+1} = \partial_x^3\hat{v}_{i+1}(x_i) - \partial_x^3\hat{v}_i(x_i) \\ \ldots \\ \left(\mathbf{h}_3^T(L) + \dfrac{1}{c}\mathbf{h}_2^T(L)\right)\mathbf{a}_N + \left(\mathbf{k}_3^T(L) + \dfrac{1}{c}\mathbf{k}_2^T(L)\right)\mathbf{d}_N = -\dfrac{1}{c}\partial_x^2\hat{v}_N(L) - \partial_x^3\hat{v}_N(L) \end{cases} \tag{6.25}$$

with $i \in \{1, \ldots, N-1\}$.

The interpolating bending $M_i^h$ and shearing $T_i^h$ interaction fields of the $i-$th element $\Omega_i$ follow from Eqs. (6.14) and (6.15), using Eqs.(6.23), that is

$$\begin{cases} M_i^h(x) = I_{Ei}\mathbf{h}_2^T(x)\mathbf{a}_i + I_{Ei}\left(\partial_x^2\hat{v}_i(x) - c^2\partial_x^4\hat{v}_i(x)\right), \\ T_i^h(x) = -I_{Ei}\mathbf{h}_3^T(x)\mathbf{a}_i - I_{Ei}\left(\partial_x^3\hat{v}_i(x) - c^2\partial_x^5\hat{v}_i(x)\right). \end{cases} \tag{6.26}$$

The generalized displacement vector $\mathbf{u}_i$ of the $i-$th element $\Omega_i$, the generalized displacement vector $\bar{\mathbf{u}}_i$ associated with the homogeneous solution and the

particular generalized displacement vector $\hat{\mathbf{u}}_i$ associated with the complementary solution are given by

$$\begin{aligned}
\mathbf{u}_i &= \begin{bmatrix} u_{i1} \\ u_{i2} \\ u_{i3} \\ u_{i4} \end{bmatrix} = \begin{bmatrix} v_i^h(x_{i-1}) \\ \varphi_i^h(x_{i-1}) \\ v_i^h(x_i) \\ \varphi_i^h(x_i) \end{bmatrix}, \quad \bar{\mathbf{u}}_i = \begin{bmatrix} \bar{u}_{i1} \\ \bar{u}_{i2} \\ \bar{u}_{i3} \\ \bar{u}_{i4} \end{bmatrix} = \begin{bmatrix} \bar{v}_i(x_{i-1}) \\ \bar{\varphi}_i(x_{i-1}) \\ \bar{v}_i(x_i) \\ \bar{\varphi}_i(x_i) \end{bmatrix}, \\
\hat{\mathbf{u}}_i &= \begin{bmatrix} \hat{u}_{i1} \\ \hat{u}_{i2} \\ \hat{u}_{i3} \\ \hat{u}_{i4} \end{bmatrix} = \begin{bmatrix} \hat{v}_i(x_{i-1}) \\ \hat{\varphi}_i(x_{i-1}) \\ \hat{v}_i(x_i) \\ \hat{\varphi}_i(x_i) \end{bmatrix}.
\end{aligned} \tag{6.27}$$

Thus Eqs.(6.16) and (6.27) yield

$$\mathbf{u}_i = \bar{\mathbf{u}}_i + \hat{\mathbf{u}}_i \quad \text{with } i \in \{1, \dots, N\}. \tag{6.28}$$

For further use, vector parameters $\mathbf{a}_i$, $\mathbf{u}_i$, $\hat{\mathbf{u}}_i$ can be collected in ($4N$,1) global vectors and vector parameter $\mathbf{d}_i$ can be collected in a ($2N$,1) global vector. That is

$$\begin{aligned}
\mathbf{a} &= \begin{bmatrix} \mathbf{a}_1^T & \dots & \mathbf{a}_N^T \end{bmatrix}^T, \quad \mathbf{d} = \begin{bmatrix} \mathbf{d}_1^T & \dots & \mathbf{d}_N^T \end{bmatrix}^T, \\
\mathbf{u} &= \begin{bmatrix} \mathbf{u}_1^T & \dots & \mathbf{u}_N^T \end{bmatrix}^T, \quad \hat{\mathbf{u}} = \begin{bmatrix} \hat{\mathbf{u}}_1^T & \dots & \hat{\mathbf{u}}_N^T \end{bmatrix}^T.
\end{aligned} \tag{6.29}$$

Then, recalling that the interpolating rotation field of the $i-$th element $\Omega_i$ is expressed as $\varphi_i^h = \partial_x v_i^h$ and using Eq.(6.24), the generalized displacement vectors $\mathbf{u}_i$ in Eq.(6.28) are rewritten in terms of the global parameter vectors $\mathbf{a}$ and $\mathbf{d}$ in the form

$$\left.\begin{aligned}
&\mathbf{u}_1 = \mathbf{A}_{11}\mathbf{a}_1 + \mathbf{A}_{12}\mathbf{d}_1 + \hat{\mathbf{u}}_1 \\
&\dots \\
&\mathbf{u}_i = \mathbf{A}_{i1}\mathbf{a}_i + \mathbf{A}_{i2}\mathbf{d}_i + \hat{\mathbf{u}}_i \\
&\dots \\
&\mathbf{u}_N = \mathbf{A}_{N1}\mathbf{a}_N + \mathbf{A}_{N2}\mathbf{d}_N + \hat{\mathbf{u}}_N
\end{aligned}\right\} \Longleftrightarrow \mathbf{u} = \mathbf{A}_1\mathbf{a} + \mathbf{A}_2\mathbf{d} + \hat{\mathbf{u}} \tag{6.30}$$

where the (4,4), (4,2) matrices $\mathbf{A}_{i1}$, $\mathbf{A}_{i2}$ and the ($4N$,$4N$), ($4N$,$2N$) matrices $\mathbf{A}_1$, $\mathbf{A}_2$ are defined in subsection Appendix (see Eq.(6.37)).

Analogously, the CBCs and the CCCs Eqs.(6.25) can be rewritten as

$$\left.\begin{aligned}
&\mathbf{H}_0\mathbf{a}_1 + \mathbf{D}_0\mathbf{d}_1 = t_0 \\
&\dots \\
&\mathbf{H}_i\mathbf{a}_i + \mathbf{D}_i\mathbf{d}_i - \mathbf{H}_i\mathbf{a}_{i+1} - \mathbf{D}_i\mathbf{d}_{i+1} = \mathbf{t}_i \\
&\dots \\
&\mathbf{H}_N\mathbf{a}_N + \mathbf{D}_N\mathbf{d}_N = t_N
\end{aligned}\right\} \Longleftrightarrow \mathbf{H}\mathbf{a} + \mathbf{D}\mathbf{d} = \mathbf{t} \tag{6.31}$$

where the (2,4), (2,2) matrices $\mathbf{H}_i$, $\mathbf{D}_i$, the $(2N,4N)$, $(2N,2N)$ matrices $\mathbf{H}$, $\mathbf{D}$, the scalars $t_0$, $t_N$ and the (2,1), $(2N,1)$ vectors $\mathbf{t}_i$, $\mathbf{t}$ are provided in subsection Appendix (see Eqs.(6.38)-(6.39)).

Unlike the classical (local) finite element method, it is necessary a preliminary step in order to express the global parameter vectors $\mathbf{a}$ and $\mathbf{d}$ in terms of the global generalized displacement vector $\mathbf{u}$.

Indeed, solving the CBCs and the CCCs in Eqs.(6.31), the global parameter vector $\mathbf{d}$ can be expressed in terms of the global parameter vector $\mathbf{a}$ as

$$\mathbf{d} = -\mathbf{D}^{-1}\mathbf{H}\mathbf{a} + \mathbf{D}^{-1}\mathbf{t}. \tag{6.32}$$

Substituting the parameter vector $\mathbf{d}$ in Eqs.(6.30), the generalized displacement vector $\mathbf{u}$ can be rewritten in the form

$$\mathbf{u} = \left(\mathbf{A}_1 - \mathbf{A}_2\mathbf{D}^{-1}\mathbf{H}\right)\mathbf{a} + \mathbf{A}_2\mathbf{D}^{-1}\mathbf{t} + \hat{\mathbf{u}} = \mathbf{A}\mathbf{a} + \mathbf{A}_2\mathbf{D}^{-1}\mathbf{t} + \hat{\mathbf{u}} \tag{6.33}$$

where the $(4N,4N)$ matrix $\mathbf{A}$ is $\mathbf{A} = \mathbf{A}_1 - \mathbf{A}_2\mathbf{D}^{-1}\mathbf{H}$. It is worth noting that the matrix $\mathbf{A}$ can be inverted since the matrix $\mathbf{A}_1$ is nonsingular and it results, see [108]

$$\mathbf{A}^{-1} = \mathbf{A}_1^{-1} + \mathbf{A}_1^{-1}\mathbf{A}_2\left(\mathbf{D} - \mathbf{H}\mathbf{A}_1^{-1}\mathbf{A}_2\right)^{-1}\mathbf{H}\mathbf{A}_1^{-1}. \tag{6.34}$$

Finally, from Eq.(6.33), we obtain the global parameter vector $\mathbf{a}$ in terms of the generalized displacement vector $\mathbf{u}$ and of the complementary vectors $\mathbf{t}$, $\hat{\mathbf{u}}$ in the form

$$\mathbf{a} = \mathbf{A}^{-1}\mathbf{u} - \mathbf{A}^{-1}\mathbf{A}_2\mathbf{D}^{-1}\mathbf{t} - \mathbf{A}^{-1}\hat{\mathbf{u}}. \tag{6.35}$$

Using Eqs.(6.32) and (6.35), the expression of the global parameter vector $\mathbf{d}$ in terms of $\mathbf{u}$, $\mathbf{t}$ and $\hat{\mathbf{u}}$ is given by

$$\mathbf{d} = -\mathbf{D}^{-1}\mathbf{H}\mathbf{A}^{-1}\mathbf{u} + \left(\mathbf{D}^{-1}\mathbf{H}\mathbf{A}^{-1}\mathbf{A}_2\mathbf{D}^{-1} + \mathbf{D}^{-1}\right)\mathbf{t} + \mathbf{D}^{-1}\mathbf{H}\mathbf{A}^{-1}\hat{\mathbf{u}}. \tag{6.36}$$

**Appendix**

The following matrices have been introduced in Eq.(6.30)

$$\mathbf{A}_{i1} = \begin{bmatrix} \mathbf{h}_0^T(x_{i-1}) \\ \mathbf{h}_1^T(x_{i-1}) \\ \mathbf{h}_0^T(x_i) \\ \mathbf{h}_1^T(x_i) \end{bmatrix}, \quad \mathbf{A}_{i2} = \begin{bmatrix} \mathbf{k}_0^T(x_{i-1}) \\ \mathbf{k}_1^T(x_{i-1}) \\ \mathbf{k}_0^T(x_i) \\ \mathbf{k}_1^T(x_i) \end{bmatrix},$$

$$\mathbf{A}_1 = diag\left[\mathbf{A}_{i1}\right] = \begin{bmatrix} \mathbf{A}_{11} & \mathbf{0} & \mathbf{0} & \mathbf{0} \\ \mathbf{0} & \mathbf{A}_{21} & \mathbf{0} & \mathbf{0} \\ \mathbf{0} & \mathbf{0} & \dots & \mathbf{0} \\ \mathbf{0} & \mathbf{0} & \mathbf{0} & \mathbf{A}_{N1} \end{bmatrix}, \tag{6.37}$$

$$\mathbf{A}_2 = diag\left[\mathbf{A}_{i2}\right] = \begin{bmatrix} \mathbf{A}_{12} & \mathbf{0} & \mathbf{0} & \mathbf{0} \\ \mathbf{0} & \mathbf{A}_{22} & \mathbf{0} & \mathbf{0} \\ \mathbf{0} & \mathbf{0} & \dots & \mathbf{0} \\ \mathbf{0} & \mathbf{0} & \mathbf{0} & \mathbf{A}_{N2} \end{bmatrix}$$

with $i \in \{1, \dots, N\}$. Moreover, the following matrices have been defined in Eq.(6.31)

$$\mathbf{H}_0 = \left[\mathbf{h}_3^T(0) - \frac{1}{c}\mathbf{h}_2^T(0)\right], \quad \mathbf{D}_0 = \left[\mathbf{k}_3^T(0) - \frac{1}{c}\mathbf{k}_2^T(0)\right]$$

$$\mathbf{H}_i = \begin{bmatrix} \mathbf{h}_2^T(x_i) \\ \mathbf{h}_3^T(x_i) \end{bmatrix}, \quad \mathbf{D}_i = \begin{bmatrix} \mathbf{k}_2^T(x_i) \\ \mathbf{k}_3^T(x_i) \end{bmatrix} \quad i \in \{1, \dots, N-1\},$$

$$\mathbf{H}_N = \left[\mathbf{h}_3^T(L) + \frac{1}{c}\mathbf{h}_2^T(L)\right], \quad \mathbf{D}_N = \left[\mathbf{k}_3^T(L) + \frac{1}{c}\mathbf{k}_2^T(L)\right]$$

$$\mathbf{H} = \begin{bmatrix} \mathbf{H}_0 & \mathbf{0} & \mathbf{0} & & \mathbf{0} \\ \mathbf{H}_1 & -\mathbf{H}_1 & \mathbf{0} & & \mathbf{0} \\ \mathbf{0} & \mathbf{H}_2 & -\mathbf{H}_2 & & \mathbf{0} \\ & & & \dots & \\ \mathbf{0} & \mathbf{0} & \mathbf{0} & & \mathbf{H}_N \end{bmatrix}, \quad \mathbf{D} = \begin{bmatrix} \mathbf{D}_0 & \mathbf{0} & \mathbf{0} & & \mathbf{0} \\ \mathbf{D}_1 & -\mathbf{D}_1 & \mathbf{0} & & \mathbf{0} \\ \mathbf{0} & \mathbf{D}_2 & -\mathbf{D}_2 & & \mathbf{0} \\ & & & \dots & \\ \mathbf{0} & \mathbf{0} & \mathbf{0} & & \mathbf{D}_N \end{bmatrix} \tag{6.38}$$

with

$$
\begin{aligned}
t_0 &= \frac{1}{c}\partial_x^2\hat{v}_1\left(0\right) - \partial_x^3\hat{v}_1\left(0\right), \quad t_N = -\frac{1}{c}\partial_x^2\hat{v}_N\left(L\right) - \partial_x^3\hat{v}_N\left(L\right) \\
\mathbf{t}_i &= \begin{bmatrix} \partial_x^2\hat{v}_{i+1}\left(x_i\right) - \partial_x^2\hat{v}_i\left(x_i\right) \\ \partial_x^3\hat{v}_{i+1}\left(x_i\right) - \partial_x^3\hat{v}_i\left(x_i\right) \end{bmatrix} \quad i \in \{1,\ldots,N-1\}, \\
\mathbf{t} &= \begin{bmatrix} t_0 & \mathbf{t}_1^T & \mathbf{t}_2^T & \ldots & t_N \end{bmatrix}^T.
\end{aligned}
\tag{6.39}
$$

### 6.3.1 Nonlocal shape functions

In order to derive the shape functions according to the proposed SD-FEM, we consider the interpolated displacement $\bar{v}_i$ Eq.(6.18) associated with the homogeneous solution of Eq.(6.12). The expressions of the corresponding global parameter vectors $\mathbf{a}$ and $\mathbf{d}$ in terms of the generalized displacement vector $\mathbf{u}$ derive from Eqs.(6.35)-(6.36) setting $\mathbf{t} = \hat{\mathbf{u}} = \mathbf{0}$. Hence we have

$$
\mathbf{a} = \mathbf{A}^{-1}\mathbf{u} \tag{6.40}
$$

and

$$
\mathbf{d} = -\mathbf{D}^{-1}\mathbf{H}\mathbf{A}^{-1}\mathbf{u}. \tag{6.41}
$$

Now, let us introduce the tensors $\mathcal{P}_{ai}$ and $\mathcal{P}_{di}$ denoting, respectively, the (4,4$N$) and (2,2$N$) extractor operators that pick up from the global parameter vectors $\mathbf{a}$ and $\mathbf{d}$ the corresponding parameters pertaining to the $i-$th element $\Omega_i$ according to the following parametric relations

$$
\mathbf{a}_i = \mathcal{P}_{ai}\mathbf{a}, \quad \mathbf{d}_i = \mathcal{P}_{di}\mathbf{d}. \tag{6.42}
$$

Then, substituting Eqs.(6.40) and (6.41) into Eq.(6.18) of the interpolated transverse displacement $\bar{v}_i\left(x\right)$ of the $i-$th element $\Omega_i$, we get

$$
\begin{aligned}
\bar{v}_i\left(x\right) &= \mathbf{h}_0^T(x)\mathcal{P}_{ai}\mathbf{A}^{-1}\mathbf{u} - \mathbf{k}_0^T(x)\mathcal{P}_{di}\mathbf{D}^{-1}\mathbf{H}\mathbf{A}^{-1}\mathbf{u} \\
&= \left(\mathbf{h}_0^T(x)\mathcal{P}_{ai}\mathbf{A}^{-1} - \mathbf{k}_0^T(x)\mathcal{P}_{di}\mathbf{D}^{-1}\mathbf{H}\mathbf{A}^{-1}\right)\mathbf{u}.
\end{aligned}
\tag{6.43}
$$

Hence, the displacement function $\bar{v}_i\left(x\right)$ of the $i-$th element $\Omega_i$ Eq.(6.43) is provided by the following compact expression

$$
\bar{v}_i\left(x\right) = \mathbf{N}_i(x)\mathbf{u} \tag{6.44}
$$

where nonlocal shape functions of the two-noded element $\Omega_i$ are collected in the (1,4$N$) matrix $\mathbf{N}_i(x) = \left[ \begin{array}{cccc} \eta_{11}^{(i)}(x) & \eta_{12}^{(i)}(x) & \dots & \eta_{N4}^{(i)}(x) \end{array} \right]$ with $i \in \{1, \dots, N\}$ so that the nonlocal shape functions matrix is given by

$$\mathbf{N}_i(x) = \mathbf{h}_0^T(x)\mathcal{P}_{ai}\mathbf{A}^{-1} - \mathbf{k}_0^T(x)\mathcal{P}_{di}\mathbf{D}^{-1}\mathbf{H}\mathbf{A}^{-1}. \tag{6.45}$$

The superscript $i$ in shape function $\eta_{jk}^{(i)}(x)$ indicates the $i-$th element $\Omega_i$ while the subscripts $j \in \{1, \dots, N\}$ and $k \in \{1, \dots, 4\}$ identify the nodal generalized displacement $u_{jk} = 1$ contributing to the displacement function $\bar{v}_i(x)$. Then, the generic shape function at the position $(1, 4(j-1)+k)$ of the matrix $\mathbf{N}_i(x)$ represents the displacement function $\bar{v}_i(x)$ of the element $\Omega_i$ due to the unit generalized displacement $u_{jk} = 1$ at the node $x_{j-1}$ if $k \in \{1, 2\}$ and at the node $x_j$ if $k \in \{3, 4\}$.

It is worth noting that we have $4N$ shape functions pertaining to the $i-$th element $\Omega_i$ since the displacement function $\bar{v}_i(x)$ of the element $\Omega_i$ depends on the generalized displacement vector $\mathbf{u}$, as shown in Eq.(6.44). The nonlocal shape functions of the $i-$th element are also determined by the matrices $\mathbf{D}$ and $\mathbf{H}$ defined by the CBCs and CCCs in Eq.(6.31) so that the nonlocal shape functions of the SD-FEM depends on the considered mesh of the nanobeam.

### 6.3.2 Nonlocal stiffness matrix and nodal force vector

The vector $\mathbf{p}_i$ of the generalized forces of the $i-$th element $\Omega_i$ is defined as the dual of the element generalized displacement vector $\mathbf{u}_i$ in the form

$$\mathbf{p}_i = \left[ \begin{array}{c} \mathcal{F}_{i1} \\ \mathcal{M}_{i2} \\ \mathcal{F}_{i3} \\ \mathcal{M}_{i4} \end{array} \right] = \left[ \begin{array}{c} -T_i^h(x_{i-1}) \\ -M_i^h(x_{i-1}) \\ T_i^h(x_i) \\ M_i^h(x_i) \end{array} \right] \tag{6.46}$$

in which the conventions on the sign of shear force $T_i^h$ and bending moment $M_i^h$ have been taken into account.

Now, let us preliminary introduce the (4,4) matrix $\mathbf{B}_i$ and the (4,1) force vector $\hat{\mathbf{f}}_i$ defined as follows

$$\mathbf{B}_i = I_{Ei} \left[ \begin{array}{c} \mathbf{h}_3^T(x_{i-1}) \\ -\mathbf{h}_2^T(x_{i-1}) \\ -\mathbf{h}_3^T(x_i) \\ \mathbf{h}_2^T(x_i) \end{array} \right], \quad \hat{\mathbf{f}}_i = I_{Ei} \left[ \begin{array}{c} \partial_x^3 \hat{v}_i(x_{i-1}) - c^2 \partial_x^5 \hat{v}_i(x_{i-1}) \\ -\partial_x^2 \hat{v}_i(x_{i-1}) + c^2 \partial_x^4 \hat{v}_i(x_{i-1}) \\ -\partial_x^3 \hat{v}_i(x_i) + c^2 \partial_x^5 \hat{v}_i(x_i) \\ \partial_x^2 \hat{v}_i(x_i) - c^2 \partial_x^4 \hat{v}_i(x_i) \end{array} \right]. \tag{6.47}$$

Then, recalling the expressions of the interpolating bending moment $M_i^h$ and shear force $T_i^h$ of the element $\Omega_i$, the element generalized force vector $\mathbf{p}_i$ can be written as follows

$$\mathbf{p}_i = \mathbf{B}_i \mathcal{P}_{ai} \mathbf{A}^{-1} \mathbf{u} - \mathbf{B}_i \mathcal{P}_{ai} \mathbf{A}^{-1} \mathbf{A}_2 \mathbf{D}^{-1} \mathbf{t} - \mathbf{B}_i \mathcal{P}_{ai} \mathbf{A}^{-1} \hat{\mathbf{u}} + \hat{\mathbf{f}}_i \,. \tag{6.48}$$

By definition, the elemental nonlocal stiffness matrix $\mathbf{K}_i$ of the $i-$th element $\Omega_i$ relates the element generalized force vector $\mathbf{p}_i$ to the element generalized displacement vector $\mathbf{u}$. Hence the (4,4$N$) nonlocal stiffness matrix $\mathbf{K}_i$ of the $i-$th element $\Omega_i$ follows from the r.h.s. of Eq.(6.48) and is given by

$$\mathbf{K}_i = \mathbf{B}_i \mathcal{P}_{ai} \mathbf{A}^{-1}. \tag{6.49}$$

Note that the (4,4$N$) nonlocal stiffness matrix $\mathbf{K}_i$ of the $i-$th element is non-symmetric. The corresponding (4,1) force vector $\mathbf{f}_i$ of the $i-$th element $\Omega_i$ is

$$\mathbf{f}_i = \mathbf{B}_i \mathcal{P}_{ai} \mathbf{A}^{-1} \mathbf{A}_2 \mathbf{D}^{-1} \mathbf{t} + \mathbf{B}_i \mathcal{P}_{ai} \mathbf{A}^{-1} \hat{\mathbf{u}} - \hat{\mathbf{f}}_i. \tag{6.50}$$

Thus, the element generalized force vector $\mathbf{p}_i$ Eq.(6.48) becomes

$$\mathbf{p}_i = \mathbf{K}_i \mathbf{u} - \mathbf{f}_i. \tag{6.51}$$

The assembled finite element formulation follows from Eq.(6.51) adding up the contributions of each element $\Omega_i$ and imposing the conforming requirement to the interpolated displacement in the form

$$\sum_{i=1}^{N} \mathbf{p}_i \cdot \delta \mathbf{u}_i = \sum_{i=1}^{N} \mathbf{K}_i \mathcal{A} \mathbf{q} \cdot \mathcal{A}_i \delta \mathbf{q} - \sum_{i=1}^{N} \mathbf{f}_i \cdot \mathcal{A}_i \delta \mathbf{q} = 0, \tag{6.52}$$

for any $\delta \mathbf{u}_i = \mathcal{A}_i \delta \mathbf{q}$, where the dot stands for the inner product.

Direct determination of nonlocal stiffness matrix and force vector as expressed by Eq.(6.52) requires the definition of the assembly operator $\mathcal{A}_i$ which provides the generalized displacement vector $\mathbf{u}_i$ of the $i-$th element $\Omega_i$ in terms of the nodal displacement parameter $\mathbf{q}$ of the assembled finite element model by means of the following parametric relations

$$\mathbf{u}_i = \mathcal{A}_i \mathbf{q} \quad \text{and} \quad \mathbf{u} = \mathcal{A} \mathbf{q} \tag{6.53}$$

being $\mathcal{A}$ the global assembly operator given by

$$\mathcal{A} = \begin{bmatrix} \mathcal{A}_1 \\ \vdots \\ \mathcal{A}_N \end{bmatrix}. \tag{6.54}$$

Hence, from Eq.(6.52) we have

$$\sum_{i=1}^{N} \mathcal{A}_i^T \mathbf{K}_i \mathcal{A}\mathbf{q} = \sum_{i=1}^{N} \mathcal{A}_i^T \mathbf{f}_i \tag{6.55}$$

where the $(4N,4N)$ nonlocal stiffness matrix $\mathbf{K}$ and the $(4N,1)$ nonlocal force vector $\mathbf{f}$ are given by

$$\mathbf{K} = \sum_{i=1}^{N} \mathcal{A}_i^T \mathbf{K}_i \mathcal{A}, \quad \mathbf{f} = \sum_{i=1}^{N} \mathcal{A}_i^T \mathbf{f}_i. \tag{6.56}$$

The solving linear equation system for the SD-FEM is then achieved, id est

$$\mathbf{K}\mathbf{q} = \mathbf{f}. \tag{6.57}$$

It is worth noting that the assemblage procedure in Eq.$(6.56)_1$ provides the $(4N,4N)$ symmetric nonlocal stiffness matrix $\mathbf{K}$. Symmetry of the nonlocal stiffness matrix $\mathbf{K}$ can be proved as follows.

**Proposition 6.3.1** *The global nonlocal stiffness matrix* $\mathbf{K}$

$$\mathbf{K} = \sum_{i=1}^{N} \mathcal{A}_i^T \mathbf{K}_i \mathcal{A} \tag{6.58}$$

*with the element nonlocal stiffness matrix* $\mathbf{K}_i$ *defined as*

$$\mathbf{K}_i = \mathbf{B}_i \mathcal{P}_{ai} \mathbf{A}^{-1} \tag{6.59}$$

*is symmetric.*

**Proof 6.3.1** *Let us consider the equality*

$$\sum_{i=1}^{N} \mathbf{u}_i^T \mathbf{p}_i = \sum_{i=1}^{N} \mathbf{p}_i^T \mathbf{u}_i. \tag{6.60}$$

*Since Eq.(6.48) with* $\mathbf{t} = \hat{\mathbf{u}} = \hat{\mathbf{f}}_i = \mathbf{0}$ *yields*

$$\mathbf{p}_i = \mathbf{B}_i \mathcal{P}_{ai} \mathbf{A}^{-1} \mathbf{u}, \tag{6.61}$$

*the l.h.s. of Eq.(6.60) can be rewritten in the following form*

$$\sum_{i=1}^{N} \mathbf{u}_i^T \mathbf{p}_i = \sum_{i=1}^{N} \mathbf{q}^T \mathcal{A}_i^T \mathbf{B}_i \mathcal{P}_{ai} \mathbf{A}^{-1} \mathbf{u} \tag{6.62}$$

*being* $\mathbf{u}_i = \mathcal{A}_i \mathbf{q}$*, see Eq.(6.53)*$_1$*. Inserting Eq.(6.53)*$_2$ *in Eq.(6.62) we have*

$$\sum_{i=1}^{N} \mathbf{u}_i^T \mathbf{p}_i = \sum_{i=1}^{N} \mathbf{q}^T \mathcal{A}_i^T \mathbf{B}_i \mathcal{P}_{ai} \mathbf{A}^{-1} \mathcal{A} \mathbf{q} = \sum_{i=1}^{N} \mathbf{q}^T \mathcal{A}_i^T \mathbf{K}_i \mathcal{A} \mathbf{q} \tag{6.63}$$

*since* $\mathbf{K}_i = \mathbf{B}_i \mathcal{P}_{ai} \mathbf{A}^{-1}$*, see Eq.(6.49).*

*On the other side, recalling Eq.(6.61), the r.h.s. of Eq.(6.60) becomes*

$$\begin{aligned} &\sum_{i=1}^{N} \mathbf{p}_i^T \mathbf{u}_i = \sum_{i=1}^{N} \mathbf{u}^T \mathbf{A}^{-T} \mathcal{P}_{ai}^T \mathbf{B}_i^T \mathbf{u}_i = \sum_{i=1}^{N} \mathbf{u}^T \mathbf{A}^{-T} \mathcal{P}_{ai}^T \mathbf{B}_i^T \mathcal{A}_i \mathbf{q} \\ &= \sum_{i=1}^{N} \mathbf{q}^T \mathcal{A}^T \mathbf{A}^{-T} \mathcal{P}_{ai}^T \mathbf{B}_i^T \mathcal{A}_i \mathbf{q} = \sum_{i=1}^{N} \mathbf{q}^T \mathcal{A}^T \mathbf{K}_i^T \mathcal{A}_i \mathbf{q} \end{aligned} \tag{6.64}$$

*being* $\mathbf{u} = \mathcal{A}\mathbf{q}$*, see Eq.(6.53)*$_2$*.*

*Hence, using Eqs.(6.63) and (6.64), the equality Eq.(6.60) yields*

$$\mathbf{q}^T \left( \sum_{i=1}^{N} \mathcal{A}_i^T \mathbf{K}_i \mathcal{A} \right) \mathbf{q} = \mathbf{q}^T \left( \sum_{i=1}^{N} \mathcal{A}^T \mathbf{K}_i^T \mathcal{A}_i \right) \mathbf{q} \tag{6.65}$$

*so that, recalling the expression Eq.(6.56)*$_1$ *of the nonlocal stiffness matrix* $\mathbf{K}$*, we get*

$$\mathbf{K} = \sum_{i=1}^{N} \mathcal{A}_i^T \mathbf{K}_i \mathcal{A} = \sum_{i=1}^{N} \mathcal{A}^T \mathbf{K}_i^T \mathcal{A}_i = \mathbf{K}^T \tag{6.66}$$

*and the symmetry of the the nonlocal stiffness matrix* $\mathbf{K}$ *is proved.*

In the post–processing phase, the generalized displacement vector $\mathbf{u}$ can be obtained in terms of the nodal displacement parameter $\mathbf{q}$ by means of the parametric relation Eq.(6.53)$_2$. Then, the global parameters $\mathbf{a}$ and $\mathbf{d}$ follow from Eqs.(6.35)-(6.36) and the element-wise parameters $\mathbf{a}_i$ and $\mathbf{d}_i$ pertaining to the $i-$th element $\Omega_i$ can be immediately obtained using the parametric relations Eq.(6.42). Accordingly interpolating displacements, rotations, bending moment and shear force in the element $\Omega_i$ can be obtained by means of Equations (6.24) and (6.26).

## 6.4 Benchmark numerical results

The above illustrated stress-driven nonlocal finite element methodology is exploited to examine exemplar case-studies, involving common boundary and loading conditions in structural mechanics. Validation of the stress-driven finite element formulation is done by making a comparison with the closed form solutions of the investigated structural schemes.

The nanobeam is supposed to be made of aluminum (Al), which is a common material adopted in Nano-Engineering. The corresponding Euler-Young modulus is thus $E = 68.5\,GPa$. The nonlocal length-scale parameter is assumed to be $c = 1\,nm$.

Structural schemes, such as cantilever (C-F) and simply supported (S-S) micro/nanobeam, are commonly applied in small-scale electromechanical systems, like sensors, actuators, or in atomic force microscopes. Hence, the SD-FEM is here applied to cantilever and simply supported nanobeams under distributed loadings and the obtained results are compared with the corresponding closed form solutions of the nonlocal stress-driven elastostatic problem provided in [62]. Moreover, the SD-FEM is adopted for a nano-cantilever under concentrated force applied at internal point and for an articulated assemblage of nanobeams under a piecewise uniformly distributed loading and a concentrated couple. Then the results are compared with the corresponding nonlocal stress-driven closed form solutions obtained through the methodology presented in [59].

### 6.4.1 Simply supported nanobeam under distributed loading

Let us examine a simply supported nanobeam of length $L = 25\,nm$ under a uniformly distributed loading $q = 1\,nN/nm$. Height and width of cross-section are assumed to be $b = h = 1\,nm$. Validation is done by comparing the results with the closed form solution provided in [62] for the stress-driven nonlocal elastic problem of equilibrium.

First, let us consider a unique two-noded element $\Omega \equiv \Omega_1 = [0, L]$ so that the generalized displacement vector $\mathbf{u} = \mathbf{u}_1$ is expressed as

$$\mathbf{u} = \begin{bmatrix} u_{11} \\ u_{12} \\ u_{13} \\ u_{14} \end{bmatrix} = \begin{bmatrix} v^h(0) \\ \varphi^h(0) \\ v^h(L) \\ \varphi^h(L) \end{bmatrix} = \mathcal{A}\mathbf{q} \tag{6.67}$$

where the nodal displacement parameter is $\mathbf{q} = \begin{bmatrix} \varphi^h(0) & \varphi^h(L) \end{bmatrix}^T$. It is worth noting that only the two CBCs in Eqs.(6.31) must be prescribed since there are no internal points in $\Omega$ and then no CCCs have to be imposed. The shape functions of the nonlocal SD-FEM follow from from Eq.(6.45) and thus are collected in the (1,4) matrix $\mathbf{N}(x) = \begin{bmatrix} \eta_{11}(x) & \eta_{12}(x) & \eta_{13}(x) & \eta_{14}(x) \end{bmatrix}$. Explicit expressions of the nonlocal shape functions are

$$\begin{cases} \eta_{11}(x) = 0.994114 + 0.00588577x - 0.00544979x^2 + 0.000145328x^3 \\ \qquad +0.00588577^{-x} \\ \eta_{12}(x) = -0.0944055 + 1.09441x - 0.0889557x^2 + 0.0018166x^3 \\ \qquad +0.0944055^{-x} \\ \eta_{13}(x) = 0.00588577 - 0.00588577x + 0.00544979x^2 - 0.000145328x^3 \\ \qquad -0.00588577^{-x} \\ \eta_{14}(x) = -0.0527388 + 0.0527388x - 0.047289x^2 + 0.0018166x^3 \\ \qquad +0.0527388^{-x}. \end{cases} \tag{6.68}$$

The (4,4) element stiffness matrix $\mathbf{K}_1$ and the (4,1) force vector $\mathbf{f}_1$ of the element $\Omega$ can be obtained from Eqs.(6.49) and (6.50), that is

$$\mathbf{K}_1 = \mathbf{B}_1\mathbf{A}^{-1}, \quad \mathbf{f}_1 = \mathbf{B}_1\mathbf{A}^{-1}\mathbf{A}_2\mathbf{D}^{-1}\mathbf{t} + \mathbf{B}_1\mathbf{A}^{-1}\hat{\mathbf{u}} - \hat{\mathbf{f}}_1. \tag{6.69}$$

Hence, the solving linear equation system for the SD-FEM is $\mathcal{A}^T\mathbf{K}_1\mathcal{A}\mathbf{q} = \mathcal{A}^T\mathbf{f}_1$, see Eq.(6.56). Using the parametric relation Eq.(6.67), the generalized displacement vector $\mathbf{u}$ of the element $\Omega$ is

$$\mathbf{u} = \begin{bmatrix} 0 & 113.044 & 0 & -113.044 \end{bmatrix}^T. \tag{6.70}$$

Then, the interpolated displacement field $v^h$ Eq.(6.24) can be written as

$$v^h(x) = \mathbf{h}_0^T(x)\mathbf{a} + \mathbf{k}_0^T(x)\mathbf{d} + \frac{x^4}{24I_E} \tag{6.71}$$

where the global parameter vectors $\mathbf{a}$ and $\mathbf{d}$ are provided by Eqs.(6.35)-(6.36) in terms of the generalized displacement vector $\mathbf{u}$ Eq.(6.70)

$$\mathbf{a} = \begin{bmatrix} 1.18248 & 111.861 & 0.0875912 & -0.364964 \end{bmatrix}^T \quad \mathbf{d} = \begin{bmatrix} -1.18248 & 0 \end{bmatrix}^T. \tag{6.72}$$

The interpolated bending moment and shear force follow from Eq.(6.26) as

$$\begin{cases} M^h(x) = I_E\mathbf{h}_2^T(x)\mathbf{a} + \dfrac{x^2}{2} - c^2, \\ T^h(x) = -I_E\mathbf{h}_3^T(x)\mathbf{a} - x. \end{cases} \tag{6.73}$$

| $x\,[nm]$ | $v\,(x)\,[nm]$ | | $\varphi\,(x)\,[-]$ | | $M\,(x)\,[nN\ nm]$ | |
|---|---|---|---|---|---|---|
| | SD-FEM | [62] | SD-FEM | [62] | SD-FEM | [62] |
| 0 | 0 | 0 | 113.044 | 113.044 | 0 | 0 |
| 5 | 521.612 | 521.612 | 89.0226 | 89.0226 | -50 | -50 |
| 12.5 | 878.521 | 878.521 | 0 | 0 | -78.125 | -78.125 |
| 20 | 521.612 | 521.612 | -89.0226 | -89.0226 | -50 | -50 |
| 25 | 0 | 0 | -113.044 | -113.044 | 0 | 0 |

Table 6.1: Simply supported nanobeam under uniformly distributed loading: comparison of results obtained by the nonlocal SD-FEM (with one element) and the SD closed form solutions.

Comparison of the interpolated displacements, rotations and bending moments of the considered simply supported nanobeam obtained from Eqs.(6.71) and $(6.73)_1$ with the closed form solutions provided in [62] are reported in Table 6.1. It can be easily checked that the proposed SD-FEM provides the exact solution obtained in [62] by considering a unique two-noded element $\Omega_1 \equiv \Omega = [0, L]$.

The nanobeam domain $\Omega = [0, L]$ is now partitioned into three elements $\Omega_i$, $i \in \{1, 2, 3\}$, with $x_0 = 0$, $x_1 = 5\ nm$, $x_2 = 12.5\ nm$, $x_3 = L = 25\ nm$. For the sake of generality, the elements have different lengths and thus the mesh is non-symmetric. The aim is to show that the same solution of that pertaining to the nonlocal one-element SD-FEM is obtained.

In this case we have two CBCs and four CBCs in Eqs.(6.31). The generalized displacement vector is

$$\mathbf{u} = \begin{bmatrix} \mathbf{u}_1 \\ \mathbf{u}_2 \\ \mathbf{u}_3 \end{bmatrix} = \mathcal{A}\mathbf{q} \tag{6.74}$$

where $\mathbf{u}_i = \begin{bmatrix} v_i^h(x_{i-1}) & \varphi_i^h(x_{i-1}) & v_i^h(x_i) & \varphi_i^h(x_i) \end{bmatrix}^T$, with $i \in \{1, 2, 3\}$, the nodal displacement parameter is $\mathbf{q} = \begin{bmatrix} \varphi_0 & v_1 & \varphi_1 & v_2 & \varphi_2 & \varphi_3 \end{bmatrix}^T$ and $\mathcal{A}$ is the global assembly operator. The nonlocal shape functions of the element $\Omega_i$ are collected in the (1,12) matrix $\mathbf{N}_i(x) = \begin{bmatrix} \eta_{11}^{(i)}(x) & \eta_{12}^{(i)}(x) & \dots & \eta_{34}^{(i)}(x) \end{bmatrix}$ according to Eq.(6.45). The nonlocal shape functions $\mathbf{N}_1(x)$ pertaining to the

element $\Omega_1 = [0, x_1]$ have the following expressions

$$\begin{cases}
\eta_{11}^{(1)}(x) = 0.64213 + 0.360645 \times 2.71828^{-x} - 0.00277509 \times 2.71828^{x} \\
\quad +0.36342x - 0.25615x^2 + 0.0348316x^3 \\
\eta_{12}^{(1)}(x) = -1.00709 + 1.01281 \times 2.71828^{-x} - 0.00571982 \times 2.71828^{x} \\
\quad +2.01853x - 0.756655x^2 + 0.0853833x^3 \\
\eta_{13}^{(1)}(x) = 0.35787 - 0.360645 \times 2.71828^{-x} + 0.00277509 \times 2.71828^{x} \\
\quad -0.36342x + 0.25615x^2 - 0.0348316x^3 \\
\eta_{14}^{(1)}(x) = -0.782263 + 0.790418 \times 2.71828^{-x} - 0.00815562 \times 2.71828^{x} \\
\quad +0.798574x - 0.524094x^2 + 0.0887746x^3 \\
\eta_{21}^{(1)}(x) = -0.0270114 + 0.0277819 \times 2.71828^{-x} - 0.000770485 \times 2.71828^{x} \\
\quad +0.0285524x - 0.0173875x^2 + 0.0034648x^3 \\
\eta_{22}^{(1)}(x) = -0.133606 + 0.137417 \times 2.71828^{-x} - 0.00381103 \times 2.71828^{x} \\
\quad +0.141228x - 0.0860034x^2 + 0.0171379x^3 \\
\eta_{23}^{(1)}(x) = 0.0270114 - 0.0277819 \times 2.71828^{-x} + 0.000770485 \times 2.71828^{x} \\
\quad -0.0285524x + 0.0173875x^2 - 0.0034648x^3 \\
\eta_{24}^{(1)}(x) = -0.0689797 + 0.0709473 \times 2.71828^{-x} - 0.00196761 \times 2.71828^{x} \\
\quad +0.0729149x - 0.0444028x^2 + 0.00884814x^3 \\
\eta_{31}^{(1)}(x) = -0.000890314 + 0.00091571 \times 2.71828^{-x} - 0.0000253957 \times 2.71828^{x} \\
\quad +0.000941105x - 0.000573103x^2 + 0.000114202x^3 \\
\eta_{32}^{(1)}(x) = -0.00740329 + 0.00761446 \times 2.71828^{-x} - 0.000211175 \times 2.71828^{x} \\
\quad +0.00782564x - 0.00476557x^2 + 0.000949632x^3 \\
\eta_{33}^{(1)}(x) = 0.000890314 - 0.00091571 \times 2.71828^{-x} + 0.0000253957 \times 2.71828^{x} \\
\quad -0.000941105x + 0.000573103x^2 - 0.000114202x^3 \\
\eta_{34}^{(1)}(x) = -0.00372564 + 0.00383191 \times 2.71828^{-x} - 0.000106272 \times 2.71828^{x} \\
\quad +0.00393818x - 0.00239823x^2 + 0.000477894x^3
\end{cases} \tag{6.75}$$

The twelve nonlocal shape functions $\mathbf{N}_i(x)$ of the element $\Omega_i$, with $i \in \{1, 2, 3\}$, are reported in Figs.6.2, 6.3 and 6.4.

The solution of SD-FEM Eq.(6.57) provides the nodal displacement parameter $\mathbf{q}$ as

$$\mathbf{q} = \begin{bmatrix} 113.044 & 521.612 & 89.0226 & 878.521 & 0 & -113.044 \end{bmatrix}^T. \tag{6.76}$$

The interpolated displacement field $v_i^h$ is given by Eq.(6.24). The interpolated bending moments $M_i^h$ and shear forces $T_i^h$ follow from Eq.(6.26).

Comparison of the interpolated displacements, rotations and bending moments of the considered simply supported nanobeam obtained by the SD-FEM

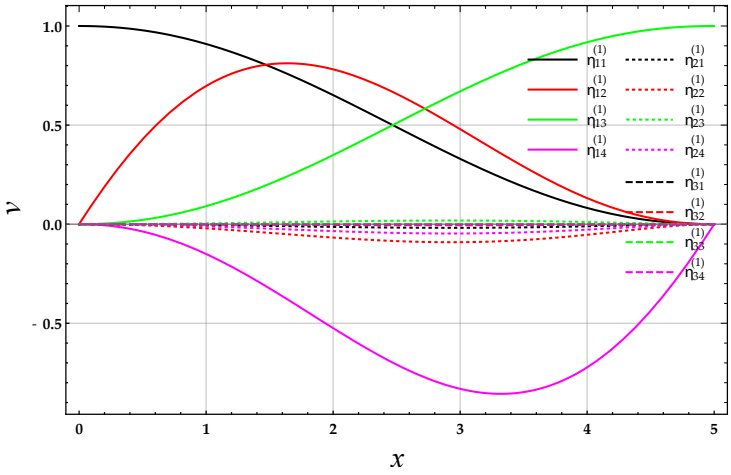


Figure 6.2: The twelve nonlocal shape functions $\mathbf{N}_1(x)$ of the element $\Omega_1$.

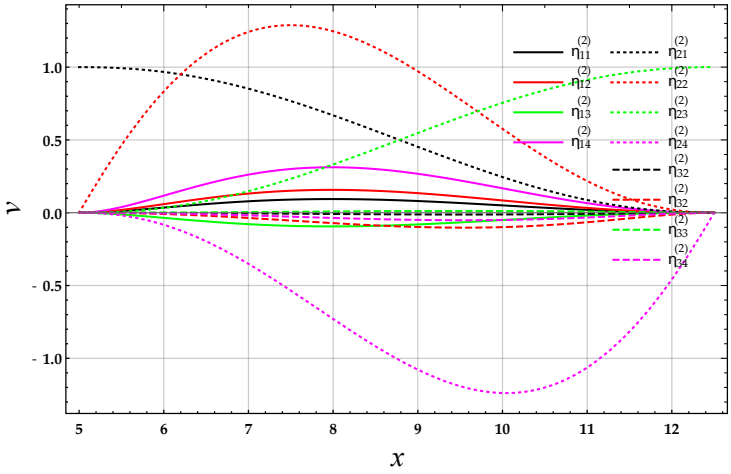


Figure 6.3: The twelve nonlocal shape functions $\mathbf{N}_2(x)$ of the element $\Omega_2$.

using three elements (SD-FEM3) with those obtained by the SD-FEM using one element (SD-FEM1) is reported in Table 6.2. It is apparent that the same

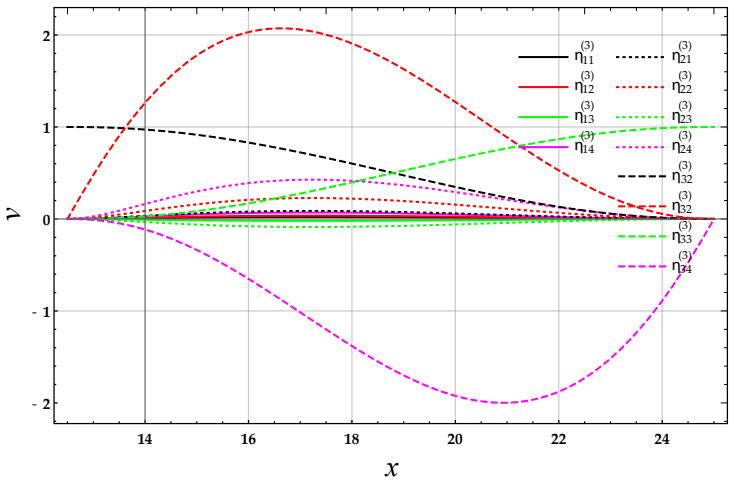


Figure 6.4: The twelve nonlocal shape functions $\mathbf{N}_3(x)$ of the element $\Omega_3$.

results are obtained by using the SD-FEM with a different number of elements.

### 6.4.2 Nanocantilever under distributed loading

Let us consider a nanocantilever of length $L = 25\ nm$ under a uniformly distributed loading $q = 1\ nN/nm$. Geometric properties of cross-section are $b = h = 1\ nm$. In order to validate the procedure, a comparison will be done with the closed form solution obtained by the nonlocal SD model provided in [62].

Let us define a unique two-noded element $\Omega_1 \equiv \Omega = [0, L]$ so that we have only the two constitutive boundary conditions in Eqs.(6.31) since there are no internal points in $\Omega$. The generalized displacement vector is

$$\mathbf{u} = \mathbf{u}_1 = \begin{bmatrix} u_{11} \\ u_{12} \\ u_{13} \\ u_{14} \end{bmatrix} = \begin{bmatrix} v^h(0) \\ \varphi^h(0) \\ v^h(L) \\ \varphi^h(L) \end{bmatrix} = \mathcal{A}\mathbf{q} \tag{6.77}$$

where the nodal displacement parameter is $\mathbf{q} = \begin{bmatrix} v^h(L) & \varphi^h(L) \end{bmatrix}^T$. The solving linear equation system for the SD-FEM is given by $\mathcal{A}^T\mathbf{K}_1\mathcal{A}\mathbf{q} = \mathcal{A}^T\mathbf{f}_1$, see

| $x\,[nm]$ | $v\,(x)\,[nm]$ | | $\varphi\,(x)\,[-]$ | | $M\,(x)$ | |
|---|---|---|---|---|---|---|
| | SD-FEM1 | SD-FEM3 | SD-FEM1 | SD-FEM3 | SD-FEM1 | SD-FEM3 |
| 0 | 0 | 0 | 113.044 | 113.044 | 0 | 0 |
| 5 | 521.612 | 521.612 | 89.0226 | 89.0226 | -50 | -50 |
| 12.5 | 878.521 | 878.521 | 0 | 0 | -78.125 | -78.125 |
| 20 | 521.612 | 521.612 | -89.0226 | -89.0226 | -50 | -50 |
| 25 | 0 | 0 | -113.044 | -113.044 | 0 | 0 |

Table 6.2: Simply supported nanobeam under uniformly distributed loading: displacements, rotations and bending moments obtained by the nonlocal SD-FEM with one and three elements.

| $x\,[nm]$ | $v\,(x)\,[nm]$ | | $\varphi\,(x)\,[-]$ | | $M\,(x)\,[nN\ nm]$ | |
|---|---|---|---|---|---|---|
| | SD-FEM | [62] | SD-FEM | [62] | SD-FEM | [62] |
| 0 | 0 | 0 | 0 | 0 | 312.5 | 312.5 |
| 12.5 | 2702.2 | 2702.2 | 371.719 | 371.719 | 78.125 | 78.125 |
| 25 | 7896.9 | 7896.9 | 430.847 | 430.847 | 0 | 0 |

Table 6.3: Nanocantilever under uniformly distributed loading: comparison of results obtained by the nonlocal SD-FEM (with one element) and the SD closed form solutions.

Eq.(6.56). The generalized displacement vector $\mathbf{u}$ is

$$\mathbf{u} = \begin{bmatrix} 0 & 0 & 7896.9 & 430.847 \end{bmatrix}^T. \tag{6.78}$$

The interpolated displacement field $v^h$ Eq.(6.24) can be written as

$$v^h\,(x) = \mathbf{h}_0^T(x)\mathbf{a} + \mathbf{k}_0^T(x)\mathbf{d} + \frac{x^4}{24 I_E} \tag{6.79}$$

where the global parameter vector $\mathbf{a}$ and $\mathbf{d}$ are provided by Eqs.(6.35)-(6.36) in terms of the displacement parameter $\mathbf{u}$ Eq.(6.78)

$$\mathbf{a} = \begin{bmatrix} 29.6496 & -29.6496 & 27.4599 & -0.729927 \end{bmatrix}^T \quad \mathbf{d} = \begin{bmatrix} -29.6496 & 0 \end{bmatrix}^T. \tag{6.80}$$

Comparison of displacements, rotations and bending moments of the nanocantilever with those obtained by the closed form solution reported in [62] are provided in Table 6.3. It can be easily checked that the proposed SD-FEM with a unique two-noded element $\Omega_1 \equiv \Omega = [0, L]$ provides the exact solution obtained in [62].

### 6.4.3 Nanocantilever under concentrated force

Let us consider a nanocantilever of length $L = 15\ nm$ under a concentrated force $F = 1\ nN$ at abscissa $x = 10\ nm$. Geometric properties of cross-section are $b = h = 1\ nm$. The closed form solution of the nonlocal SD model can be obtained following the procedure provided in [59]. The domain $\Omega = [0, L]$ of the nanocantilever is partitioned according to the following three meshes:

*Mesh* 1. Two elements $\Omega_1 = [0, 10]$ and $\Omega_2 = [10, 15]$ with $x_0 = 0$, $x_1 = 10\ nm$ and $x_2 = L = 15\ nm$. The generalized displacement vector is $\mathbf{u} = \begin{bmatrix} \mathbf{u}_1 & \mathbf{u}_2 \end{bmatrix}^T = \mathcal{A}\mathbf{q}$ where $\mathbf{q} = \begin{bmatrix} v_1 & \varphi_1 & v_2 & \varphi_2 \end{bmatrix}^T$;

*Mesh* 2. Three elements $\Omega_1 = [0, 5]$, $\Omega_2 = [5, 10]$ and $\Omega_3 = [10, 15]$ with $x_0 = 0$, $x_1 = 5\ nm$, $x_2 = 10\ nm$ and $x_3 = L = 15\ nm$. The generalized displacement vector is $\mathbf{u} = \begin{bmatrix} \mathbf{u}_1 & \mathbf{u}_2 & \mathbf{u}_3 \end{bmatrix}^T = \mathcal{A}\mathbf{q}$ where the nodal displacement vector is $\mathbf{q} = \begin{bmatrix} v_1 & \varphi_1 & v_2 & \varphi_2 & v_3 & \varphi_3 \end{bmatrix}^T$;

*Mesh* 3. Three elements $\Omega_1 = [0, 10]$, $\Omega_2 = [10, 12]$ and $\Omega_3 = [12, 15]$ with $x_0 = 0$, $x_1 = 10\ nm$, $x_2 = 12\ nm$ and $x_3 = L = 15\ nm$. The generalized displacement vector is $\mathbf{u} = \begin{bmatrix} \mathbf{u}_1 & \mathbf{u}_2 & \mathbf{u}_3 \end{bmatrix}^T = \mathcal{A}\mathbf{q}$ where the nodal displacement parameter vector is $\mathbf{q} = \begin{bmatrix} v_1 & \varphi_1 & v_2 & \varphi_2 & v_3 & \varphi_3 \end{bmatrix}^T$.

The three different meshes are considered in order to show that the SD-FEM provides the same solution for all the considered meshes. Solution of Eq.(6.57) provides the following nodal displacement parameters

$$\begin{aligned}
&\textit{Mesh } 1 \quad \mathbf{q} = \begin{bmatrix} 49.8101 & 7.88325 & 89.5772 & 7.97021 \end{bmatrix}^T \\
&\textit{Mesh } 2 \quad \mathbf{q} = \begin{bmatrix} 14.3882 & 5.61292 & 49.8101 & 7.88325 & 89.5772 & 7.97021 \end{bmatrix}^T \\
&\textit{Mesh } 3 \quad \mathbf{q} = \begin{bmatrix} 49.8101 & 7.88325 & 65.676 & 7.95895 & 89.5772 & 7.97021 \end{bmatrix}^T.
\end{aligned} \tag{6.81}$$

The interpolated displacement field $v_i^h$ is given by Eq.(6.24). The interpolated bending moments $M_i^h$ and shear forces $T_i^h$ follow from Eq.(6.26).

Comparison of the interpolated displacements, rotations and bending moments following from the SD-FEM using the three meshes defined above with those obtained by the closed form solution (CFS) of the stress-driven method are reported in Table 6.4. It can be easily checked that the proposed SD-FEM provides the exact solution obtained in [62].

It must be noted that unlike the local (classical) structural response, although the bending interaction field is vanishing between the abscissae $x_2 = 10\,nm$ and $x_3 = L = 15\,nm$, the nanocantilever has not a rigid behavior in that interval due to the long range interactions effect. Indeed, rotations $\varphi(x_2)$ and

| $x\,[nm]$ | $v\,(x)\,[nm]$ | | | | $\varphi\,(x)\,[-]$ | | | |
|---|---|---|---|---|---|---|---|---|
| | SD-FEM | | | CFS | SD-FEM | | | CFS |
| | Mesh 1 | Mesh 2 | Mesh 3 | | Mesh 1 | Mesh 2 | Mesh 3 | |
| 0 | 0 | 0 | 0 | 0 | 0 | 0 | 0 | 0 |
| 5 | 14.3882 | 14.3882 | 14.3882 | 14.3882 | 5.61292 | 5.61292 | 5.61292 | 5.61292 |
| 10 | 49.8101 | 49.8101 | 49.8101 | 49.8101 | 7.88325 | 7.88325 | 7.88325 | 7.88325 |
| 15 | 89.5772 | 89.5772 | 89.5772 | 89.5772 | 7.97021 | 7.97021 | 7.97021 | 7.97021 |

Table 6.4: Nanocantilever under concentrated force: comparison of displacements and rotations obtained by the nonlocal SD-FEM and the closed form solutions.

$\varphi(L)$ obtained by the SD-FEM differ. Non-dimensional maximum displacement $v_{\max}/v_l$ versus thickness to nonlocal parameter ratio is depicted in Fig.6.5, being $v_l$ the maximum local displacement. In order to make a comparison, the trend predicted by the classical (local) model is shown. It can be observed that the response predicted by the SD-FEM tends to converge to the one predicted by the classical theory of elasticity for increasing thickness to nonlocal parameter ratio. Accordingly, if the ratio is large the SD-FEM shows that effects of

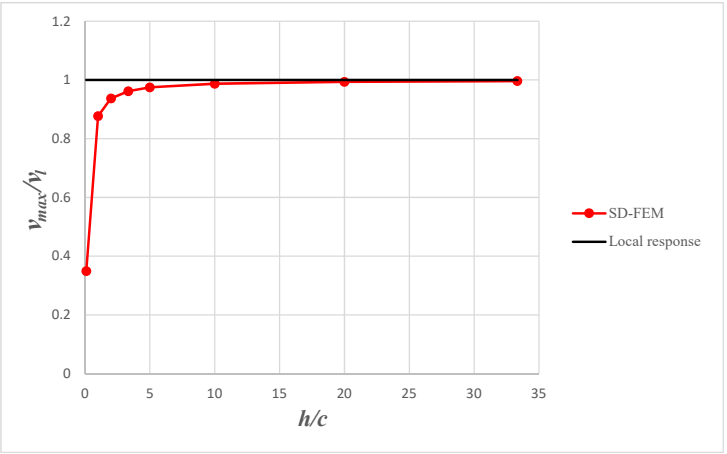


Figure 6.5: Non-dimensional maximum displacement $v_{\max}/v_l$ versus thickness to nonlocal parameter ratio.

long range interactions are negligible while, when the thickness approaches the length-scale, nonlocal effects cannot be overlooked.

### 6.4.4 Complex nonlocal structural system

Let us consider an assemblage of nanobeams under a concentrated couple $\mathcal{M} = 1\,nNnm$ and a piecewise uniformly distributed loading $q = 1\,nN/nm$ (see Fig.6.6). The geometric properties are $L_1 = L_2 = L_3 = 1\,nm$ and $b = h = 1\,nm$. The structure is meshed with three elements $\Omega_1 = [0, 1]$, $\Omega_2 = [1, 2]$ and $\Omega_3 = [2, 3]$ with $x_0 = 0$, $x_1 = 1\,nm$, $x_2 = 2\,nm$ and $x_3 = L = 3\,nm$. The closed form solution associated with the stress-driven nonlocal model can be obtained following the procedure provided in [59]. The twelve nonlocal shape

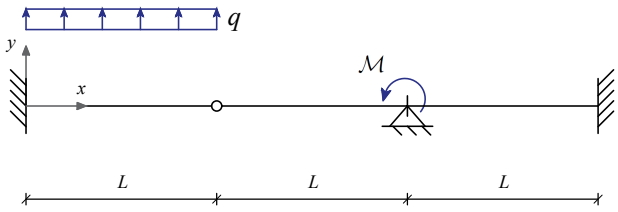


Figure 6.6: Sketch of an articulated assemblage of beams under concentrated couple and piecewise smooth distributed loading.

functions $\mathbf{N}_i(x)$ of the elements $\Omega_i$, with $i \in \{1, 2, 3\}$, are reported in Figs.6.7, 6.8 and 6.9.

The nodal displacement parameter is $\mathbf{q} = \begin{bmatrix} q_1 & q_2 & q_3 & q_4 \end{bmatrix}^T$ and its components represent displacement of the hinge at $x_1$, rotation of the section just left the hinge at $x_1$, rotation of the section just right the hinge at $x_1$, rotation of the section at $x_2$.

Solution of Eq.(6.57) provides the nodal displacement parameter as

$$\mathbf{q} = \begin{bmatrix} 0.000712727 & 0.00157794 & -0.00264855 & 0.000875735 \end{bmatrix}^T. \tag{6.82}$$

The interpolated displacement field $v_i^h$, with $i \in \{1, 2, 3\}$, is given by Eq.(6.24)

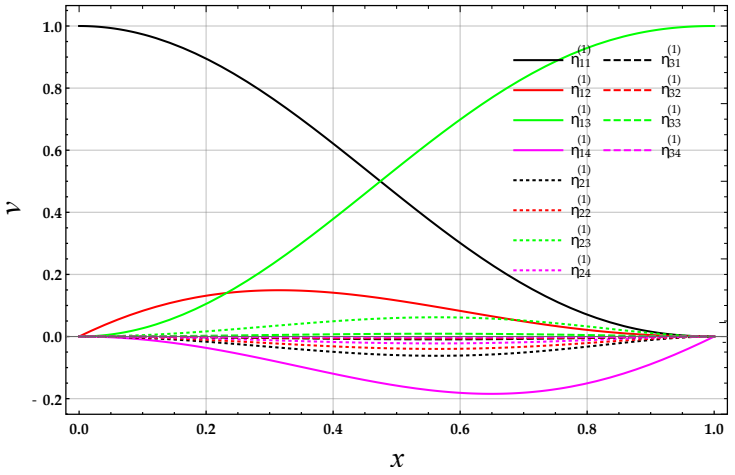


Figure 6.7: Articulated assemblage of nanobeams: shape functions of the element $\Omega_1$.

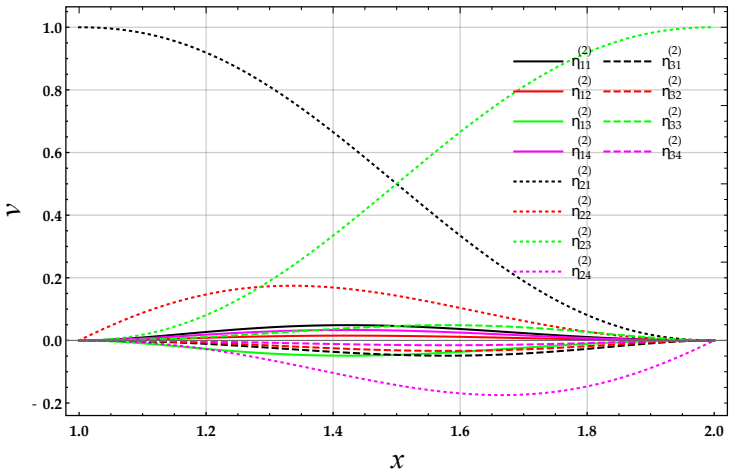


Figure 6.8: Articulated assemblage of nanobeams: shape functions of the element $\Omega_2$.

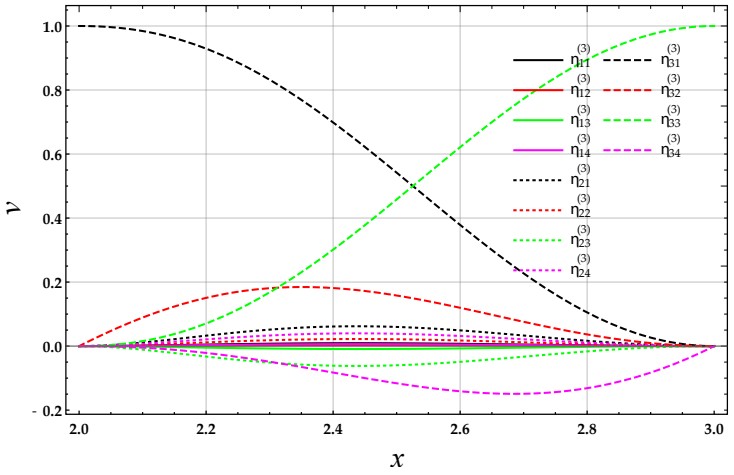


Figure 6.9: Articulated assemblage of nanobeams: shape functions of the element $\Omega_3$.

and can be written as

$$\begin{aligned} v_1^h(x) &= \mathbf{h}_0^T(x)\mathbf{a}_1 + \mathbf{k}_0^T(x)\mathbf{d}_1 + \frac{x^4}{24I_E} \\ v_2^h(x) &= \mathbf{h}_0^T(x)\mathbf{a}_2 + \mathbf{k}_0^T(x)\mathbf{d}_2 \\ v_3^h(x) &= \mathbf{h}_0^T(x)\mathbf{a}_3 + \mathbf{k}_0^T(x)\mathbf{d}_3 \end{aligned} \tag{6.83}$$

where the global parameter vectors $\mathbf{a}$ and $\mathbf{d}$ are provided by Eqs.(6.35)-(6.36) as follows

$$\begin{aligned} \mathbf{a} = \big[ & \ 0.198159 \quad -0.113512 \quad 0.0998157 \quad -0.0186733 \quad -0.0676874 \\ & \ 0.0866408 \quad -0.0315712 \quad 0.0105237 \quad -0.986294 \quad 0.790759 \\ & \ -0.23708 \quad 0.0301767 \ \big]^T \\ \mathbf{d} = \big[ & \ -0.155836 \quad -0.0423234 \quad 0.082262 \quad -0.0101004 \\ & \ 1.16513 \quad -0.00622538 \ \big]^T \end{aligned} \tag{6.84}$$

Interpolated bending moments $M_i^h$ and shear forces $T_i^h$ follow from Eq.(6.26). Comparison of displacements, rotations and bending moments of the considered nanocantilever with those obtained by the closed form solution (CFS) are re-

| $x\,[nm]$ | $v\,(x)\,[nm]$ | | $\varphi\,(x)\,[-]$ | | $M\,(x)\,[nN\ nm]$ | |
|---|---|---|---|---|---|---|
| | SD-FEM | CFS | SD-FEM | CFS | SD-FEM | CFS |
| 0 | 0 | 0 | 0 | 0 | 0.139562 | 0.139562 |
| 0.5 | 0.000180286 | 0.000180286 | 0.000687645 | 0.000687645 | -0.055219 | -0.055219 |
| 1 left | 0.000712727 | 0.000712727 | 0.00157794 | 0.00157794 | 0 | 0 |
| 1 | 0.000712727 | 0.000712727 | / | / | 0 | 0 |
| 1 right | 0.000712727 | 0.000712727 | -0.00264855 | -0.00264855 | 0 | 0 |
| 1.5 | -0.00015543 | -0.00015543 | -0.000659419 | -0.000659419 | 0.180219 | 0.180219 |
| 2 left | 0 | 0 | 0.000875735 | 0.000875735 | 0.360438 | 0.360438 |
| 2 | 0 | 0 | 0.000875735 | 0.000875735 | / | / |
| 2 right | 0 | 0 | 0.000875735 | 0.000875735 | -0.639562 | -0.639562 |
| 2.5 | 0.000161892 | 0.000161892 | -0.000309315 | -0.000309315 | -0.122786 | -0.122786 |
| 3 | 0 | 0 | 0 | 0 | 0.393989 | 0.393989 |

Table 6.5: Comparison of displacements, rotations and bending moments obtained by the nonlocal SD-FEM and the closed form solutions.

ported in Tables 6.5. The labels "1 left" and "1 right" mean node 2 of element $\Omega_1$ and node 1 of element $\Omega_2$, respectively, and "2 left" and "2 right" mean node 2 of element $\Omega_2$ and node 1 of element $\Omega_3$, respectively. It can be immediately checked that the proposed SD-FEM provides same results of the closed form SD method.

# Conclusions

Nonlocal fields theory is a branch of Continuum Mechanics accounting for size effects in those material bodies where long range interactions cannot be overlooked. Due to the recent interest in Nanoscience and Nanotechnology, one of the most promising applications of nonlocal continuum theories deals with modeling and optimization of smaller and smaller smart devices. Thus, during the last decade many efforts have been devoted to provide consistent nonlocal formulations leading to well-posed structural problems in Continuum Mechanics.

The present thesis aims at facing challenging topics of current interest in nonlocal mechanics, both from the theoretical and the computational point of view. To approach the topic, fundamental concepts of nonlocality have been first elucidated with a comprehensive and detailed illustration. A variational formulation has been proposed to derive the general constitutive law of nonlocal elasticity from which the main theories can be derived and exploited to provide some benchmark results in nonlocal mechanics.

Then, a challenging issue in the framework of nonlocal fields theory has been faced concerning the reproducibility of a continuum structural problem according to which general physical laws, expressed with reference to a given placement of a continuous body, must be applicable to its any sub-part. Thus, a nonlocal model of elasticity based on the well-posed stress-driven formulation has been conceived for assembled structural systems. A constitutive differential formulation has been provided to model the size-dependent behavior of nonlocal elastic structures involving concentrated and non-smooth distributed loadings, internal kinematic constraints and piecewise regular elastic and geometric properties. The presented differential formulation, involving prescription of constitutive boundary and interface conditions, has been exploited to conceive a finite element (FE) nonlocal formulation.

The proposed FE methodology is based on a two-noded nonlocal finite element and the obtained nonlocal shape functions account for long range interac-

tions on the whole structural domain, so that nonlocal effects are not confined to the single finite element. Indeed, the number of nonlocal shape functions is four times the number of elements in the mesh. A direct approach has been proposed to derive nonlocal stiffness matrix and nodal force vector and then an assemblage procedure has been exploited to get the relevant structural problem.

Validation of the proposed stress-driven nonlocal FE formulation has been performed and benchmark numerical results of structural assemblages have been provided. The presented methodology has been shown to provide exact stress-driven nonlocal solutions and to reproduce the typical stiffening size-dependent structural behavior in agreement with the smaller-is-stiffer phenomenon. Moreover, unlike previous contributions where nonlocal effects were confided to the single finite element, according to the proposed nonlocal FE formulation long range interactions involve the whole structural domain.

Further contributions may concern the application of the proposed nonlocal computational technique to accurately solve static, dynamic and buckling problems of nanoscopic beams and frames involved in modern electromechanical devices.

# Bibliography

[1] Allameh M., Shafai C., 2021. Tri-electrode MEMS electrostatic actuator with lower control voltage and higher stroke for actuator array implementations, Journal of Electrostatics 114, 103635.

[2] Chand C.G., Maity R., Srinivasa Rao K., Maity N.P., 2021. Electromagnetic modelling and analysis of RF MEMS capacitive shunt switch for 5G applications, Microelectronics Journal 117, 105262.

[3] Kumar P.A., Rao K.S., Sravani K.G., Balaji B., Aditya M., Guha K., Elsinawi A., 2021. An intensive approach to optimize capacitive type RF MEMS shunt switch, Microelectronics Journal 112, 105050.

[4] Ouakad H.M., Valipour A., Żur K.K., Sedighi H.M., Reddy J.N., 2020. On the nonlinear vibration and static deflection problems of actuated hybrid nanotubes based on the stress-driven nonlocal integral elasticity, Mechanics of Materials 148, 103532.

[5] Farajpour A., Żur K.K., Kim J., Reddy J.N., 2021. Nonlinear frequency behaviour of magneto-electromechanical mass nanosensors using vibrating MEE nanoplates with multiple nanoparticles, Composite Structures 260, 113458.

[6] Wang S., Wang J., Zeng M., Yang J., Hu N., Su Y., Zhou Z., Pang H., Yang Z., 2021. Synthesis of nickel-metal organic framework nanoplates with pyridine modulation and application to supercapacitors, Journal of Energy Storage 38, 102528.

[7] Furletov A., Apyari V., Garshev A., Dmitrienko S., Zolotov Y., 2022. Fast and sensitive determination of bioflavonoids using a new analytical system based on label-free silver triangular nanoplates, Sensors 22(3), 843.

[8] Aryasomayajula A. et al., 2017. Springer Handbook of Nanotechnology, Springer. Bharat Bhushan (ed.), Columbus, USA.

[9] Xiao D., Li Q., Hou Z., Xia D., Xu X., Wu X., 2017. A double differential torsional micro-accelerometer based on V-shape beam, Sensors and Actuators A 258, 182-192.

[10] Algamili A.S., Khir M.H.M., Dennis J.O., Ahmed A. Y., Alabsi S.S., Ba Hashwan S.S., Junaid M.M., 2021. A review of actuation and sensing mechanisms in MEMS-based sensor devices, Nanoscale Research Letters 16, 16.

[11] Khaniki H.B., Ghayesh M.H., Amabili M., 2021. A review on the statics and dynamics of electrically actuated nano and micro structures, International Journal of Non-Linear Mechanics 129, 103658.

[12] Iijima S., Ichihashi T., 1993. Single-shell carbon nanotubes of 1 nm diameter, Nature 363, 603-605.

[13] Bethune D.S., Kiang C.H., de Vries M.S., Gorman G., Savoy R., Vazquez J., Bayers R., 1993. Cobalt-catalysed growth of carbon nanotubes with single-atomic layer walls, Nature 363, 605-607.

[14] Barretta R., Brcić M., Ĉanadija M., Luciano R., Marotti de Sciarra F., 2017. Application of gradient elasticity to armchair carbon nanotubes: Size effects and constitutive parameters assessment. European Journal of Mechanics A/Solids 65, 1-13.

[15] Javaid M., Haleem A., Singh R.P., Rab S., Suman R., 2021. Exploring the potential of nanosensors: A brief overview, Sensors International 2, 100130.

[16] Asad M., Sheikhi M.H., Pourfath M., Moradi M., 2015. High sensitive and selective flexible $H_2S$ gas sensors based on Cu nanoparticle decorated SWCNTs, Sensors and Actuators B: Chemical 210, 1-8.

[17] Song H., Li Q., Zhang Y., 2020. CNT-based sensor array for selective and steady detection of $SO_2$ and NO, Materials Research Bulletin, 124, 110772.

[18] Besley N., 2020. A. vibrational analysis of carbon nanotube-based nanomechanical resonators, Journal of Physical Chemistry C 124, 16714-16721.

[19] Clement K. et al., 2021. Requirements and attributes of nano-resonator mass spectrometry for the analysis of intact viral particles. Analytical and Bioanalytical Chemistry. https://doi.org/10.1007/s00216-021-03511-4

[20] Morassi A., Dilena M., Fedele Dell'Oste M., Fernández-Sáez J., Zaera R., 2019. Monitoring mass changes using nanoresonator sensors, Procedia Structural Integrity 17, 98-104.

[21] Dilena M., Fedele Dell'Oste M., Fernández-Sáez J., Morassi A., Zaera R., 2020. Hearing distributed mass in nanobeam resonators, International Journal of Solids and Structures 193–194, 568-592.

[22] Zhang C., Akbarzadeh A., Kang W., Wang J., Mirabolghasemi A., 2018. Nano-architected metamaterials: Carbon nanotube-based nanotrusses, Carbon 131, 38-46.

[23] Chao M., Wang Y., Ma D., Wu X., Zhang W., Zhang L., Wan P., 2020. Wearable MXene nanocomposites-based strain sensor with tile-like stacked hierarchical microstructure for broad-range ultrasensitive sensing, Nano Energy 78, 105187.

[24] Bi L., Yin J., Huang X., Wang Y., Yang Z., 2020. Graphene pillared with hybrid fullerene and nanotube as a novel 3D framework for hydrogen storage: A DFT and GCMC study, International Journal of Hydrogen Energy 45, 17637-17648.

[25] Navier C.L.M.H., 1827. Mémoire sur les lois de l'équilibre et du mouvement des corps solides élastiques, Mémoire de l'Académie des Sciences de l'Institut de France 7, 375-393.

[26] Poisson S.D., 1829. Mémoire sur l'équilibre et du mouvement des corps élastiques, Mémoire de l'Académie des Sciences de l'Institut de France 8, 357-570.

[27] Cauchy A.L., 1829. Sur l'équilibre et le mouvement intérieur des corps considérés comme des masses continues, Exercices de Mathématiques 4, 293-319.

[28] Meo M., Rossi M., 2006. Prediction of Young's modulus of single wall carbon nanotubes by molecular-mechanics based finite element modelling, Composites Science and Technology, 66(11–12), 1597-1605.

[29] Malagù M., Benvenuti E., Simone A., 2015. One-dimensional nonlocal elasticity for tensile single-walled carbon nanotubes: A molecular structural mechanics characterization, European Journal of Mechanics A/Solids 54, 160-170.

[30] Duan K., Li L., Hu Y., Wang X., 2017. Enhanced interfacial strength of carbon nanotube/copper nanocomposites via Ni-coating: Molecular-dynamics insights, Physica E: Low-dimensional Systems and Nanostructures 88, 259-264.

[31] Rogula D., 1965. Influence of spatial acoustic dispersion on dynamical properties of dislocations, Bull. Acad. Pol. Sci. Ser. Sci. Tech. 13, 337-343.

[32] Rogula D., 1982. Introduction to nonlocal theory of material media. Nonlocal theory of material media, CISM courses and lectures, Springer, Wien, 268, 125-222.

[33] Lakes R.S., 1991. Experimental micro mechanics methods for conventional and negative Poissons ratio cellular solids as Cosserat continua, Journal of Engineering Materials and Technology 113(1), 148-155.

[34] Arash B., Wang Q., 2012. A review on the application of nonlocal elastic models in modeling of carbon nanotubes and graphenes, Computational Materials Science 51(1), 303-313.

[35] Eringen A.C., 1972. Linear theory of nonlocal elasticity and dispersion of plane waves, International Journal of Engineering Science 10(5), 425-435.

[36] Eringen, A.C., 1983. On differential equations of nonlocal elasticity and solutions of screw dislocation and surface waves, Journal of Applied Physics 54, 4703.

[37] Peddieson J., Buchanan G.R., McNitt R.P., 2003. Application of nonlocal continuum models to nanotechnology. International Journal of Engineering Science 41(3-5), 305-312.

[38] Challamel N., Wang C.M., 2008. The small length scale effect for a nonlocal cantilever beam: a paradox solved, Nanotechnology 19, 345703.

[39] Li C., Yao L., Chen W., Li S., 2015. Comments on nonlocal effects in nanocantilever beams, International Journal of Engineering Science 87, 47-57.

[40] Romano G., Barretta R., Diaco M., Marotti de Sciarra F., 2017. Constitutive boundary conditions and paradoxes in nonlocal elastic nano-beams, International Journal of Mechanical Sciences 121, 151-156.

[41] Zhang P., Qing H., Gao C.F., 2020. Exact solutions for bending of Timoshenko curved nanobeams made of functionally graded materials based on stress-driven nonlocal integral model, Composite Structures 245, 112362.

[42] Sidhardh S., Patnaik S., Semperlotti F., 2020. Geometrically nonlinear response of a fractional-order nonlocal model of elasticity, International Journal of Non-Linear Mechanics 125, 103529.

[43] Dilena M., Fedele Dell'Oste M., Fernández-Sáez J., Morassi A., Zaera R., 2019. Mass detection in nanobeams from bending resonant frequency shifts, Mechanical Systems and Signal Processing 116, 261-276.

[44] Shahsavari D., Karami B., Fahham H.R., Li L., 2018. On the shear buckling of porous nanoplates using a new size-dependent quasi-3D shear deformation theory, Acta Mechanica 229(11), 4549-4573.

[45] Vila J., Fernández-Sáez J., Zaera R., 2017. Nonlinear continuum models for the dynamic behavior of 1D microstructured solids, International Journal of Solids and Structures 117, 111-122.

[46] Romano G., Luciano R., Barretta R., Diaco M., 2018. Nonlocal integral elasticity in nanostructures, mixtures, boundary effects and limit behaviours, Continuum Mechanics and Thermodynamics, 30(3), 641-655.

[47] Benvenuti E., Simone A., 2013. One-dimensional nonlocal and gradient elasticity: closed-form solution and size effects, Mechanics Research Communications 48, 46-51.

[48] Eringen A.C., 1987. Theory of nonlocal elasticity and some applications, Res Mechanica 21, 313-342.

[49] Wang Y., Zhu X., Dai H., 2016. Exact solutions for the static bending of Euler-Bernoulli beams using Eringen two-phase local/nonlocal model, AIP Advances 6(8), 085114.

[50] Khodabakhshi P., Reddy J.N., 2015. A unified integro-differential nonlocal model, International Journal of Engineering Science 95, 60-75.

[51] Fernández-Sáez J., Zaera R., 2017. Vibrations of Bernoulli-Euler beams using the two-phase nonlocal elasticity theory, International Journal of Engineering Science 119, 232-248.

[52] Zhang P., Qing H., Gao C., 2019. Theoretical analysis for static bending of circular Euler-Bernoulli beam using local and Eringen's nonlocal integral mixed model, ZAMM 99(8), e201800329.

[53] Romano G., Barretta R., Diaco M., 2017. On nonlocal integral models for elastic nano-beams, International Journal of Mechanical Sciences 131-132, 490-499.

[54] Romano G., Barretta R., 2017. Nonlocal elasticity in nanobeams: the stress-driven integral model, International Journal of Engineering Science 115, 14-27.

[55] Romano G., Barretta R., 2017. Stress-driven versus strain-driven nonlocal integral model for elastic nano-beams, Composites Part B: Engineering 114, 184-188.

[56] Barretta R., Marotti de Sciarra F., Vaccaro M.S., 2019. On nonlocal mechanics of curved elastic beams, International Journal of Engineering Science 144, 103140.

[57] Romano G., Barretta R., Diaco M., 2019. Iterative methods for nonlocal elasticity problems, Continuum Mechanics and Thermodynamics 31, 669–689.

[58] Romano G., Diaco M., 2020. On formulation of nonlocal elasticity problems, Meccanica 56(3–5).

[59] Vaccaro M.S., Marotti de Sciarra F., Barretta R., 2021. On the regularity of curvature fields in stress-driven nonlocal elastic beams, Acta Mechanica 232, 2595–2603.

[60] Sedighi H., Malikan M., 2020. Stress-driven nonlocal elasticity for nonlinear vibration characteristics of carbon/boron-nitride hetero-nanotube subject to magneto-thermal environment, Physica Scripta 95, 055218.

[61] Farajpour A., Howard C.Q., Robertson W.S., 2020. On size-dependent mechanics of nanoplates, International Journal of Engineering Science 156, 103368.

[62] Barretta R., Ĉanadija M., Feo L., Luciano R., Marotti de Sciarra F., Penna R., 2018. Exact solutions of inflected functionally graded nano-beams in integral elasticity, Composites Part B, 142, 273-286.

[63] Barretta R., Luciano R., Marotti de Sciarra F., Ruta G., 2018. Stress-driven nonlocal integral model for Timoshenko elastic nano-beams, European Journal of Mechanics / A Solids 72, 275-286.

[64] Apuzzo A., Barretta R., Luciano R., Marotti de Sciarra F., Penna R., 2017. Free vibrations of Bernoulli-Euler nano-beams by the stress-driven nonlocal integral model, Composites Part B: Engineering 123, 105-111.

[65] Barretta R., Fabbrocino F., Luciano R., Marotti de Sciarra F., 2018. Closed-form solutions in stress-driven two-phase integral elasticity for bending of functionally graded nano-beams, Physica E: Low-dimensional Systems and Nanostructures 97, 13-30.

[66] Vaccaro M.S., Pinnola F.P., Marotti de Sciarra F., Ĉanadija M., Barretta R., 2021. Stress-driven two-phase integral elasticity for Timoshenko curved beams, Proceedings of the Institution of Mechanical Engineers, Part N: Journal of Nanomaterials, Nanoengineering and Nanosystems 235(1-2), 52-63.

[67] Apuzzo A., Barretta R., Fabbrocino F., Faghidian S.A., Luciano R., Marotti de Sciarra F., 2019. Axial and torsional free vibrations of elastic nano-beams by stress-driven two-phase elasticity, Journal of Applied and Computational Mechanics 5(2), 402-413.

[68] Fuschi P., Pisano A.A., Polizzotto C., 2019. Size effects of small-scale beams in bending addressed with a strain-difference based nonlocal elasticity theory, International Journal of Mechanical Sciences 151, 661-671.

[69] Aifantis E.C., 1994. Gradient effects at macro, micro and nano scales, Journal of the Mechanical Behavior of Biomedical Materials 5, 355-375.

[70] Aifantis E.C., 2003. Update on a class of gradient theories. Mechanics of Materials, 3–6(35), 259-280.

[71] Lim C.W., Zhang G., Reddy J.N., 2015. A higher-order nonlocal elasticity and strain gradient theory and its applications in wave propagation, Journal of the Mechanics and Physics of Solids 78, 298-313.

[72] Barretta R., Marotti de Sciarra F., 2018. Constitutive boundary conditions for nonlocal strain gradient elastic nano-beams, International Journal of Engineering Science 130, 187-198.

[73] Barretta R., Marotti de Sciarra F., 2019. Variational nonlocal gradient elasticity for nano-beams, International Journal of Engineering Science 143, 73-91.

[74] Abazari A.M., Safavi S.M., Rezazadeh G., Villanueva L.G., 2015. Modelling the size effects on the mechanical properties of micro/nano structures, Sensors 15, 28543-28562.

[75] Pisano A.A., Fuschi P., 2003. Closed form solution for a nonlocal elastic bar in tension, International Journal of Solids and Structures 40, 13-23.

[76] Tricomi F.G., 1957. Integral Equations, Interscience, New-York, USA. Reprinted by Dover Books on Mathematics, 1985.

[77] Polyanin A.D., Manzhirov A.V., 2008. Handbook of integral equations, Chapman & Hall/CRC, Boca Raton, USA.

[78] Mikhasev G., Nobili A., 2020. On the solution of the purely nonlocal theory of beam elasticity as a limiting case of the two-phase theory, International Journal of Solids and Structures 190, 47-57.

[79] Mikhasev G., 2021. Free high-frequency vibrations of nonlocally elastic beam with varying cross-section area. Continuum Mechanics and Thermodynamics 33, 1299–1312.

[80] Romano G., 2002. Scienza delle Costruzioni. Tomo I, Hevelius, Benevento, Italia.

[81] Vaccaro M.S., 2022. On geometrically nonlinear mechanics of nanocomposite beams, International Journal of Engineering Science 173, 103653.

[82] Nemat-Nasser S., Hori M., 1999. Micromechanics: overall properties of heterogeneous materials. North Holland.

[83] Shen H.S., 2011. Postbuckling of nanotube-reinforced composite cylindrical shells in thermal environments, part I: Axially-loaded shells, Composite Structures 93, 2096–2108.

[84] Liew K.M., Pan Z., Zhang L.W., 2020. The recent progress of functionally graded CNT reinforced composites and structures, Science China Physics, Mechanics, and Astronomy 63, 234601.

[85] Civalek Ö., Dastjerdi S., Akbaș Ș. D., Akgoz B., 2021. Vibration analysis of carbon nanotube-reinforced composite microbeams, Mathematical Methods in the Applied Sciences. doi:10.1002/mma.7069.

[86] Barretta R., Ĉanadija M., Marotti de Sciarra F., 2019. Modified nonlocal strain gradient elasticity for nano-rods and application to carbon nanotubes, Applied Sciences 9, 514.

[87] Zhu X., Li L., 2017. Closed form solution for a nonlocal strain gradient rod in tension, International Journal of Engineering Science 119, 16–28.

[88] Caporale A., Darban H., Luciano R., 2020. Exact closed-form solutions for nonlocal beams with loading discontinuities, Mechanics of Advanced Materials and Structures 1-11. https://bit.ly/3nDcf56.

[89] Bachtold A., Hadley P., Nakanishi T., Dekker C., 2001. Logic circuits with carbon nanotube transistors, Science 294(5545), 1317-1320.

[90] Zi Y., Wang Z.L., 2017. Nanogenerators: An emerging technology towards nanoenergy, APL Materials 5, 074103.

[91] Kazmi S.N.R., Hafiz A.A., Chappanda K.N., Ilyas S., Holguin J., Costa P.M.F.J., Younis M.I., 2017. Tunable nanoelectromechanical resonator for logic computations, Nanoscale 9, 3449-3457.

[92] Kumar R., Singh R., Hui D., Feo L., Fraternali F., 2018. Graphene as biomedical sensing element: state of art review and potential engineering applications, Composites Part B 134, 193-206.

[93] Talebitooti R., Rezazadeh S., Amiri A., 2019. Comprehensive semi-analytical vibration analysis of rotating tapered AFG nanobeams based on nonlocal elasticity theory considering various boundary conditions via differential transformation method, Composites Part B: Engineering 160, 412-435.

[94] Khaniki H., 2018. Vibration analysis of rotating nanobeam systems using Eringen's two-phase local/nonlocal model, Physica E: Low-dimensional Systems and Nanostructures 99, 310-319.

[95] Aghababaei J.R., 2009. Nonlocal third-order shear deformation plate theory with application to bending and vibration of plates, Journal of Sound and Vibration 326(1-2), 277-289.

[96] Żur K., Arefi M., Kim J., Reddy J.N., 2020. Free vibration and buckling analyses of magneto-electro-elastic FGM nanoplates based on nonlocal modified higher-order sinusoidal shear deformation theory, Composites Part B: Engineering 182, 107601.

[97] Farajpour A., Rastgoo A., Farajpour M.R., 2017. Nonlinear buckling analysis of magneto-electro-elastic CNT-MT hybrid nanoshells based on the nonlocal continuum mechanics, Composite Structures 180, 179-191.

[98] Sahmani S., Aghdam M., 2018. Nonlocal strain gradient shell model for axial buckling and postbuckling analysis of magneto-electro-elastic composite nanoshells, Composites Part B: Engineering 132, 258-274.

[99] Eltaher M.A., Emam S.A., Mahmoud F.F., 2012. Free vibration analysis of functionally graded size-dependent nanobeams, Applied Mathematics and Computation 218(14), 1737-1741.

[100] Aria A.I., Friswell M.I., 2019. A nonlocal finite element model for buckling and vibration of functionally graded nanobeams, Composites Part B, Engineering 166, 233-246.

[101] Srividhya S., Raghu P., Rajagopal A., Reddy J.N., 2018. Nonlocal nonlinear analysis of functionally graded plates using third-order shear deformation theory, International Journal of Engineering Science 125, 1-22.

[102] Raghu P., Rajagopal A., Reddy J.N., 2018. Nonlocal nonlinear finite element analysis of composite plates using TSDT, Composite Structures 185, 38-50.

[103] Civalek Ö., Numanoğlu H.M., 2020. Nonlocal finite element analysis for axial vibration of embedded love–bishop nanorods, International Journal of Mechanical Sciences 188, 105939.

[104] Bacciocchi M., Fantuzzi N., Ferreira A.J.M., 2021. Static finite element analysis of thin laminated strain gradient nanoplates in hygro-thermal environment, Continuum Mechanics and Thermodynamics 33, 969-992.

[105] Sedighi H.M., Malikan M., Valipour A., Żur K.K., 2020. Nonlocal vibration of carbon/boron-nitride nano-hetero-structure in thermal and magnetic fields by means of nonlinear finite element method, Journal of Computational Design and Engineering 7(5), 591-602.

[106] Alotta G., Failla G., Zingales M., 2017. Finite-element formulation of a nonlocal hereditary fractional-order Timoshenko beam, Journal of Engineering Mechanics 143(5), 5D4015001.

[107] Pinnola F.P., Vaccaro M.S., Barretta R., Marotti de Sciarra F., 2022. Finite element method for stress-driven nonlocal beams, Engineering Analysis with Boundary Elements 134(5545), 22-34.

[108] Henderson H.V., Searle S.R., 1981. On deriving the inverse of a sum of matrices, SIAM Review 23(1), 53-60.